Division of Biomedical Engineering
Department of Human Biology
University of Cape Town

Design and Development of a Device to Diagnose and Treat Obstructive Sleep Apnoea

In partial fulfilment of the requirements for the degree of

Master of Science in Biomedical Engineering

by coursework and dissertation

By:
Joel Philpott

Supervisor:
Prof. Sudesh Sivarasu

June 12, 2024

Plagiarism Declaration

I, **Joel Philpott**, hereby declare that the work on which this thesis is based is my original work (except where acknowledgements indicate otherwise) and that neither the whole work nor any part of it has been, is being, or is to be submitted for another degree in this or any other university. I authorise the University to reproduce for the purpose of research either the whole or any portion of the contents in any manner whatsoever.

Signature: Signed by candidate **Date:** June 12, 2024

Acknowledgements

Firstly, I would like to thank the Wisconsin Sleep Cohort for granting access to their database. This Wisconsin Sleep Cohort Study was supported by the U.S. National Institutes of Health, National Heart, Lung, and Blood Institute (R01HL62252), National Institute on Aging (R01AG036838, R01AG058680), and the National Center for Research Resources (1UL1RR025011). The National Sleep Research Resource was supported by the U.S. National Institutes of Health, National Heart Lung and Blood Institute (R24 HL114473, 75N92019R002).

I would also like to thank merSETA, the manufacturing, engineering, and related services SETA for funding this research. I would also like to thank the Groote Schuur hospital departments of clinical engineering and clinical skills for allowing me to use their facilities for testing.

The thesis presented here is by no means an individual effort. It is the culmination of years of educators conveying their knowledge and support, as well as advice from family and friends during the master's degree. Some of these people are mentioned below, but to all those who have put time and energy into teaching me to enjoy the learning and development process, I am eternally grateful.

Thank you to the members of the University of Cape Town Medical devices laboratory. The culture of support and camaraderie created among us has been incredibly encouraging, and it has been a privilege to work with people so passionate about what we do. Special mention must go to Jonathan Oehley and Brandon Reabow, our Thursday lunches were often the highlight of the week. Thank you to Prof. Sudesh Sivarasu for your encouragement. I have enjoyed learning from and being challenged by you.

Thank you to the Nel family of whom I became a member in the course of my thesis. Your cumulative assistance has got me through the most frustrating and exhausting times. Thank you for all your prayers and support.

To the Philpott family, thank you for all you have done to get me to this point. I appreciate that you instilled in me pride in the work that I do, and for encouraging me to tackle tasks that seemed insurmountable at times. Thank you for the hours spent editing, and for the many encouraging phone calls.

Finally, Candace, thank you for allowing me time for all the after-hours work that I needed to do, and for supporting me whenever possible (including coming to have dinner at the laboratory). You have been an incredible photographer/engineering consultant/wife. This thesis is as much yours as it is mine.

Isaiah 40:31
"Even youths shall faint and be weary, and young men shall fall exhausted;
but they who wait for the Lord shall renew their strength;
they shall mount up with wings like eagles;
they shall run and not be weary;
they shall walk and not faint."
Soli Deo Gloria.

Abstract

Sleep apnoea is the repeated cessation of breathing during sleep and can result in impaired concentration, excessive unexplained sleepiness, and sleep fragmentation. Long-term effects of the condition can include hypertension, stroke and cardiovascular disease, diabetes and glucose intolerance, and obesity. Sleep apnoea is linked to a hazard ratio of 1.97, indicating that individuals with this condition face almost twice the risk of experiencing a stroke or death compared to those without sleep apnoea.

It is estimated that 425 million adults between the ages of 30 and 69 have moderate to severe sleep apnoea. A study conducted in Wisconsin, America, found that 82% of men and 93% of women with moderate to severe sleep apnoea had not been diagnosed. This is likely to be even higher in low-middle-income countries like South Africa, where there is limited access to healthcare. Limited access to healthcare also affects sleep apnoea treatment. A study conducted in Latin America found that of the 880 patients diagnosed with sleep apnoea, only 55.7% started Positive Airway Pressure (PAP) therapy, as many of the study participants could not afford a basic level of treatment.

This study describes the development of a device that could reduce the prevalence of undiagnosed sleep apnoea cases and improve access to treatment. The developed system makes use of standard breathing effort and pulse oximetry sensors as well as a flow sensor to provide the necessary information to conduct a home sleep test for the diagnosis of sleep apnoea, as required by the American Academy of Sleep Medicine (AASM). The diagnostic algorithm proposed by the AASM is also used to identify apnoea events and present this information to a clinician.

The system also provides a basic level of Continuous Positive Airway Pressure (CPAP) treatment, the most common treatment modality used for patients with sleep apnoea. The system performance specifications are tested according to the EN ISO 80601-2-70 testing protocol for the mean static pressure, dynamic pressure accuracy, and maximum flow rate. The ISO standard does not dictate minimum performance requirements; however, the device meets most of the requirements dictated by the Association for Respiratory Technology and Physiology (ARTP), except the requirements for the dynamic pressure accuracy where the device exceeded the maximum pressure range by $1.69\,\mathrm{cmH_2O}$.

The study has demonstrated that a single device could be used to address the high prevalence of undiagnosed and untreated sleep apnoea and thereby prevent associated health risks. Using a single device for the diagnosis and treatment of the condition may also allow clinicians to monitor the efficacy of treatment and ensure that the correct pressure level of the CPAP treatment is being used. However, further development and testing would be required before the device can meet all of the minimum performance requirements. These developments include improving the pressure control and adding the ability for the device to connect to the internet.

Contents

List of Figures

List of Tables

List of Acronyms

AASM	American Academy of Sleep Medicine
AAST	American Association of Sleep Technologists
ADC	Analog to Digital Converter
AHI	Apnoea Hypopnoea Index
APAP	Autotitrating Positive Airway Pressure
ARTP	Association for Respiratory Technology and Physiology
BiPAP	Bi-level Positive Airway Pressure
BMI	Body Mass Index
CFD	Computational Flow Dynamics
CNC	Computer Numerical Control
CPAP	Continuous Positive Airway Pressure
CSA	Central Sleep Apnoea
CSV	Comma-separated Values
DAC	Digital to Analogue Converter
EDF	European Data Format
EEG	Electroencephalography
EMG	Electromyography
EOG	Electrooculography
FDM	Fused Deposition Modelling
HST	Home Sleep Test
I^2C	Inter-Integrated Circuit
IEC	International Electrotechnical Commission
ISO	International Organisation for Standardisation
JST	Japan Solderless Terminal
LDO	Low Dropout
MRA	Mandibular Repositioning Appliance
OSA	Obstructive Sleep Apnoea
PAP	Positive Airway Pressure
PAT	Peripheral Arterial Tonometry

PCB Printed Circuit Board

PID Proportional Integral Derivative

PLA Polyactic Acid

PSG Polysomnography

PWM Pulse Width Modulation

SD Secure Digital

SDB Sleep Disordered Breathing

SLA Stereolithography

SPI Serial Peripheral Interface

SpO_2 Saturation of Peripheral Oxygen

TRD Tongue Retaining Device

UART Universal Asynchronous Receiver-Transmitter

USB Universal Serial Bus

VAT Ventilator Assessment Tool

WSC Wisconsin Sleep Cohort

1 Introduction

In this chapter, the clinical problem of sleep apnoea and its diagnosis is introduced. There is discussion regarding the inadequacy of current methods of diagnosis and treatment of the condition, which leads to the formation of the research question, aim, and objectives of this study. Additionally, the scope, limitations, and development plan are identified.

1.1 Background

Sleep apnoea is the repeated cessation of breathing during sleep, leading to a reduction in blood oxygen saturation (Young et al., 1993). Symptoms include impaired concentration, excessive sleepiness, and sleep fragmentation (Epstein et al., 2009). Untreated sleep apnoea can cause severe health problems, including cardiovascular disease and respiratory failure (Epstein et al., 2009).

Different pathophysiological pathways can cause sleep apnoea and can manifest in varying degrees of severity (Young et al., 1993). It can either be caused by physical obstruction of the oropharyngeal airway (obstructive sleep apnoea OSA), or through the interruption of neurological stimulation of the respiratory muscles (central sleep apnoea CSA) (Jaradat & Rahhal, 2015). OSA is more common than CSA, with CSA affecting roughly 0.9% of the population, while OSA affects roughly 22% (Benjafield et al., 2019).

The exact prevalence of OSA is challenging to determine. However, Benjafield et al. (2019) estimated the global prevalence based on 17 OSA local studies from 16 countries. They found that approximately 936 million adults aged 30 to 69 have mild to severe OSA (95% confidence interval: 903 - 970 million), with 425 million adults in the same age group having moderate to severe OSA (95% confidence interval: 399 - 450 million).

The different methods of diagnosing sleep apnoea are divided into four levels. Typically, an overnight polysomnography (PSG) test (Level 1 diagnosis method) is used, or a home sleep test (Level 3) is performed (Shayeb et al., 2014). An PSG test is typically regarded as the gold standard for sleep apnoea diagnosis, however, home sleep tests have been found to have no statistically significant difference in their ability to diagnose OSA compared to polysomnography tests as patients with an inconclusive home sleep test are asked to do a polysomnography study (Zancanella et al., 2021).

Once diagnosed with sleep apnoea, various treatment modalities are available, classified as medical, surgical, or behavioural interventions (Epstein et al., 2009). Positive airway pressure (PAP) therapy is generally the preferred treatment, applying positive air pressure through a nasal, oral, or oro-nasal interface to prevent upper airway closure (Epstein et al., 2009). Some side effects include nasal irritation or dryness due to continuous airflow from the CPAP machine, claustrophobia from wearing a mask, and skin irritation and pressure sores (Llamas & Clifton, 2022).

1.2 Project Rationale

Despite the methods available for diagnosis, many cases of sleep apnoea remain undetected. A sleep study conducted in Wisconsin, USA found that of the participants with sleep apnoea, 93% of women and 82% of men were not aware that they had the condition (Domínguez-Mayoral et al., 2021). This demonstrates that a large proportion of the population with sleep apnoea are undiagnosed and not receiving treatment. This is likely due to the requirements of an overnight test during which the patient must sleep at the hospital, the limited accessibility of existing home sleep test kits, the absence of symptoms in some patients, and misdiagnosis by healthcare providers. Additional devices focused on increased accessibility capable of conducting home sleep tests are therefore required to reduce the number of patients with undiagnosed sleep apnoea.

A further challenge is that once diagnosed, many patients still do not have access to, or stop using, PAP therapy treatment devices. A study conducted in South America found that only 55.7% of patients diagnosed with sleep apnoea were using a PAP therapy device a year later (Nogueira et al., 2020). A large proportion of the patients not receiving treatment indicated that the reason for this was the lack of health insurance coverage (Nogueira et al., 2020). Commercially available PAP therapy devices are expensive and not aimed at lower-income customers. Therefore, a more cost-effective device that performs the basic requirements of PAP therapy is required.

1.3 Research Question

Based on the project rationale, a research question is formulated. The purpose of this study is, therefore, to address the following research question:

Can a device be developed that can diagnose and treat sleep apnoea such that the prevalence of untreated and undiagnosed patients is reduced?

1.4 Aims and Objectives

Based on the research question, the aim of this study can be described as follows: To design and develop a device capable of diagnosing sleep apnoea as well as providing CPAP therapy. The aim will be achieved through the following objectives:

1. To incorporate existing sensors that measure a patient's airflow, breathing effort, and blood oxygen saturation into a device.
2. To develop and test a threshold-based algorithm that uses the patient's breathing effort, blood oxygen saturation, and airflow to identify sleep apnoea events and report this information to a clinician.
3. To incorporate the ability to provide CPAP therapy that adheres to the relevant sections of the EN ISO 80601-2-70 (2020) standard into the device.

1.5 Scope and Limitations

The focus of this study is to develop a first prototype of the device and demonstrate that it meets the performance requirements for diagnosing and treating sleep apnoea. It will not be tested on patients but will be evaluated based on laboratory testing. The device will act as a proof of principle and is therefore not expected to adhere to all relevant medical device regulatory standards. The research project is completed as part of a master's degree in biomedical engineering by coursework and dissertation, the latter being only 90 credits.

1.6 Thesis outline

Figure 1 below shows the outline of the project development. The literature review will focus on sleep apnoea, its diagnosis and treatment, and the user requirements of a device to diagnose and treat sleep apnoea. Any additional research relating to subsystems of the device is discussed in the Design and Manufacturing chapter.

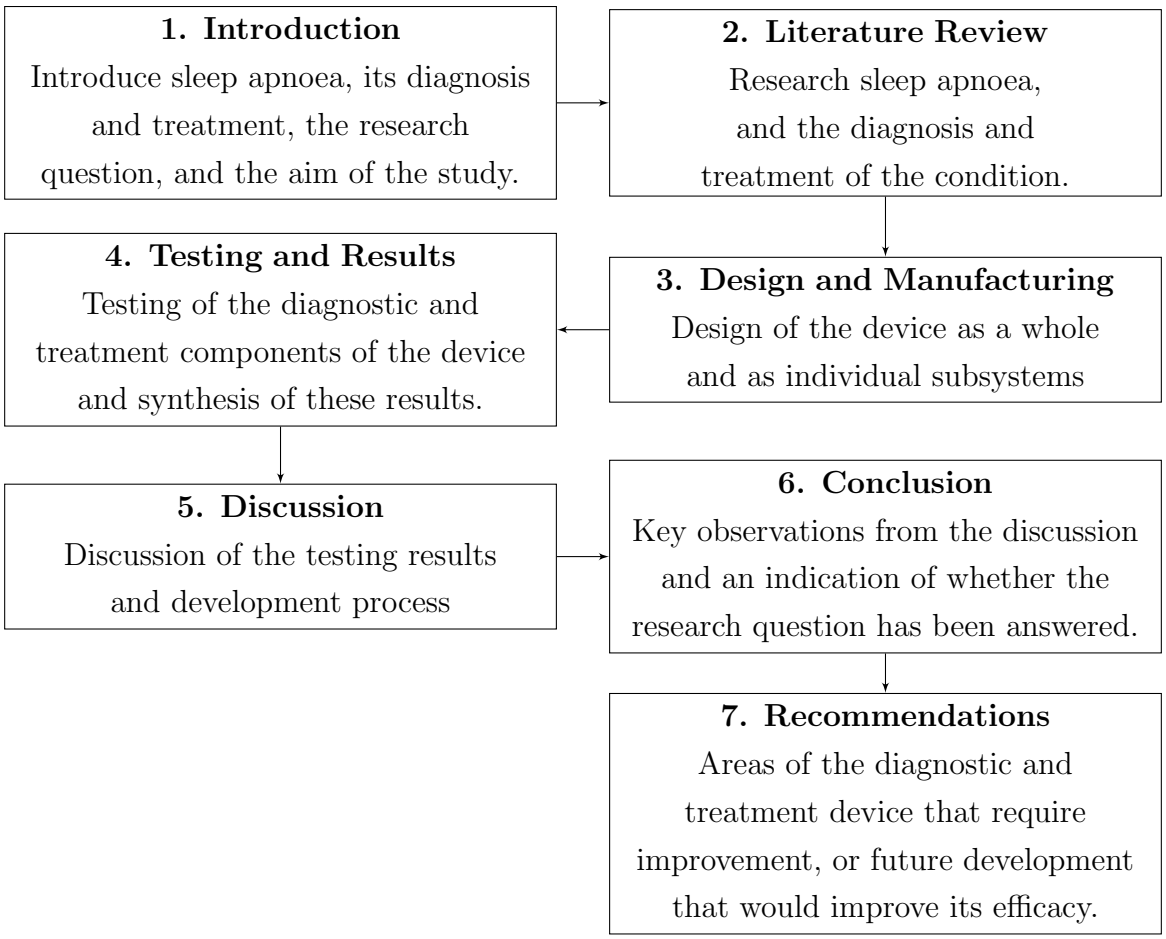

Figure 1: Plan of Development

2 Literature Review

This chapter serves to introduce sleep apnoea and explain the clinical characteristics of the condition, including its causes, symptoms, and prevalence. A detailed explanation of how sleep apnoea is diagnosed and the requirements for diagnosis are presented. The different treatment options available to clinicians are then explained, followed by a discussion of the different types of PAP therapy. Finally, the functional and performance requirements of a device to diagnose and treat sleep apnoea are summarised.

2.1 Fundamentals of Sleep Apnoea

Roughly one-third of a person's life is spent sleeping, and the quality of their sleep profoundly impacts their health (Colten & Altevogt, 2006). Some of the potential health implications of insufficient or interrupted sleep include an increased risk of hypertension, obesity, heart attack, stroke, diabetes, and depression (Colten & Altevogt, 2006). A person's sleep quality can be affected by external factors, such as a bright or noisy environment, or the consumption of alcohol and caffeine before sleeping (Man Lo et al., 2017). Sleep disorders also significantly impact sleep quality (Young et al., 2009).

There are different types of sleep disorders, but the two most common are insomnia and Sleep Disordered Breathing (SDB) (Ferrie et al., 2011). SDB can be further sub-categorised into Obstructive Sleep Apnoea (OSA), Central Sleep Apnoea (CSA), sleep-related hyperventilation disorder, and sleep-related hypoxemia disorder, with the most common of these being OSA (AASM, 2014).

OSA and CSA are both characterised by the repeated cessation of breathing during sleep, which in turn decreases the person's blood oxygen saturation (Young et al., 1993). Both of these conditions also result in reduced airflow; however, normal breathing effort is maintained in OSA, but the breathing effort is reduced in CSA (Jaradat & Rahhal, 2015). These two disorders are discussed in more detail below.

2.1.1 Causes of Sleep Apnoea

While CSA and OSA have similar effects, their aetiology is different. CSA is caused by a temporary cessation of stimulation from the pontomedullary pacemaker which is responsible for maintaining the breathing rhythm (Javaheri & Dempsey, 2013). The mechanism that causes this is poorly understood and depends on the patient's underlying conditions. However, almost all patients with CSA have a reduced reserve PCO_2. This is the difference in the partial pressure of carbon dioxide in the blood during eupnoea (normal breathing) and apnoea (cessation of breathing) and is thought to contribute to the onset of CSA (Javaheri & Dempsey, 2013). As a result of the lack of neural

stimulation, the muscles responsible for expanding the rib cage and increasing the lung volume (the external intercostals and the diaphragm) are not activated and inhalation does not occur (Javaheri & Dempsey, 2013). A variety of disorders could predispose a patient to CSA, with the most common of these being chronic opioid use and congestive cardiac failure (Javaheri & Dempsey, 2013).

In contrast to CSA, OSA is caused by a physical obstruction in the upper airway (Gottlieb & Punjabi, 2020). The obstruction may completely block the airway (apnoea event) or may partially block the airway (hypopnea event) (Gottlieb & Punjabi, 2020). Apnoea/hypopnea events are more likely to happen to patients with a reduced airway cross-section (Gottlieb & Punjabi, 2020). Some factors that reduce airway cross-sectional area are discussed below.

Elongated Uvula: In this case, the uvula (labelled in Figure 2) extends posteriorly and inferiorly, such that the space between the tip of the uvula and the posterior pharyngeal wall is reduced (Gottlieb & Punjabi, 2020). When the patient is in a supine position, the uvula falls posteriorly and can completely block the airway.

Reduced Mandibular Length: Patients with a reduced mandibular length, have a reduced maxillo-mandibular volume (Gottlieb & Punjabi, 2020). This causes the tongue (labelled in Figure 2) to be pushed posteriorly, thus reducing the airway cross-sectional area.

Tongue Fat Deposits: Fat deposits in the tongue increase its volume. This will both cause a bulge in the geniohyoid muscle (between the mandible and hyoid bones) and reduce the cross-sectional area between the tongue and the posterior pharyngeal wall (Gottlieb & Punjabi, 2020).

Fat Deposits in the Pharyngeal Wall: Fat deposits in the pharyngeal wall are typically on the lateral aspects of the wall. They cause a bulge in the wall that reduces the cross-sectional area of the airway (Gottlieb & Punjabi, 2020).

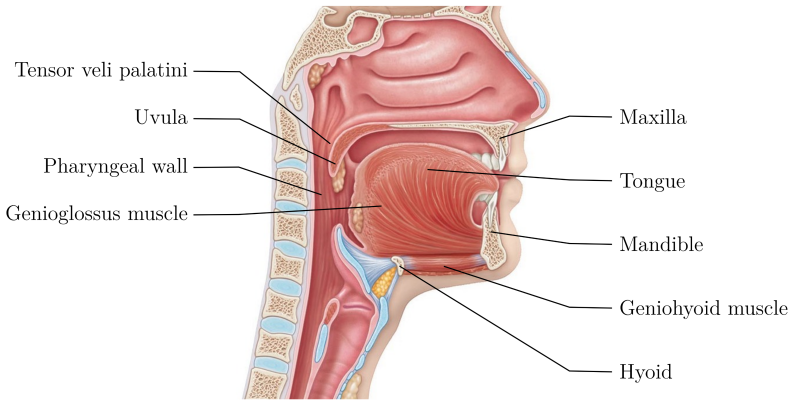

Figure 2: Cross-section of Upper Airway (Bailey Maimilian, 2010)

Muscles in the upper airway, labelled in Figure 2, help to maintain the airway. The genioglossus muscle (a fan-shaped muscle that forms most of the volume of the tongue) is activated during inhalation in order to keep the airway open. It is assisted by the hyoid and tensor veli palatini muscles to maintain airway integrity (Gottlieb & Punjabi, 2020). If the airway is already restricted by the factors described above then the muscles may not be able to maintain the airway, and an apnoea or hypopnea event will occur.

2.1.2 Symptoms of Sleep Apnoea

An apnoea or hypopnea event reduces the air entering and leaving the lungs, leading to hypoxemia (reduced blood oxygen saturation) and hypercapnia (increased blood carbon dioxide concentration). This stimulates the sympathetic nervous system, increasing the pharyngeal wall's muscle tone to maintain airway patency (Colten & Altevogt, 2006).

When an apnoea event disrupts sleep, the patient may wake up gasping for air. This disruption of sleep results in some of the primary symptoms of sleep apnoea listed below:

Daytime Hypersomnia: Excessive daytime sleepiness (hypersomnia) is usually the most prominent and noticeable symptom of sleep apnoea (Bikov & Dragonieri, 2020). It can negatively affect daytime work performance and increase the chance of vehicle accidents (Bikov & Dragonieri, 2020).

Loud Snoring: Excessive snoring is a standard indicator of sleep apnoea and a patient presenting with hypersomnia and loud snoring should be referred for a sleep test (Stradling & Crosby, 1991).

Waking up Gasping or Witnessed Apnoeas: If the patient frequently wakes up gasping, or if their partner reports observing them stop breathing during sleep, then the patient is likely to have sleep apnoea (Patil et al., 2007).

Morning Headaches: Morning headaches or not waking up feeling refreshed after a sufficient sleep period can be indicators of sleep apnoea (Colten & Altevogt, 2006).

Insomnia: Difficulty staying asleep, or sleep fragmentation is often observed in patients with sleep apnoea (Colten & Altevogt, 2006).

Mental Health Decline: A sustained and observable decline in the patient's mental health (anger, anxiety, depression, difficulty with short-term memory or concentration) is a common symptom of sleep apnoea (Patil et al., 2007).

There are other symptoms of sleep apnoea, but they are more difficult to observe and many of them require specialised equipment to detect. For example, patients with sleep apnoea typically spend more time in light sleep (sleep stages 1 and 2), than deep sleep (sleep stages 3 and 4) (Colten & Altevogt, 2006).

2.1.3 Long-term Effects of Sleep Apnoea

Without treatment, prolonged symptoms can lead to severe health conditions, some of which are discussed below.

Hypertension

Apnoea events cause a temporary rise in blood pressure and increased sympathetic nervous system activity which become more sustained if sleep apnoea remains untreated (Colten and Altevogt, 2006; Narkiewicz and Somers, 2003). The relationship between sleep apnoea and hypertension has been found to be causal as increasing the severity of sleep apnoea results in increased blood pressure, and providing sleep apnoea treatment subsequently reduces blood pressure (Peppard et al., 2000). Although the pathophysiology of hypertension resulting from sleep apnoea is not well understood, Patel et al. (2004) found that patients with sleep apnoea display markers consistent with increased cardiovascular risk (increased blood pressure variability, increased heart rate, and reduced heart rate variability).

Stroke and Cardiovascular Disease

Epidemiological studies have indicated an association between sleep apnoea and various cardiovascular diseases, including increased risk of myocardial infarction, arrhythmias, stroke, and coronary artery disease (Colten & Altevogt, 2006). Shahar et al. (2001) conducted a cross-sectional study of 6 424 participants to investigate the relationship between self-reported cardiovascular disease and Sleep Disordered Breathing (SDB). The study found that when the participants are ranked according to the severity of OSA, the participants with the most severe OSA were 42% more likely to have self-reported cardiovascular disease than those with the least severe OSA. This result is consistent with other studies which also found an increased risk of cardiovascular disease for patients with sleep apnoea, even when the effects of hypertension are accounted for (Parra et al., 2000; Yaggi et al., 2005; Bradley et al., 2005). Furthermore, sleep apnoea treatment has been shown to reduce the risk of cardiovascular disease (Doherty et al., 2005).

Diabetes and Glucose Intolerance

Punjabi et al. (2004) found a causal relationship between OSA and reduced glucose tolerance, where reduced glucose tolerance was more common in patients with more severe OSA. The same study also found that OSA contributes to insulin resistance and when combined with reduced glucose tolerance, leads to the onset of diabetes. This relationship has been confirmed by Harsch et al. (2004), who found that treating OSA led to a rapid and sustained increase in insulin sensitivity. Although the mechanism through which OSA may induce reduced glucose tolerance (and thus diabetes) is not fully understood, diabetes is known to be a risk factor for cardiovascular disease. This may explain why OSA increases a patient's risk of cardiovascular disease (Punjabi & Beamer, 2005).

Obesity

OSA and obesity are both risk factors and potential side effects of each other. A patient who is obese is more likely to have OSA, and having OSA can lead to obesity (Colten & Altevogt, 2006). Most patients with OSA either have a reduced sensitivity to appetite suppressing hormone leptin, or because of changes in the concentration of leptin during the course of the day, have a reduced effective level of the hormone (Patel et al., 2004). The reduced effective level of the hormone leads to an increase in the appetite of the patient and further contributes to obesity (Patel et al., 2004).

This is a partial list of the long-term implications of sleep apnoea, and as more longitudinal studies are conducted, more health implications may be discovered. Additional studies are therefore required to understand the physiological pathway that links SDB to each of the health conditions listed above.

The net effect of increased risk of the health conditions associated with OSA is an increase in mortality. Ge et al. (2013) conducted a meta-analysis involving six different studies (involving 11 932 patients) to identify whether OSA is an independent predictor of mortality. The study found that patients with severe OSA have a 67% increase in the risk of all-cause mortality and a 267% increase in the risk of mortality due to cardiovascular disease. Yaggi et al. (2005) confirmed this association. They found that OSA almost doubles a patient's risk of death from any cause when other risk factors are accounted for (a hazard ratio of 1.97, 95% confidence interval: 1.12 to 3.48, p=0.01). These results are also supported by the increase in mortality rate found in the Wisconsin Sleep Cohort study (Nieto et al., 2012). The latter also found that patients with sleep apnoea also have higher mortality due to cancer, as shown in Figure 3. The Apnoea Hypopnoea Index (AHI) is the number of apnoea events per hour of sleep and is used to indicate the severity of a patient's OSA.

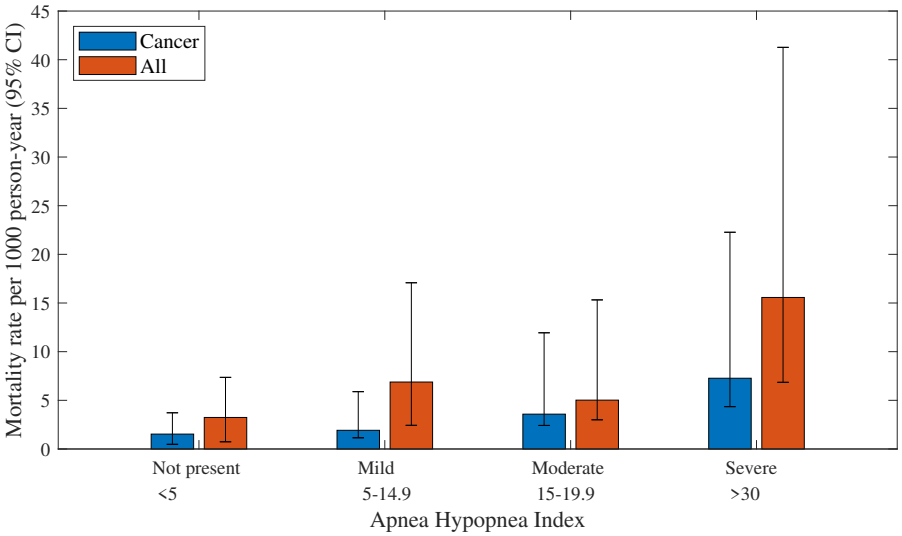

Figure 3: Mortality Rates of Patients with SDB (Nieto et al., 2012)

2.1.4 Prevalence of Obstructive Sleep Apnoea

Very few OSA prevalence studies are found in the literature before 1990 (Punjabi, 2008). Since then, multiple studies have been conducted, but it is difficult to compare the findings as the metrics used to diagnose sleep apnoea are different. However, two literature-based analyses conducted by Punjabi (2008) and Benjafield et al. (2019) have collated the existing prevalence studies to estimate the global prevalence of sleep apnoea.

Punjabi (2008) used seven studies conducted in five countries between 1993 and 2004, including 3 793 patients. However, five studies limited the age range to middle-aged patients, and many of the studies focused on either men or women (Punjabi, 2008). Based on the available information, Punjabi (2008) estimated the global prevalence of sleep apnoea to be between 3% and 7%. Still, it stated that the prevalence is likely higher than this and that further systematic surveys are required.

Benjafield et al. (2019) conducted a more comprehensive analysis using 17 studies conducted in 16 countries, between 2001 and 2016. The analysis included 15 685 participants, but the age range was limited to patients between 30 and 69 years old. Benjafield et al. (2019) then constructed a regression model using factors known to affect the prevalence of OSA (BMI, age, sex, race) to estimate the prevalence in countries where local prevalence studies were not available. The model was tested by estimating the prevalence in the countries where a study was completed. For mild to moderate sleep apnoea, the average difference between the actual and measured values was -33% and for moderate to severe sleep, the average difference was -48%, indicating an underestimation of the prevalence of OSA (Benjafield et al., 2019). Despite this, the analysis estimated that 425 million adults between the ages of 30 and 69 have moderate to severe OSA. In contrast, 925 million people in the same age category have mild to moderate OSA (Benjafield et al., 2019). The distribution of patients with moderate to severe OSA is shown in Figure 4. Countries where Benjafield et al. (2019) have not provided data are coloured grey.

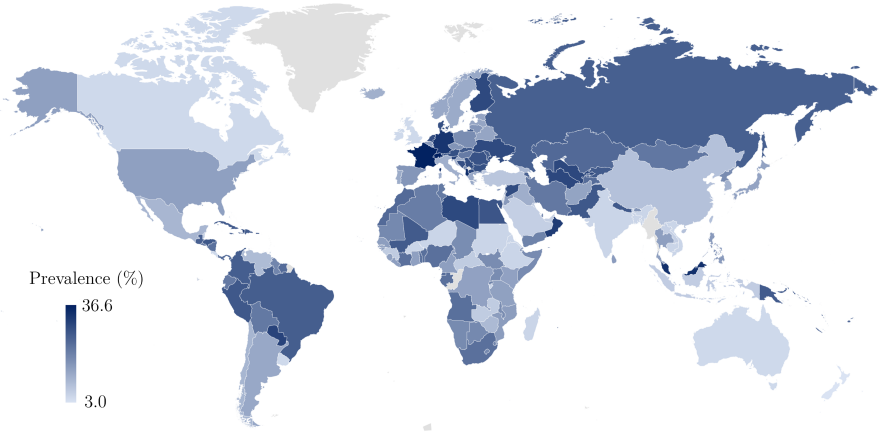

Figure 4: Prevalence of Obstructive Sleep Apnoea (Benjafield et al., 2019)

Benjafield et al. (2019) estimated that of the people in South Africa between the age of 30 and 69, 8.5 million (40.4%) have mild to severe OSA, while 4.8 million (22.8%) have moderate to severe OSA and require treatment. Roche et al. (2021) conducted a study in rural South Africa and found a prevalence of moderate to severe sleep apnoea of 29.3%. This confirms the high local prevalence of sleep apnoea, higher than predicted by Benjafield et al. (2019). In the study by Roche et al. (2021), all the participants with sleep apnoea had not been diagnosed. This trend of undiagnosed sleep apnoea is observed worldwide and the reasons for this are discussed below.

2.2 Diagnosis of Sleep Apnoea

A patient's diagnosis is their first step in the treatment pathway and therefore the lack of a diagnosis can be one of the main inhibitors to receiving adequate treatment. This subsection highlights the current challenges related to the diagnosis of sleep apnoea, gives an overview of what methods are used to diagnose sleep apnoea, and outlines the requirements of a sleep apnoea diagnostic device.

2.2.1 Current State of Diagnosis

A significant proportion of the population with sleep apnoea is not aware that they have the condition and that could benefit from treatment. Young et al. (1997) conducted a study to estimate the prevalence of undiagnosed sleep apnoea in a sample of 4 925 government employees in Wisconsin, America. The study found that 82% of men and 93% of women with moderate to severe sleep apnoea had not been diagnosed, while 90% of men and 98% of women with mild to moderate sleep apnoea had not. This is likely to be even higher in low-middle income countries like South Africa, with limited healthcare access. The reasons for the high prevalence of undiagnosed sleep apnoea are discussed below.

Access to suitable healthcare: Many patients do not have access to clinicians with the necessary skills to be diagnosed (Flemons et al., 2004). A diagnosis cannot be made is if a patient's symptoms are not recognised as OSA.

Clinical ignorance: A clinician must manage the diagnosis and treatment of a patient's sleep apnoea. Ball et al. (1997) found that many primary care physicians do not recognise the symptoms of OSA and therefore do not consider sleep tests. However, once they were further educated about the condition, the number of sleep tests ordered increased by 7.8-fold (Ball et al., 1997).

Access to diagnostic equipment: In many countries, the diagnostic capacity needs to be improved to serve their population. Flemons et al. (2004) found that in the five first-world countries considered in the study, only 10% of the required diagnostic capacity was available (assuming all patients who required a sleep test were referred to a sleep clinic).

2.2.2 Diagnosis Methods

Sleep apnoea is traditionally diagnosed using an overnight polysomnography (PSG) test, an expensive and cumbersome process. This means that very few patients have access to sleep test equipment, and even those with access have long waiting times. As a result of this and stringent requirements of a conventional overnight PSG test, alternative methods of diagnosing sleep apnoea are being developed and implemented. Subsequently, there are various diagnostic methods, some with more stringent requirements than others. To categorise types of sleep tests, they have been divided into four different levels:

Level 1: In this level, Polysomnography (PSG) is used to diagnose OSA in a sleep laboratory (Patil et al., 2007). PSG uses at least 7 channels (usually more than 16) to monitor the patient's limb movement, body position, airflow, sleep stages, heart rate and rhythm, and oxygen saturation (Rundo & Downey, 2019). This requires multiple sensors to be connected to the patient and for them to sleep in the clinic overnight with a sleep technician present for the test duration (Shayeb et al., 2014).

Level 2: The same process is used as in Level 1, but a technician is not present throughout and can be conducted in a sleep clinic or the patient's home (Shayeb et al., 2014).

Level 3: In this level of test, between 4 and 7 data channels are recorded, with the following necessary channels: airflow, respiratory effort, heart rate, and blood oxygen saturation (A. N. Natsky et al., 2021). This level also does not require observation by a sleep technician and is therefore often conducted in the patient's home (Shayeb et al., 2014).

Level 4: A level 4 test requires between 1 and 3 data channels to be recorded, with one of these being blood oxygen saturation (A. N. Natsky et al., 2021).

Level 1 studies are considered the gold standard for sleep apnoea diagnosis and can be used to diagnose many sleep conditions (Shayeb et al., 2014). Level 3 and 4 studies are significantly less costly than level 1 and 2 studies (A. Natsky et al., 2021). Shayeb et al. (2014) conducted a systematic review of 28 studies to investigate the difference in the accuracy of level 1 and 3 sleep studies and the results are shown in Figure 5.

Figure 5 shows that despite using significantly fewer data channels, and without having a sleep technician present for the test, level 3 sleep tests have a comparable sensitivity and specificity to level 1. The level 3 studies do, however, have a low specificity for patients with fewer than 5 apnoea events per hour. Based on these results, Shayeb et al. (2014) concluded that level 3 sleep tests are suitable for cases where there is a high likelihood that the patient has moderate to severe OSA. Level 1 studies, should however, be used for patients with underlying conditions, and for patients with suspected mild OSA (Shayeb

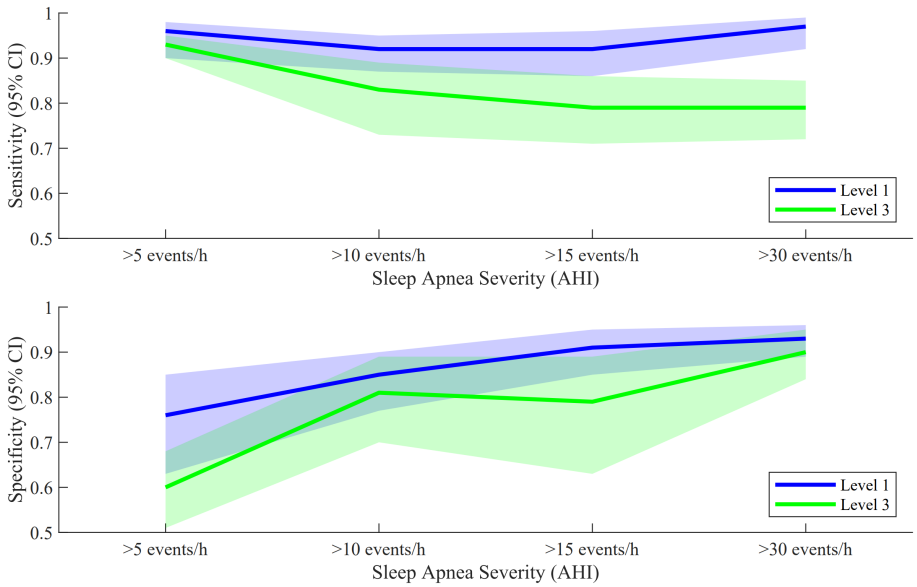

Figure 5: Sensitivity and Specificity of Level 1 and 3 Sleep Studies (Shayeb et al., 2014)

et al., 2014). Because level 3 tests do not require a dedicated sleep laboratory, these tests are more suitable for areas without access to one.

As biomedical sensor technology improves and as more advanced algorithms are developed, alternative methods of sleep apnoea diagnosis are created that no longer fit into the categories discussed above. Some of the new technologies are discussed below.

Peripheral Arterial Tone (PAT)

Airway obstruction during sleep elicits a response from the sympathetic nervous system. One of the effects of this response is peripheral vasoconstriction (Yalamanchali et al., 2013). A PAT sensor measures the change in peripheral arterial volume to help detect apnoea events. This is used in conjunction with blood oxygen saturation and heart rate sensors to diagnose sleep apnoea (Yalamanchali et al., 2013). This method does not measure airflow or breathing effort and therefore is not a level 3 diagnostic tool. This does, however, mean that it is significantly more comfortable for the patient. The diagnostic rules published by the AASM have been updated to allow for diagnosis using PAT.

Machine Learning and Load Cells

Mosquera-Lopez et al. (2019) have developed a method of diagnosing sleep apnoea using load cells placed at strategic locations under a patient's mattress. The data from the sensors is processed by a two-stage machine learning classifier that detects the occurrence of an apnoea event. This method of diagnosis was tested on 14 different patients and the system was found to have a sensitivity of 88.9% and a specificity of 76.5% (Mosquera-Lopez et al., 2019).

Ultrasound for Airflow Detection

The Doppler effect can be observed in ultrasound waves when a patient inhales and exhales (Arlotto et al., 2014). This can therefore be used for airflow detection, and thus sleep apnoea diagnosis. The signal is, however, noisy and requires advanced signal processing to identify the airflow. The signal is also disrupted during patient movement, meaning apnoeas cannot be detected accurately (Arlotto et al., 2014). Furthermore, multiple sensors are required to increase the accuracy of the system, making the diagnostic method cumbersome (Arlotto et al., 2014).

The methods mentioned above are used to detect the occurrence of an apnoea event. To measure the severity of a patient's sleep apnoea, the frequency of apnoea or hypopnea events is recorded. This is known as the Apnoea Hypopnoea Index (AHI) and is the number of apnoea or hypopnea events that occur per hour of sleep.

2.2.3 Requirements for Sleep Apnoea Diagnosis

Sleep apnoea is considered a non-life-threatening condition and therefore the International Organization for Standardization ISO does not specify performance requirements for diagnosing and treating sleep apnoea. Instead, the ISO standards specify the testing protocol for the devices and that the performance specifications of the device must be displayed in the user manual. The American Academy of Sleep Medicine (AASM) has, however, published a list of performance requirements for devices that treat and diagnose sleep apnoea. These requirements specify the performance and functional requirements of diagnostic and treatment devices as well as the algorithm to be used to identify apnoea events. The algorithm is shown in Figure 6. To satisfy the requirements of the algorithm, the device must be able to measure blood oxygen saturation, breathing effort, and airflow (Berry et al., 2020).

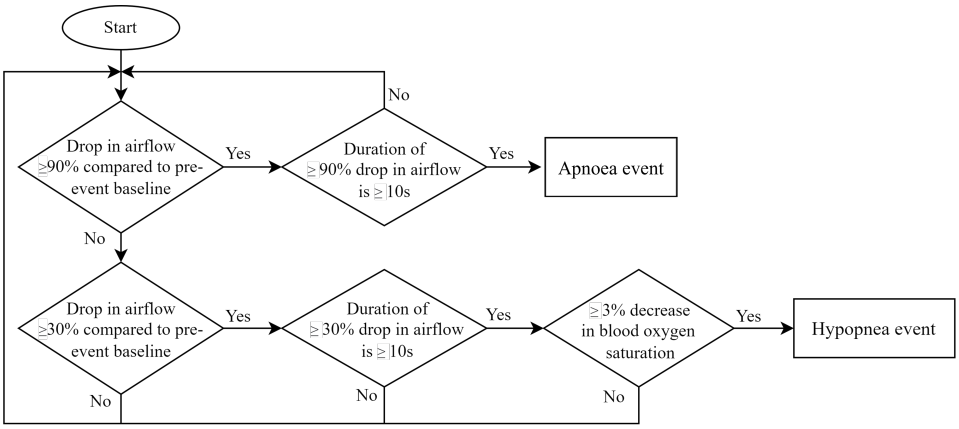

Figure 6: Diagnostic Algorithm (Berry et al., 2020)

The AASM requires that the apnoea events be classified as either obstructive, central, or mixed based on the data obtained from the respiratory effort sensor, as, shown in

Figure 7. Based on the sleep test results, the clinician classifies the sleep apnoea as either OSA, CSA, or mixed, determines its severity, and prescribes treatment if necessary.

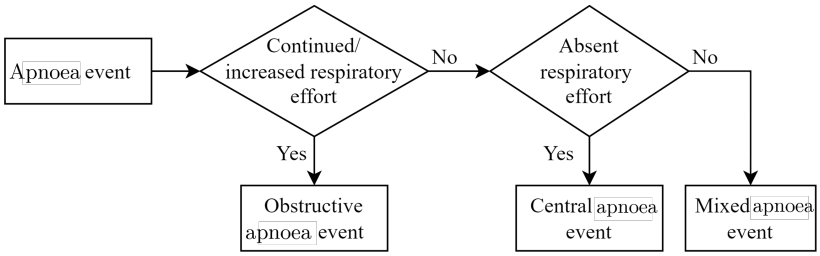

Figure 7: Apnoea Event Classification (Berry et al., 2020)

2.3 Treatment of Sleep Apnoea

Sleep apnoea treatment is vital in mitigating the effects of long-term exposure to its symptoms. There are numerous treatment modalities available to clinicians and each has its own clinical indications. The treatment modalities as well as their efficacy and indications are discussed below.

2.3.1 Surgical Treatment

Description

Surgical treatment for sleep apnoea targets four different areas of the upper airway. These include the nasal region, the soft palate, the tongue, and the mandible, as shown in Figure 8 (Won et al., 2008).

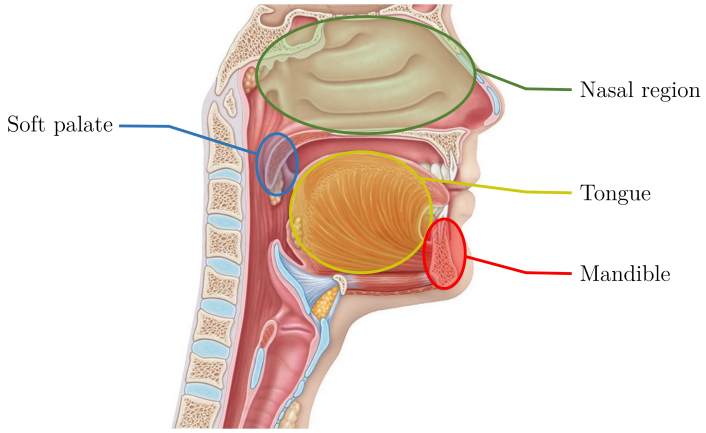

Figure 8: Sites of Possible Surgical Intervention (Bailey Maimilian, 2010)

Surgery in the nasal region is usually ineffective at reducing the severity of sleep apnoea, but is frequently used to improve PAP therapy adherence, as it unblocks the nasal passage and reduces mouth breathing (Maurer, 2009). Surgical procedures focused on the soft palate generally move the soft palate anteriorly and inferiorly towards the hard palate, resulting in increased volume behind the soft palate (Won et al., 2008). Surgical procedures on the tongue usually involve either reducing the volume of the tongue, or moving it anteriorly (Won et al., 2008).

Indications

Surgery is indicated in cases where abnormal anatomy is the cause of sleep apnoea (Won et al., 2008). For example, patients with retrognathia (unusual positioning of the mandible) would benefit significantly from surgery.

Efficacy

The efficacy of surgical treatment varies depending on the suitability of the procedure for the patient, and the type of surgery conducted. For example, surgery conducted on the mandible for patients with retrognathia has a 90% success rate, whereas surgery on the soft palate has a 50% success rate (Maurer, 2009; Won et al., 2008). In some patients, different surgical procedures can be combined, with a success rate of 70% to 99% (Won et al., 2008). In many cases, surgery is not a long-term solution and alternative treatment must be sought after 5 years, or additional surgical procedures must be undertaken (Won et al., 2008).

2.3.2 Behavioural Therapy

Description

This treatment method is aimed at addressing the habits and elements of a patient's lifestyle that may be contributing to their condition. These therapies include weight loss, positional therapy (changing their sleeping position), exercise, and avoidance of sedatives or alcohol before sleeping (Epstein et al., 2009).

Indications

This treatment is often considered before other treatment methods or is considered in parallel to receiving other treatment. It is also advised for patients with mild sleep apnoea who do not tolerate PAP therapy (Sánchez et al., 2009). This is because it is minimally invasive and produces good long-term results as it reduces the effects of underlying habits that cause or exacerbate sleep apnoea.

Efficacy

The efficacy of the treatment is patient-specific as it depends on the cause of sleep apnoea (Epstein et al., 2009). For example, weight loss would be an effective form of long-term treatment for an overweight patient whose tongue fat deposits are causing their apnoea events. However, weight loss for a patient whose sleep apnoea is caused by retrognathia may reduce the severity of their condition but would not be an effective long-term solution. Behavioural therapy is not a short-term treatment option, especially for patients with moderate to severe sleep apnoea. PAP therapy is still usually advised initially for such patients. In instances where behaviour therapy is used as a treatment modality towards long-term behaviour changes, it is not able to mitigate the effects of sleep apnoea immediately (Sánchez et al., 2009).

2.3.3 Oral Devices

Description

Oral devices are used while the patient is asleep. They can have long-term effects on dental health, including bite changes, and so benefits need to be weighed against the long-term effects (Pantin et al., 1999). There are two main types of oral devices. Mandibular repositioning appliances (MRA) consist of two plastic moulds of the patient's teeth (one for the upper jaw and one for the lower jaw) which are joined by a spring so that when the patient uses the device, the spring pulls the mandible anteriorly (Merchant, 2022). The device must be fitted by a qualified dental healthcare provider (Merchant, 2022). The second type of oral device, tongue retaining devices (TRD), operates by holding the tongue in an anterior position (Merchant, 2022). To do this, the device fits over the patient's front teeth and holds a small plastic bubble between their incisors (front middle teeth), as seen in Figure 9. When the patient places their tongue into the bubble, the air is pushed out and a negative pressure is created at the front of the tongue, holding it in the device (Merchant, 2022).

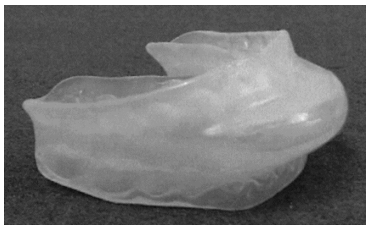

Figure 9: Tongue Retaining Device (Higurashi et al., 2002)

Indications

A TRDs is suitable for patients with macroglossia (enlarged tongue) or for patients whose condition worsens when in the supine position (Merchant, 2022). MRAs are suitable for patients who do not exceed their ideal body weight by more than 30% or for patients with retrognathia (Merchant, 2022). Both devices are only suitable for patients with mild sleep apnoea and are only considered if they do not tolerate PAP therapy.

Efficacy

A study conducted on 58 participants with the necessary clinical indications for an oral device found that after treatment, the average AHI score decreased by 10.4 events per hour (Skalna et al., 2019). Oral devices are therefore an effective form of treatment for patients with mild sleep apnoea and who do not tolerate PAP therapy.

2.3.4 Positive Airway Pressure (PAP) Therapy

Description

PAP therapy is regarded as the gold standard for treating sleep apnoea and the AASM suggest that PAP therapy is the treatment of choice for all patients with sleep apnoea (Epstein et al., 2009). PAP therapy is the application of positive air pressure to the patient's upper airway so that the airway is supported and does not collapse (Epstein et al., 2009). The pressure is applied via a mask that either covers the nose and mouth or just the nose. The different mask options are shown in Figure 10. The full-face mask

Full-face mask Nasal mask Nasal pillows

Figure 10: Types of PAP Therapy Masks (Vasta, 2022)

fits over both the nose and mouth and is typically used for patients who frequently sleep with their mouths open (Ebben et al., 2012). The nasal mask fits over just the nose and is more comfortable as the patient can still cough and mouth breathe if the PAP therapy becomes uncomfortable (Ebben et al., 2012). The nasal pillows fit into the nostrils and have a similar effect as the nasal mask. The nasal mask or pillows are more effective at treating sleep apnoea and a lower pressure level is required to reduce the patients AHI in comparison to full-face masks (Ebben et al., 2012).

There are different modes of PAP therapy, with each of them being used for different situations. The most common form is Continuous Positive Airway Pressure (CPAP) and is used for patients with mild, moderate, and severe sleep apnoea (Epstein et al., 2009). It is used for the vast majority of patients with sleep apnoea. However, patients with severe sleep apnoea require a greater level of pressure support which may make it uncomfortable to exhale. To mitigate this, BiPAP therapy can be used (Antonescu-Turcu & Parthasarathy, 2010). As the name implies, Bi-level Positive Airway Pressure therapy makes use of two different pressure levels; a higher pressure during the inhalation phase, and a reduced pressure during the exhalation phase, thus making it more comfortable to exhale (Antonescu-Turcu & Parthasarathy, 2010). Figure 11 below shows the typical difference in flow rate, lung volume, and airway pressure for patients being treated by CPAP and BiPAP therapy.

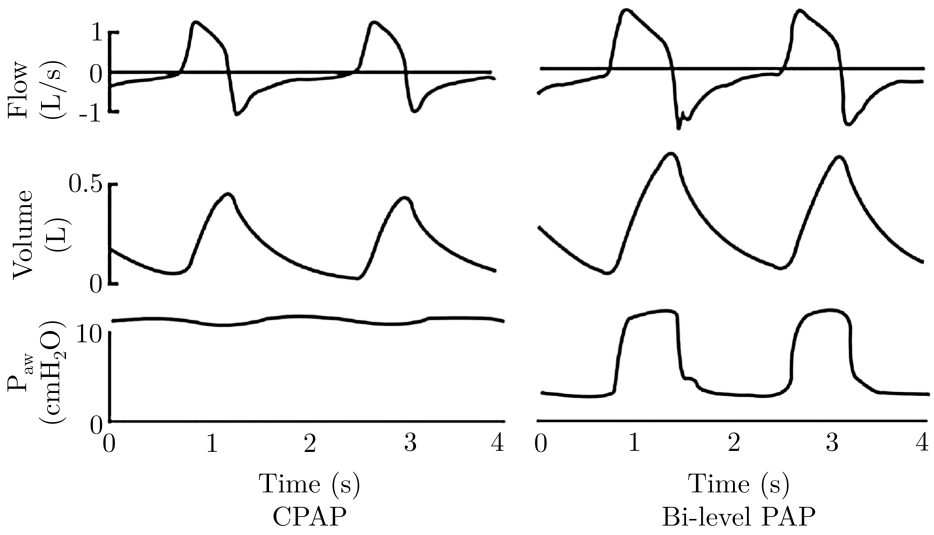

Figure 11: Bi-level and Continuous PAP Therapy (Antonescu-Turcu & Parthasarathy, 2010)

One of the major challenges with PAP therapy is adherence. A significant proportion of patients who have been prescribed PAP therapy use it for less than four hours per night (Antonescu-Turcu & Parthasarathy, 2010). One way of mitigating this is to make sure that the pressure level prescribed to the patient is as low as possible to improve patient comfort but is still high enough to prevent apnoea events (Antonescu-Turcu & Parthasarathy, 2010). This can be achieved by doing a pressure titration or using an autotitrating PAP (APAP) device. This device monitors the patient's AHI and increases the pressure level in response. This is shown in Figure 12, where the pressure increases after the occurrence of an apnoea event.

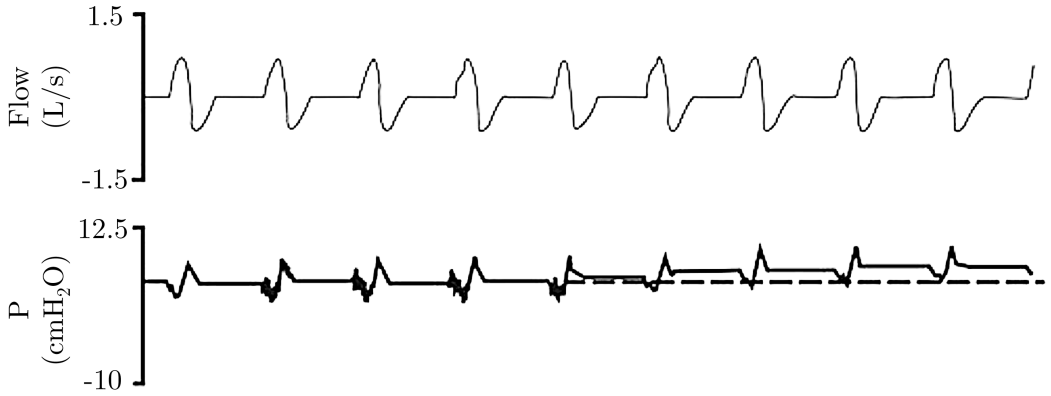

Figure 12: APAP Therapy Pressure Increase (Antonescu-Turcu & Parthasarathy, 2010)

Indications

PAP therapy is generally the preferred treatment method for patients with OSA (Epstein et al., 2009). CPAP therapy is used for patients with mild, moderate, and severe OSA and is generally advised for patients who require pressure support less than 15 cmH_2O. For patients requiring a higher level of pressure support, BiPAP therapy is generally recommended while patients who require a pressure support level of less than 15 cmH_2O but struggle to comply with CPAP may be prescribed APAP therapy (Antonescu-Turcu & Parthasarathy, 2010).

Efficacy

McDaid et al. (2009) conducted a systematic review and found that the use of CPAP therapy was an effective treatment for OSA and improved the sleep quality of patients who received treatment. Ge et al. (2013) also found that the use of CPAP therapy significantly reduced the risk of mortality due to cardiovascular disease. PAP therapy is, therefore, effective for all patients, regardless of the cause of their OSA.

2.3.5 Therapy Accessibility

Although PAP therapy is the preferred method of treatment and has been shown to mitigate the long-term effects of OSA, a patient's access to PAP therapy is not guaranteed. A study conducted in Latin America found that of the 880 patients diagnosed with sleep apnoea, only 490 (55.7%) started PAP therapy (Nogueira et al., 2020). The reason for this is reported to be limited health insurance coverage, and unclear or no indication from the treating physicians (Nogueira et al., 2020). A greater proportion of patients with severe OSA (AHI $\geq$ 30) who did not start PAP therapy indicated that the reason for this was the lack of health insurance coverage (Nogueira et al., 2020). A similar study conducted in Argentina found that of the 213 patients needing PAP therapy that participated in the study, 28.2% did not start therapy (Nogueira et al., 2018). On average, patients with access to PAP therapy had full treatment coverage from their health insurance (Nogueira et al., 2018). Access to PAP therapy is significantly reduced for those without private health insurance as the treatment is often only available to a select few who the hospital deems most deserving (Nogueira et al., 2018). In South Africa, only 17% of the population has access to private health insurance, meaning a large proportion of those requiring PAP therapy would have to pay for it themselves, or would need to wait for access through a government hospital (Stats SA, 2017).

3 Design and Manufacturing

This chapter describes the process followed to design and produce the electronic and mechanical components of the system. First, the user requirements of a device to diagnose and treat sleep apnoea are established, followed by the specifications based on the functional requirements. The device is then broken into different subsystems and the interaction between these subsystems is discussed. Because the device's core is the pressure support and the flow rate measurement, these are designed first. The electronics required for the pressure support and flow rate measurement are then designed around the pressure delivery and flow rate measurement components. Lastly, the mechanical design of the system is completed in order to house the rest of the electronic components.

3.1 Treatment and Diagnosis Requirements

Any device used to diagnose and treat sleep apnoea must meet several functional requirements, from which performance requirements can be drawn. This subsection details the functional requirements for the diagnosis and treatment components of the device and then describes the performance requirements that result from these.

In order to provide basic CPAP therapy, the device must be able to perform the functions as listed in Table 1 . These functional requirements are obtained from those dictated by the Association for Respiratory Technology and Physiology (ARTP, 2018). The requirements for a home sleep test (Level 3 diagnostic test) are dictated by the American Academy of Sleep Medicine (Berry et al., 2020) and are listed in Table 2.

Table 1
Treatment Component User Requirements

Number	Requirement
1	Provide a constant pressure to the user
2	Provide a range of pressures to treat different severity of sleep apnoea
3	Provide sufficient flow rate to accommodate for leaks
4	The device must be suitable for use by both the clinician prescribing its use and the user
5	The device must be comfortable for the user
6	Device must report the number of hours it is used per night to a clinician
7	The device must be powered by a conventional wall socket in South Africa

The functional requirements (Table 1 and 2) were used to inform the performance requirements of the device. Each functional requirement was divided into multiple performance requirements and a value was assigned to each. These values and requirements are shown in Table 3 for the treatment component of the device, and

Table 2
Diagnostic Component User Requirements

Number	Requirement
8	Measure Pulse oximetry
9	Measure Breathing effort
10	Measure the flow rate of the air entering the patient
11	Execute the apnoea event identification algorithm
12	Present the information to a clinician

Table 4 for the diagnostic component of the device. Requirements that are not suitable for a proof of principle device (such as the maximum volume of the device), or require specialised equipment to test and are not paramount to the functioning of the device have been excluded (such as the noise level during operation, which requires a dome of microphones to test according to EN ISO 80601-2-70). The requirements in Table 3 are obtained from the Association for Respiratory Technology & Physiology (2018).

Table 3
Treatment Component Requirement Specifications

No.	Characteristic	Value
1.1	Mean static pressure	$\pm 0.5\,\text{hPa}$ for $P < 10\,\text{hPa}$ $\pm 1.0\,\text{hPa}$ for $10\,\text{hPa} \leq P < 20\,\text{hPa}$
1.2	Dynamic Airway Pressure Accuracy	$< 1.0\,\text{hPa}$
2.1	Minimum pressure	$4\,\text{hPa}$
2.2	Maximum pressure	$20\,\text{hPa}$
2.3	Pressure increments	$\leq 0.5\,\text{hPa}$
3.1	Maximum flow rate	$80\,\text{L}\,\text{min}^{-1}$
3.2	Leak compensation	Automatic
4.1	Operational modes	Clinician and user modes
4.2	Features of clinician mode	All settings are adjustable
4.3	Features of user mode	Limited settings are adjustable
5.1	Pressure ramp	User able to initiate ramp at their discretion
5.2	Ramp period	User adjustable from 1 min to 45 min
5.3	Ramp starting pressure	User adjustable from $4\,\text{hPa}$ in $\leq 0.5\,\text{hPa}$ increments
6.1	Connection Detection	Device must identify when the patient's mask is on
6.2	Information reporting	Device must store historical data regarding its use for review by a clinician
7.1	Input power supply frequency	$50\,\text{Hz}$ to $60\,\text{Hz}$
7.2	Input power supply voltage	$220\,\text{V}$ to $240\,\text{V}$

Table 4
Diagnostic Component Requirement Specifications

No.	Characteristic	Value
8.1	Interface type	USB
8.2	Reading averaging time	$\leq 3\,\mathrm{s}$[1]
8.3	Minimum sampling frequency	$10\,\mathrm{Hz}$[1]
9.1	Interface type	USB
9.2	Minimum sampling frequency	$25\,\mathrm{Hz}$[1]
9.3	Low frequency filter cut-off frequency	$0.1\,\mathrm{Hz}$[1]
9.4	High frequency filter cut-off frequency	$15\,\mathrm{Hz}$[1]
9.5	Sensor Type	Single/dual thoracoabdominal RIP/PVDF/Piezo belt (calibrated or uncalibrated)[2]
10.1	Sensor Type	Oronasal thermal airflow sensor or nasal pressure transducer[2]
10.2	Sensor Accuracy	$\pm 5\%$ [1]
10.3	Maximum reading	$80\,\mathrm{L\,min^{-1}}$ [1]
10.4	Minimum reading	$10\,\mathrm{L\,min^{-1}}$ [1]
11.1	Identify a drop in flow rate	$\geq 30\,\%$ decrease in flow rate in comparison to pre-event baseline [2]
11.2	Identify duration of a drop in flow rate	$\geq 10\,\mathrm{s}$ duration of decrease in flow rate[2]
11.3	Identify a drop in blood oxygen saturation	$\geq 3\,\%$ drop in blood oxygen saturation[2]
11.4	Identify a cessation of breathing effort	Decrease of $20\,\%$ in amplitude of breathing effort[2]
11.5	Apnoea event identification	Combine breathing effort, flow rate, and blood oxygen saturation event identifications to identify obstructive or central sleep apnoea[2]
12.1	Present event identification	Present all events to a clinician as well as AHI score[2]
12.2	Present sensor readings	Present raw sensor readings[2]

[1] American Academy of Sleep Technologists (2020).
[2] American Academy of Sleep Medicine (2020).

3.2 System Architecture and Breakdown

A device comprising multiple subsystems is required to satisfy the requirements listed in Table 3 and 4. These are named and discussed briefly below.

Pressure Supply: In order to provide PAP therapy, a pressure supply that can provide the required pressure level is required. Therefore, a suitable fan or blower must be selected that can satisfy the flow and pressure requirements.

Flow and Pressure Sensing: CPAP therapy requires accurate control of the pressure and flow of air delivered to the patient. A method of sensing the flow rate, pressure, and direction of flow is therefore required. To achieve this, a flow meter will be placed between two pressure sensors. If the difference between the two pressure sensors is positive, then the flow is in the forward direction and if the pressure difference is negative, then the flow is in the reverse direction. This will also be used to measure the flow rate during diagnosis.

System Control: A microcontroller processes the signals from the pressure and flow sensors. Based on this information, it controls the speed of the fan. Furthermore, it interfaces with other subsystems including the user interface, data storage, and sensor subsystem.

User Interface: The interface is required so that the patient can start and stop the treatment, adjust the pressure ramp settings, and view usage history. The interface must therefore be able to receive information from the user and display relevant information.

Data Storage: During both the diagnosis and treatment, the device must have the capacity to store data that a clinician can later review. The device must also be able to store settings, with some of them not being adjustable by the user, for example, the pressure setting prescribed by the clinician. An SD card will be used to store the data and settings.

Sensor Subsystem: To limit the computational requirements of the microcontroller used in the device, a sensor hub that interfaces with the pulse oximeter and breathing effort sensor will be used. This will then convey data from the sensors to the microcontroller in the device.

Power Management: All of the subsystems need to be powered, with the blower fan requiring 24V, while the rest of the system requires 5V. A method of providing the required voltage from a conventional South African wall socket is necessary.

A system architecture diagram (shown in Figure 13) illustrates the required subsystems and how they will interact.

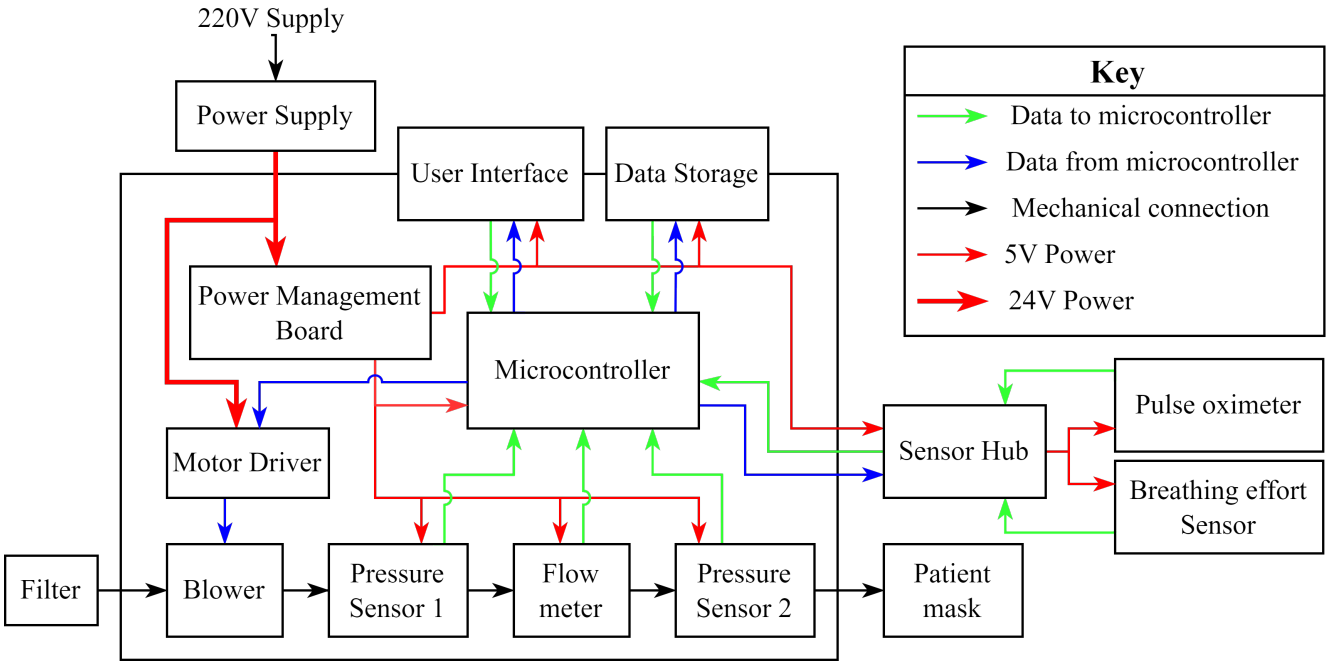

Figure 13: System Architecture Diagram

3.3 Off-the-Shelf Component Selection

Some of the components or subsystems shown in Figure 13 can be purchased as off-the-shelf products, while others require detailed design and manufacturing. The selection of the off-the-shelf components is detailed in Appendix B. The selected components are summarised in Table 5.

Table 5
Summary of Selected Off-the-Shelf Components

Component Description	Selected Component
Blower	WM7040 Brushless DC Blower Fan
Microcontroller	Arduino Mega (Atmega2560)
Filter	Resmed Airsense disposable filter
Pressure Sensors	XGZP6847 Pressure Sensor Module
User Interface	128 x 64 LCD and Push-Button Rotary Encoder
Data Storage	MicroSD Card and Card Reader Module
Pulse Oximeter	Contec CMS60C Pulse Oximeter
Breathing Effort Sensor	Plux Biosignals piezo-electric respiration sensor
Sensor Hub	Raspberry Pi 4B
Power Supply	24V, 2.5A Power Brick

3.4 Flow Path Design

The flow path includes the inlet filter, the blower, the pressure and flow sensors, and the patient mask, as seen in Figure 13. The inlet filter, pressure sensors, and blower are purchased as off-the-shelf components. A more detailed design is required for the flow sensor. The different types of sensors used to measure airflow in the pressure and flow range of CPAP devices are discussed below.

Hot-wire Sensors: These sensors function by applying a voltage to a heating element within the airflow and then monitoring the temperature of this element. The greater the temperature of the wire, the less the flow and vice versa (Wang et al., 2009).

Calorimetric Sensors: In these sensors, two temperature sensors are placed either side of a heating element. The heating element heats the fluid while temperature sensors monitor the temperature of the fluid around the heater. The higher the temperature of the fluid downstream from the heating element, the greater the flow. This type of sensor can also monitor the direction of flow (Wang et al., 2009).

Resonating Sensors: These sensors make use of a thin sheet of material with thin resistors embedded in the bridge. Applying a voltage to the resistors heats them up and forces them to expand and vibrate. The frequency of the vibration varies depending on the flow rate of air passing over the sensor (Wang et al., 2009).

Lift-force Sensors: In these sensors, a thin, angled plate, whose edges deflect when air flows over it, is placed in the flow path. The direction and angle of deflection can be measured to determine the airflow direction and flow rate (Wang et al., 2009).

Differential Pressure Sensors: These sensors rely on the Venturi effect, where increasing the flow rate of a fluid decreases the static pressure. Measuring the pressure difference in the flow at points of higher and lower velocity allows the flow rate to be calculated using Bernoulli's equation (Wang et al., 2009).

The differential pressure sensor type of flow meter is selected as it is mechanically robust, and the sensor is durable under harsh conditions. It is also simple to construct and maintain. A Venturi tube (tube with two different cross-sectional areas at different points in the tube used to accelerate the fluid) can be constructed and if the differential pressure sensor gets damaged or malfunctions, it is simple to replace.

The limitation of this type of sensor is that it is unable to indicate the direction of flow. A Venturi tube in combination with pressure sensors is therefore used, where the pressure drop over the sensor is monitored. If the pressure drop is positive, then the flow is in the forward direction and if the pressure drop is negative, then the flow is in the reverse direction. The dimensions of the Venturi tube need to be calculated and the geometry optimised. These are discussed below.

3.4.1 Venturi Tube Dimension Calculation

The Venturi effect can be described as the decrease in static pressure of a fluid when it is accelerated (Gallitto et al., 2021). This effect can be described using the Bernoulli Equation:

$$p_1 + \frac{1}{2}\rho v_1^2 + \rho g h_1 = p_2 + \frac{1}{2}\rho v_2^2 + \rho g h_2 \tag{1}$$

In the equation, p represents the fluid static pressure, ρ represents the fluid density, v represents the fluid velocity, g represents acceleration due to gravity, and h represents the height of the fluid. The two locations at which the pressure will be measured to determine the flow rate (Q) are shown in Figure 14.

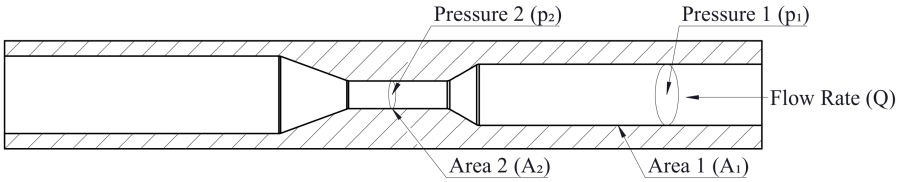

Figure 14: Equation Symbol Diagram

Equation 1 requires that the flow is laminar and the fluid flowing through the tube is incompressible. This is a reasonable approximation in this case as the pressure drop across the component is sufficiently small, and the flow rate through the component is sufficiently low. Rearranging Equation 1, and equating the flow rate to $A_2 v_2$ and $A_1 v_1$, results in the following equation:

$$Q = A_1 \sqrt{\frac{2}{\rho} \frac{(p_1 - p_2)}{\left(\frac{A_1}{A_2}\right)^2 - 1}} \tag{2}$$

Using this equation, the geometry of the Venturi tube can be calculated. The following inputs and assumptions are made in the calculation:

- The density of air is $1.225\,\mathrm{kg\,m^{-3}}$ (this is true at 15 °C and 101.325 kPa).
- The maximum flowrate is $80\,\mathrm{L\,min^{-1}}$ (as per the performance requirement).
- The diameter at A_1 is 12 mm (to match the fan outlet diameter).

These inputs, as well as Equation 2, are used to generate the function shown in Figure 15. The function describes the difference between p_1 and p_2 while varying the throat diameter (varying A_2). Choosing a diameter with a larger pressure difference would result in more accurate flow readings, however, the smaller diameter restricts the flow and increases the pressure drop across the component. A pressure sensor with a maximum range of greater than 25 hPa is therefore selected in conjunction with a throat diameter of 5.2 mm. At $80\,\mathrm{L\,min^{-1}}$, the pressure difference will be 23.29 hPa, which is within the maximum pressure range of the sensor.

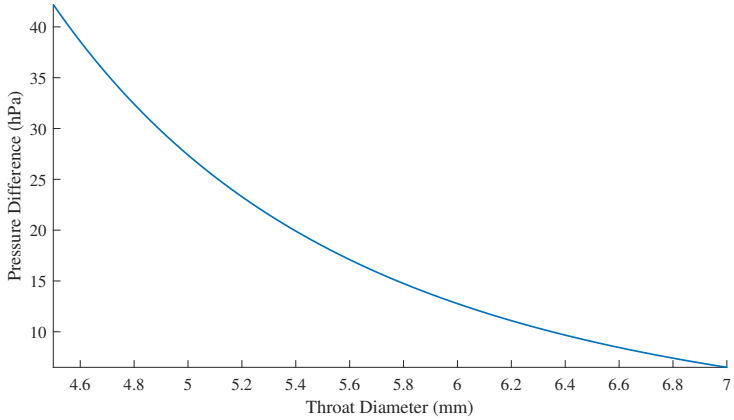

Figure 15: Pressure Difference as a Function of Throat Diameter

3.4.2 Venturi Tube Geometry Optimisation

The Venturi tube houses the pressure sensors, whose readings are used as inputs to the Proportional Integral Derivative (PID) control loop. It is crucial that the pressure readings are accurate and have minimal signal noise. To do this, a parametric Computational Flow Dynamics (CFD) study is done to investigate the effect of varying the inlet and outlet angles of the Venturi tube on the flow characteristics. The rest of the Venturi tube's geometry, including the pressure sensor position, is limited by the device's physical constraints, as depicted in Figure 16.

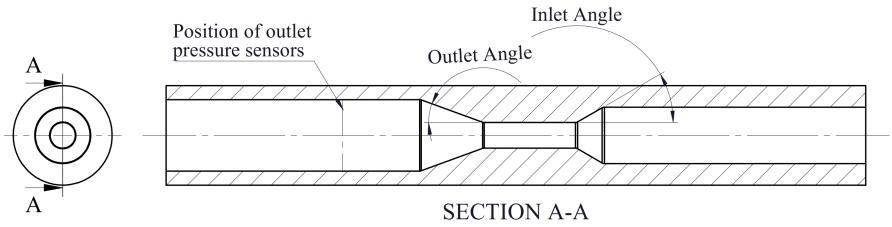

Figure 16: Venturi Tube Optimisation Parameters

Setting Up the CFD Simulation

The accuracy of the CFD simulation hinges on two factors: the refinement of the computational mesh and the stability of output values. Increasing mesh cells enhances accuracy but extends computational time. A larger mesh is used at the inlet for the Venturi tube, assuming laminar flow, while a finer one is applied at the throat and outlet to analyse flow behaviour in detail. The simulation comprises 57,026 cells (shown in Figure 17) and takes about 10 minutes. A similar CFD study conducted by Pushpak R. Shinde et al. (2020) used 70 950 cells but used a throat diameter of greater than 25 mm and a pipe diameter of 40 mm. The mesh density being considered here is, therefore, greater than in the study conducted by Pushpak R. Shinde et al. (2020). The mesh density is therefore determined to be sufficient for this study.

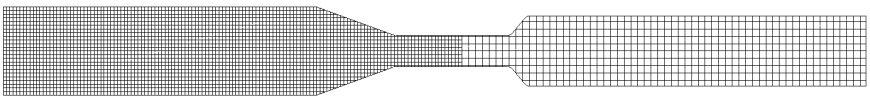

Figure 17: Computational Mesh Cut Plot

Initial static CFD studies were done that indicated that the results may not reach a steady state and a transient study would be required. This observation is based on the fact that the flow seemed to follow one side of the tube (either the top or the bottom surface). An initial transient study was therefore done, the results of which indicated that the output of the output flow does not fluctuate, but rather tends to follow either one side of the tube. The flow sticking to one surface is likely due to the Coandă effect and thus a steady state investigation is suitable.

Assumptions

In order to simplify the simulation, the following assumptions are made regarding the physical design of the Venturi tube:

1. The flow entering the Venturi tube is fully developed and is therefore laminar.
2. The inlet to the pressure ports does not have any effect on the flow.
3. The walls of the Venturi tube are perfectly smooth, with no surface roughness.
4. There is constant flow of $30\,\mathrm{L\,min^{-1}}$ flowing through the component.
5. The outlet of the component has a set pressure of 20 hPa.

Results

The parametric study is run, where the input and output angles are varied with set increments, and the results are synthesized. One example of the results is shown below. Figure 18 shows a velocity cut plot of a typical CFD simulation and Figure 19 shows the pressure variation across the length of the component for the same simulation. It is noted that in many of the simulations, and in the results shown below, the flow seems to follow one of the surfaces on the outlet, clearly displaying the Coandă effect (fluid flowing next to a solid surface tends to follow the curvature of the surface) (McCormick, 2003). In Figure 19, it is noted that the pressure after the throat is not uniformly distributed. This could affect the accuracy of the pressure sensors or could produce a significant difference between the readings of each pressure sensor.

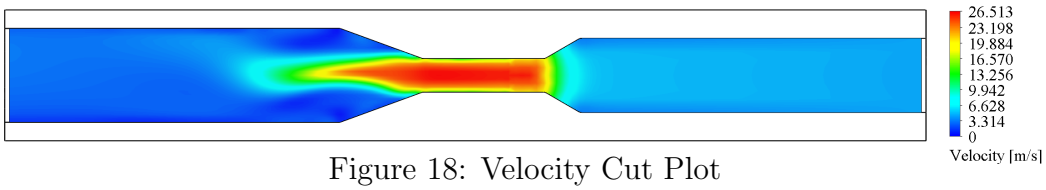

Figure 18: Velocity Cut Plot

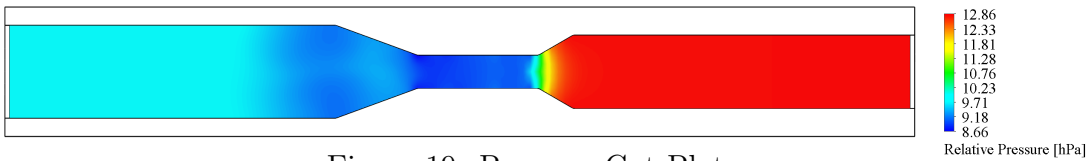

Figure 19: Pressure Cut Plot

A parametric study is conducted to understand the effect of the inlet and outlet angles on the flow characteristics. Two of these of particular interest are discussed below.

1. **The pressure drop across the Venturi tube**
   This gives an indication of how much the flow is restricted by the Venturi tube. Reducing the pressure drop reduces the pressure required from the fan, thus making the device quieter and reducing wear on the fan.
2. **The pressure range at the pressure sensors**
   To measure this in the CFD study, a virtual disk is placed on the same cross-sectional plane as the pressure sensors. The difference between the maximum pressure and the minimum pressure on this disk is recorded. This metric gives an indication of how developed the flow is through this plane. The difference between the pressure on the inner surface of the tube (where the sensors are located) and the pressure in the middle of the tube must be minimised, to ensure the pressure sensor readings are accurate.

The results of the parametric study are shown in Figures 20 and 21. In the study, both the inlet and outlet angles are varied from 7.5° to 90°. Figure 20 illustrates how the pressure drop across the Venturi tube is affected by changing the inlet and outlet angles.

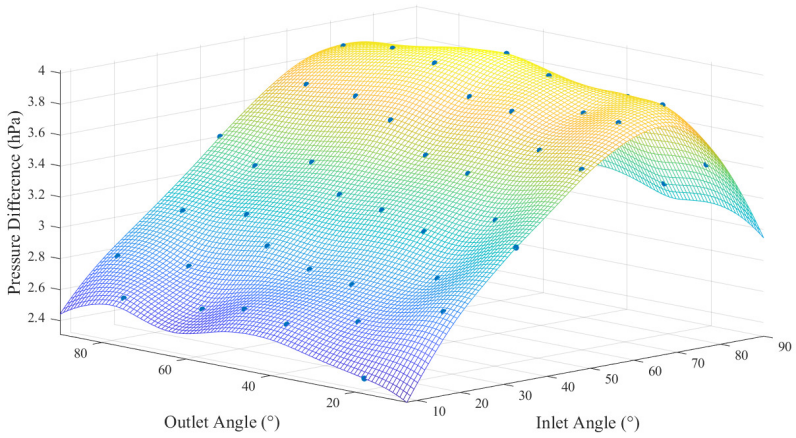

Figure 20: Pressure Drop Across the Venturi Tube

It is noted from Figure 20 that the inlet angle has a significant effect on the pressure drop, while the outlet angle has a minimal effect. It is also noted that the pressure drop increases with an increasing inlet angle until 70° and decreases after this point. The surface plot indicates that the smallest inlet angle should be selected to minimise the pressure drop across the Venturi tube. However, it does not give a clear indication regarding the outlet angle. An inlet angle of 7.5° is therefore selected. Figure 21 shows a relatively constant and small difference between the maximum and minimum pressure on the cross-sectional plane, on which the pressure sensors are located, if the outlet angle is above 30°. The Figure also illustrates that the inlet angle does not have a significant impact on this pressure range. An outlet angle of 30° is therefore selected.

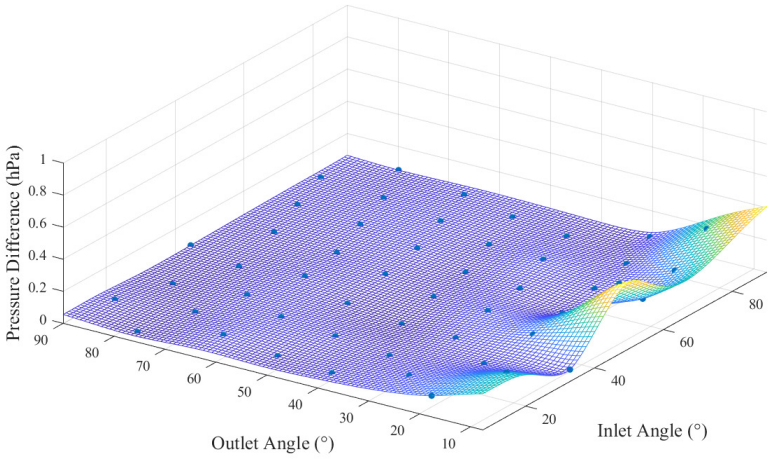

Figure 21: Pressure Range at Pressure Sensors

The tube diameters and angles are used to design a component, shown in Figure 22, that connects to the end of the blower and to the breathing circuit.

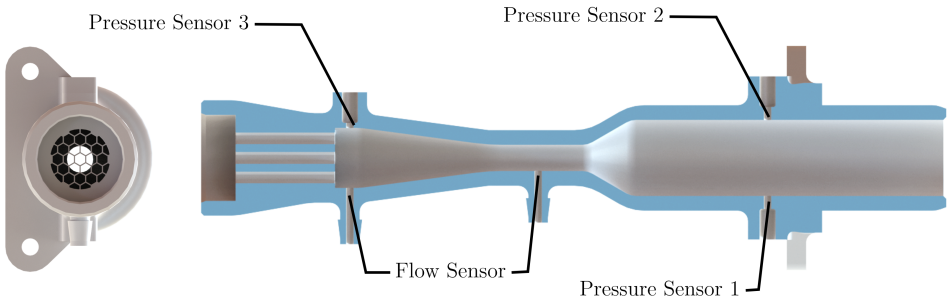

Figure 22: Cross-section of Air Inlet and Fan Mount

A laminar flow grid (tightly packed hexagonal tubes seen on the left-hand side of Figure 22) is included in the design to reduce the turbulence of the airflow coming from the blower. Pressure sensor housings are also included in the component design. The outlet of the component has a slight conical shape to adhere the ISO 5356-1 standard (for conical connectors used in anaesthetic and respiratory Equipment). The component is manufactured using a resin printer, allowing the surface to be relatively smooth and for the thin walls of the laminar flow grid to main produced.

3.4.3 Flow Path Mechanical Design

The flow path consists of the filter, the blower, and the Venturi tube. A mechanical design of the path must allow for these components to be mounted securely and connected appropriately.

The filter and blower are considered first. The filter needs to be mounted securely so that its position is not affected by airflow through it. It must also be easy to replace without having to open the device. The blower must be securely mounted with an airtight seal. Figure 23 shows a cross-section of the components used to mount the fan and filter.

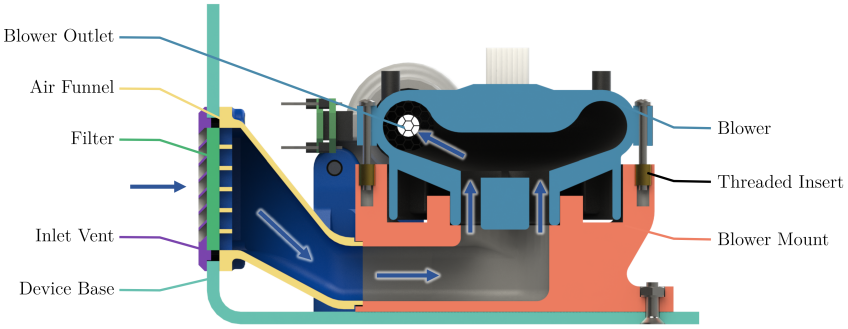

Figure 23: Cross-section of Air Inlet and Fan Mount

The inlet vent, with angled vanes to protect the filter while still allowing air to pass through, is mounted to the device base using four 2 mm bolts which screw into threaded inserts on the air funnel. The filter is pressed between the inlet vent and a grid on the air funnel (seen more clearly in Figure 24), thus preventing it from moving during use. Once through the filter, the air flows via the air funnel into the blower mount. A locating lip is used to join the air funnel and blower mount and Silicone glue is used to ensure the join is sealed.

The blower is secured using four bolts which screw into threaded inserts in the blower mount. An interference fit is also used at the blower inlet. The interference fit and silicone glue at this join ensure it is airtight. The blower mount is connected to the device base at three points using 3 mm bolts and nuts which slot into the blower mount. This ensures that when the user pushes the breathing circuit onto the Venturi tube, the force transferred to the blower and the blower mount does not cause any components to move or any seals to break.

The Venturi tube is connected to the blower outlet with an interference fit and silicone glue. The three pressure sensors mounted directly to the Venturi tube are connected to the Venturi tube using the same method. The differential pressure sensor is connected via silicone tube pushed over the barb on the sensor and the Venturi tube, as shown in Figure 24. A bracket is designed to support the front of the Venturi tube, ensuring it is stable when the user is connecting the breathing circuit.

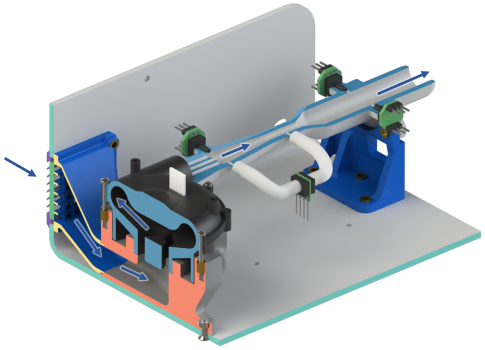

Figure 24: Flow Path Mechanical Design

3.5 Circuit Design

The device requires a circuit in order to connect the different electronic components. In this subsection, the circuit is broken down into smaller subsystems and components to illustrate how the subsystems interact. This is followed by a brief discussion of the design of the hardware filter used for the sensor signals, and the communication method with the motor driver. The detailed schematic for each PCB is given in Appendix C.

3.5.1 System Circuit Design and Subsystem Breakdown

The circuit must be designed and understood at a system level before individual subsystems can be designed. The basic components required to satisfy the system requirements are identified to design the circuit architecture. The peripheral components required to make sure these basic components can function correctly are presented. The circuit is then broken into subsystems which in turn are placed either on their own PCB or joined to the main PCB. The mechanical design is used to inform which subsystems to include in the main PCB, or which should have their own PCB. The resulting circuit architecture is shown in Figure 25.

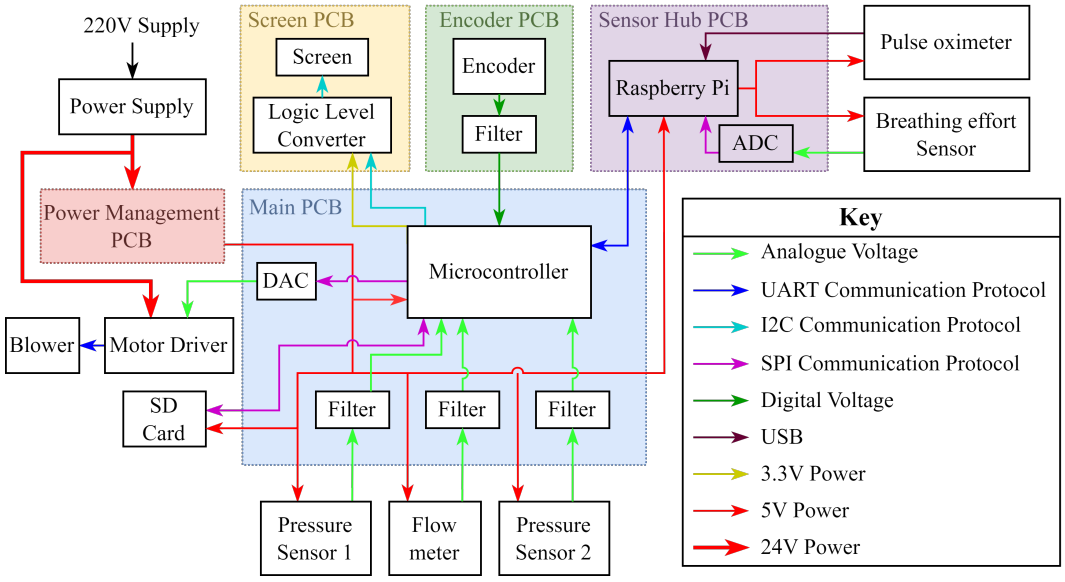

Figure 25: Circuit Architecture

The design and manufacturing of the PCBs, including the screen PCB, encoder PCB, power management PCB, sensor hub PCB, and main PCB, are shown in Appendix C. Two elements of the design of the main PCB are discussed below.

3.5.2 Signal Filtering

The pressure sensors (for pressure sensing and flow sensing) produce analogue output voltages and thus need to be processed by an analogue to digital converter (ADC). The

Arduino has a built-in ADC which will be used to process the signal. During the initial testing of the sensors, it is noted that the signal has a significant amount of high-frequency noise. To reduce this, a hardware low-pass RC filter is used. The cut-off frequency for RC filters can be calculated using the following equation:

$$f_c = \frac{1}{2\pi RC} \tag{3}$$

A cut-off frequency of 300 Hz is selected as it is sufficiently higher than the maximum signal frequency but is also lower than the noise frequency. A resistor and capacitor combination is selected that allows for the closest cutoff frequency to 300 Hz. A 4.7 kΩ resistor and 100 nF capacitor are selected and produce a cut-off frequency of 338 Hz. The RC filter is applied to the inputs from all the sensors. The resulting circuit is shown in Figure 26. A similar filter is also used for filtering the input from the encoder.

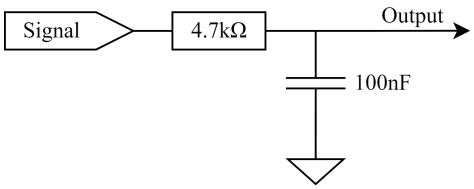

Figure 26: Low-pass Hardware Filter

3.5.3 Blower Control

Accurate control of the blower is critical to ensure that the correct pressure is delivered to the patient. The standard motor driver designed for the blower is purchased. The motor driver requires a PWM or analogue voltage to control the speed of the blower.

Pulse width modulation works by varying the proportion of time a signal is high or low, thus changing the average voltage of the signal. Figure 27 shows an example of a PWM signal with a frequency of 1 Hz. The signal changes from 25% to 50% at 3 seconds, and then from 50% to 75% at 6 seconds. This method of switching a signal on and off a signal rapidly while controlling the time the signal is high and the time the signal is low, allows a digital system to produce a seemingly analogue signal.

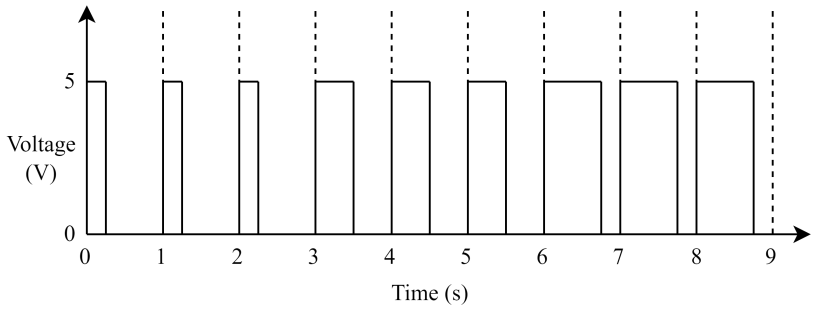

Figure 27: PWM Signal Example

The Arduino is capable of outputting a PWM signal, making it the obvious choice to control the blower speed. If the Arduino PWM function is used, then a timer interrupt is required which is set at the desired PWM frequency. The Arduino, however, has limited processing capacity so placing additional processing requirements on the microcontroller that are required to run at the PWM frequency may interrupt and slow down the processing of other signals. Limiting the processing requirements on the Arduino allows the rest of the software to run smoothly. Another issue highlighted during initial testing is that the blower does not respond consistently to the same PWM value when different PWM frequencies are used. This is likely due to the electrical characteristics of the motor driver and the method being used by the motor driver to interpret the input signal.

For these two reasons, a digital to analogue (Digital to Analogue Converter (DAC)) will be used to control the fan speed. The Arduino can communicate with the DAC over the SPI communication protocol, and the DAC will output an analogue voltage. Communication with the DAC only needs to happen when the fan speed changes reducing the processing requirements on the Arduino. No additional timers will be required as the timer for the SPI bus is already being used to communicate with the SD card. This allows for more timers to be allocated to other functions of the device.

3.6 Mechanical Design and Assembly

A method of securing the components and circuitry is required to ensure that the device operates as designed. Different mechanical components are designed, manufactured, and assembled to satisfy this requirement. A detailed discussion of the assembly and manufacturing of the subsystems and the device is given in Appendix D. A brief discussion of the manufacturing of the casing and of the Venturi tube is given below.

3.6.1 Venturi Tube Manufacturing

It is crucial that the geometry of the Venturi tube is maintained in the manufacturing process. Because the component has complex internal geometry, including the laminar flow grid, 3D printing is used to manufacture it. In future revisions, the component could be turned on a lathe and then the flow grid glued in place after this. For prototyping purposes, 3D printing is the most efficient method to produce and test the component.

First, a fused deposition modelling (FDM) type printer (Ultimaker 2+) with PLA filament is used to produce the component. The component is printed vertically to minimise the internal support required. This means that the laminar flow grid was printed on top of the support material. The resulting laminar flow grid is shown in Figure 28 on the left.

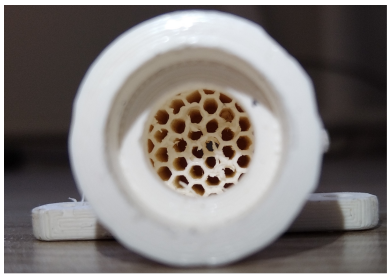

FDM Printed Venturi Tube

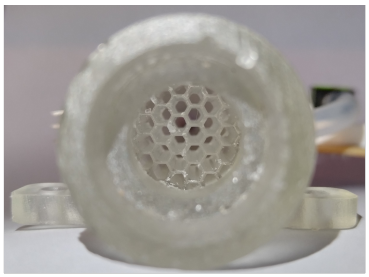

SLA Printed Venturi Tube

Figure 28: Printed Venturi Tubes

It is noted that the entry to the laminar flow grid is damaged from the support removal process. The surface finish of the FDM printed component is relatively rough as it is printed with a layer height of 200 µm. A rough surface finish and a poor laminar flow grid will negatively impact the performance of the component. An alternative method of producing the component is therefore required.

Stereolithography (SLA) is the process whereby an ultraviolet laser is used to heat up a point in a photosensitive resin bath. This causes the resin to polymerise when it is exposed to the laser. This process can be used to 3D print components with a significantly smaller layer height. The laminar flow grid manufactured using this process is shown in Figure 28 on the right. While not perfect, the entry to the laminar flow grid is much cleaner and the component has a smoother surface finish, as it has been printed with a layer height of 100 µm and washed and cured after printing to get rid of any excess resin, and then ensure all the resin is fully cured. The component is also printed at a 45° angle, so the laminar flow grid does not need any support and all the support is still external.

The shape of the laminar flow grid is chosen to be hexagonal. Typically, to get laminar flow, round tubes are stacked within a larger tube to force all the flow to go in one direction. Tubes, however, have a poor stacking efficiency (91%), whereas hexagons have a much higher stacking efficiency (100%). This means that if circular tubes are used, 9% of the cross-sectional area is blocked purely to the shape of the tube, whereas if hexagonal tubes are used, 0% of the surface area is blocked due to the shape of the tube. This means the grid will have a lower pressure drop across it.

After printing, the component is washed and cured. The pressure ports are then reamed to ensure the holes are the correct size and are not blocked. The pressure sensors are then glued to the venturi tube using silicone glue. The component is then fitted in place and the inlet is glued to the fan using silicone glue. The assembled device with the Venturi tube in it is shown in Figure 29.

The outlet of the device is designed in accordance with the ISO 5356-1 which specifies the requirements and dimensions for conical connectors used in anaesthetic and respiratory equipment. This ensures the device can interface with existing breathing

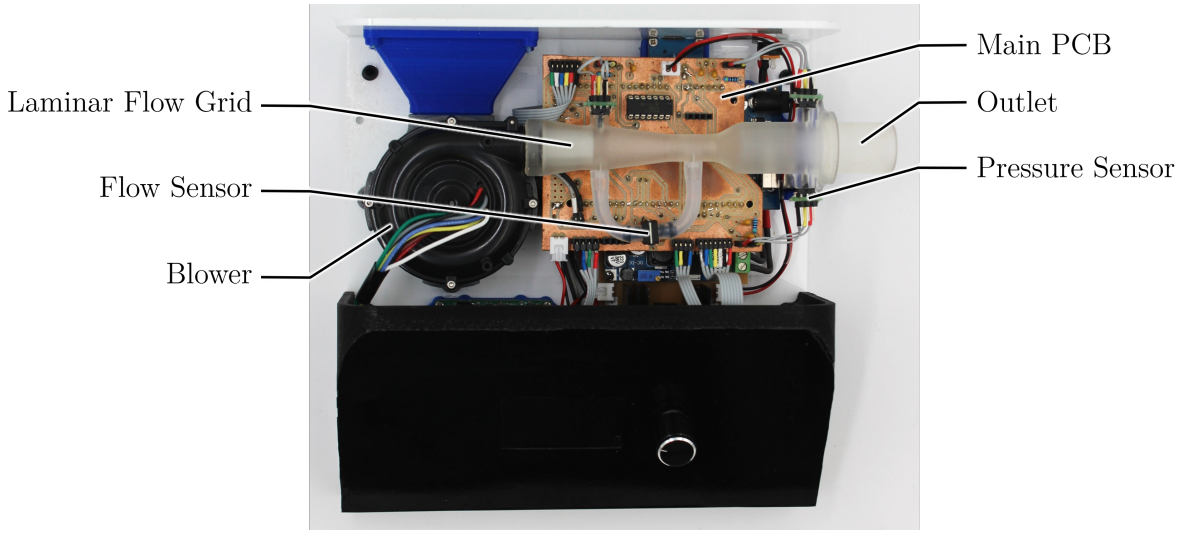

Figure 29: Assembled Device with Venturi Tube

circuits. The resin used to print the component is not biocompatible, so if future versions of the device are used on patients, the component must be printed using a biocompatible resin. Biocompatible resins are expensive and not necessary for a prototype device that is not intended to be used on patients.

3.6.2 Casing Manufacturing

The device requires a casing to enclose and protect the components. Perspex is selected as it is relatively simple to cut and bend while still being rigid and provides a good surface finish. The net for the enclosure components is designed and the net for the top and bottom casing components is laser cut from 3 mm white perspex. A template which can be used for bending the perspex is manufactured from low-density fibre board. The perspex is clamped as shown in Figure 30. The bend regions are heated using a heat gun and the sides are bent until they are flush with the template.

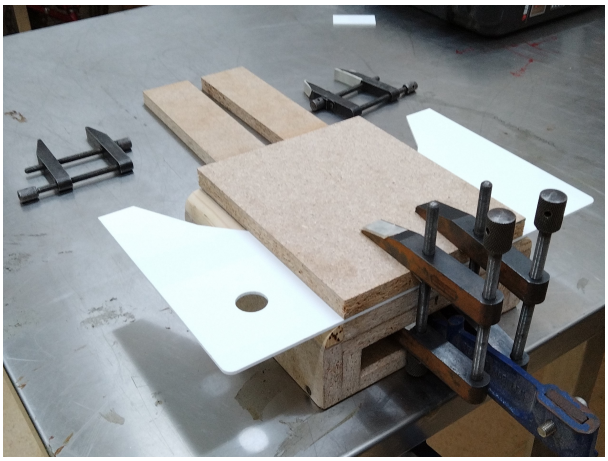

Figure 30: Top Casing Bending Process

The process of bending perspex was imprecise, especially without a uniform heat source. As a result, portions of the perspex cooled during the bending process, resulting in cracks along the bend, or sharp bends in the perspex. Multiple attempts were made at bending the perspex before it was successful. One of the key learnings from this process was to maintain a uniform temperature of the perspex through the bending process while ensuring the perspex does not become too hot and therefore malleable. if this happens, the perspex tended to bend too sharply and not follow the template. A uniform heat source should be used with temperature feedback for future iterations to ensure the perspex is maintained at the correct temperature.

3.7 Software Architecture

The device receives data from different sources, interprets these inputs, and performs some resulting action. Software is required to interpret the inputs and generate the output. This subsection discusses the broad outline of how this software works, including the initialisation sequence, treatment component, diagnostic component, and sensor hub. After the outline, a more detailed description is given for the more complex software components.

3.7.1 Software Outline

The software architecture is subdivided into treatment and diagnostic components, with the device mode determined by the SD card settings. Upon powering on the device, the initialization sequence in Figure 31 identifies whether it is configured in diagnostic or treatment mode. Reading the SD card also retrieves settings for each mode, such as the treatment mode pressure setting. Once the mode is determined, the device enters the corresponding mode of operation, which is discussed below.

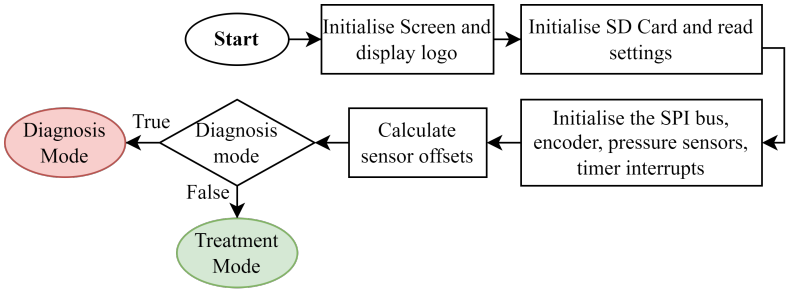

Figure 31: Software Initialisation Sequence

Treatment Mode

In treatment mode, the device calculates the ramp increment based on input settings, which is updated if the user adjusts the ramp duration or starting pressure. The software enters the main loop where the user interface is updated and the flag is lowered when the button or encoder flag is raised. If the encoder is pushed or rotated, an interrupt is generated, and the interrupt handler raises a flag. The home screen values are updated if

the user interface is currently on the home screen, or the mask-off message is displayed. Figure 32 illustrates this logic flow.

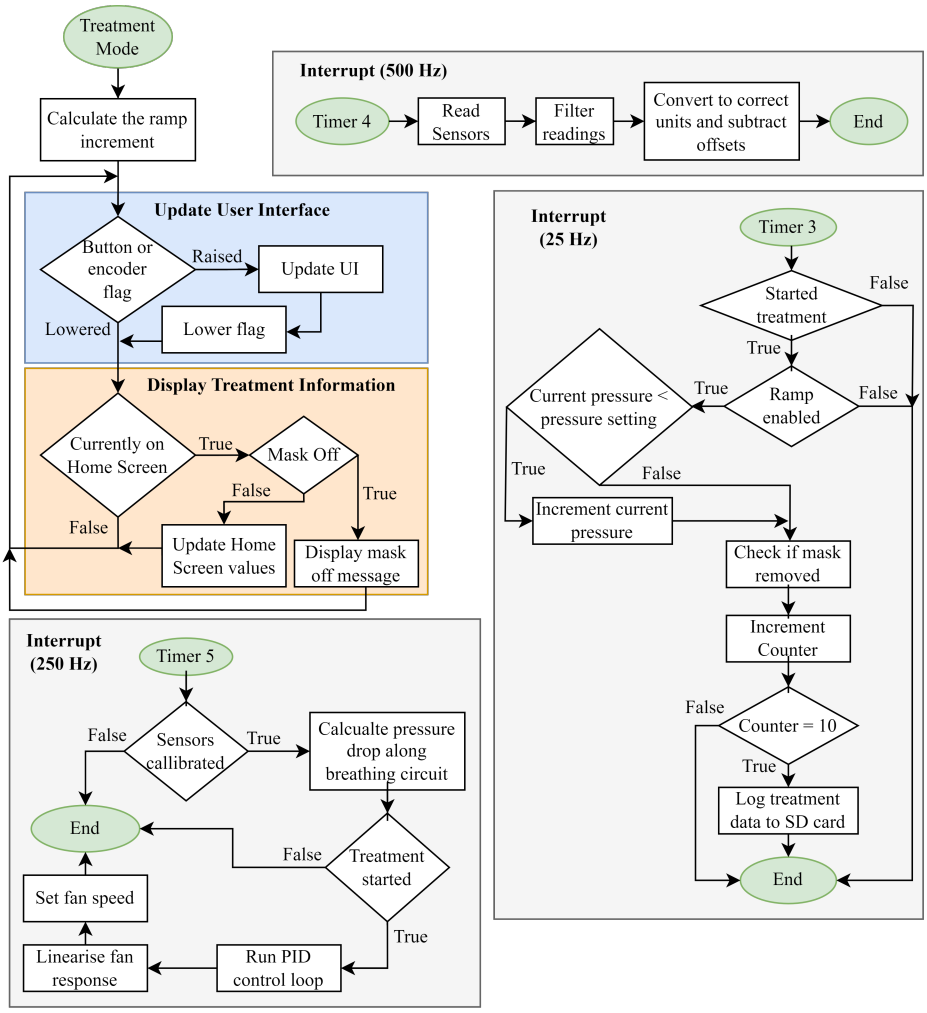

Figure 32: Outline of Treatment Component Software

Most of the computation and control is handled in the timer interrupts. Three interrupts are used, one at 500 Hz, one at 250 Hz, and one at 25 Hz as discussed below.

500 Hz: This interrupt is used to sample the pressure sensor ADC values, filter the readings using a fading memory filter, and convert the readings to cmH_2O for the pressure readings and $L\,min^{-1}$ for the flow rate readings.

250 Hz: The control loop is run in this interrupt. If the sensors have been calibrated, it calculates the pressure drop along the tube based on the current flow rate, executes the control loop if the treatment has been started, and finally linearises the control loop output before sending the new fan speed to the fan.

25 Hz: This interrupt is used for ramping the pressure setting (which is fed to the control loop) when ramp mode is enabled and logging the treatment data to the SD card at 2.5 Hz. The reduced logging frequency is achieved through the use of a counter, where the counter increments each time the interrupt runs, but the data is only logged when the counter reaches 10, after which the counter is reset to zero.

Diagnostic Mode

The diagnostic mode uses a similar structure; however, the data logging is run slightly differently. During diagnosis, the data must be logged at a frequency of 25 Hz. Therefore, the data logging function was put in the 25 Hz interrupt handler. This, however, resulted in unstable data transmission and errors in the logged data (discussed in more detail in the testing chapter). To mitigate this, the logging function is placed in the main loop and is executed when the diagnostic log flag is raised (it is raised in the interrupt handler).

The start bit is sent to request data from the sensor hub, followed by a "1", and then the stop bit. To receive data, the device waits for the start byte, reads the six bytes after that, and then checks that the last byte is the stop byte. The data is then processed before being logged. One of the bytes in the data is an error code, where an error code of "1" is when the user's finger is not inserted in the pulse oximeter, and an error code of "2" indicates the finger is inserted and then pulse oximeter is waiting to obtain a correct reading. The breathing effort sensor value is read a 12-bit number from the ADC and so the value is separated into two bytes, then recombined after communication.

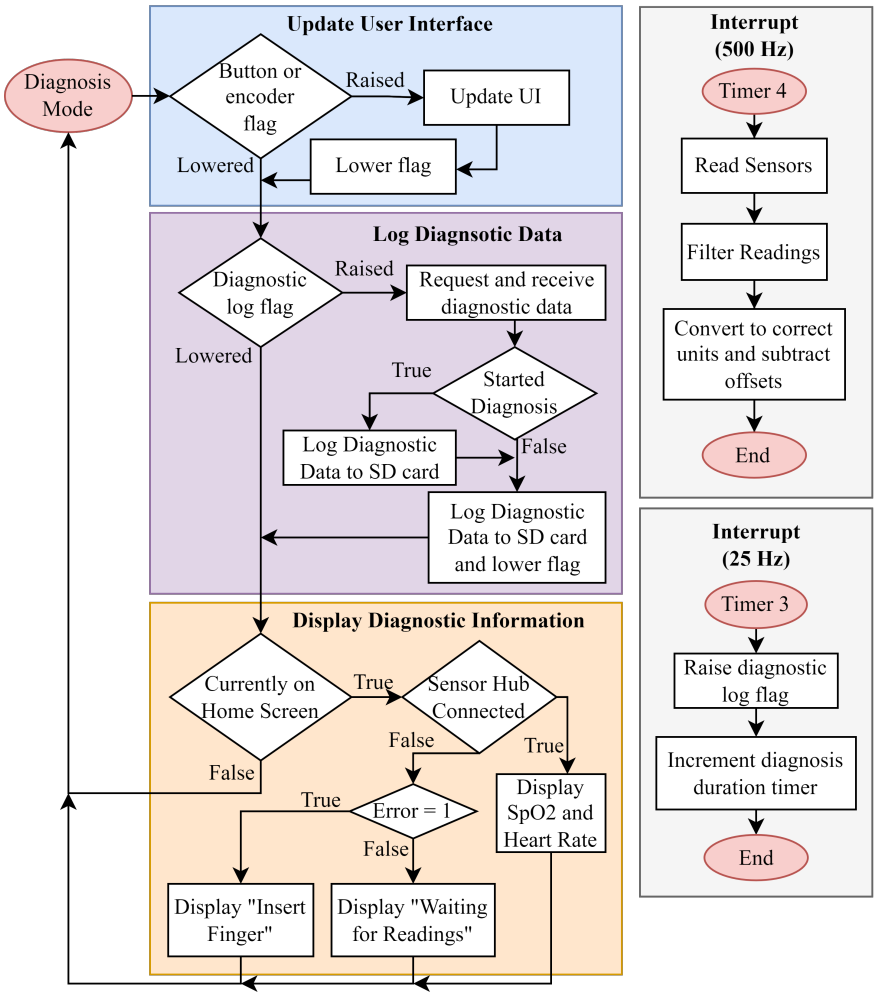

Figure 33: Outline of Diagnostic Component Software

Sensor Hub

Two different pieces of software are required for the device to operate. This includes the software developed for the sensor hub and the Arduino. The software for the sensor hub is required to receive data from the pulse oximeter and the breathing effort sensor and transmit it to the Arduino. Figure 34 shows how these functions interface with each other, and the outline of the software architecture used in the sensor hub.

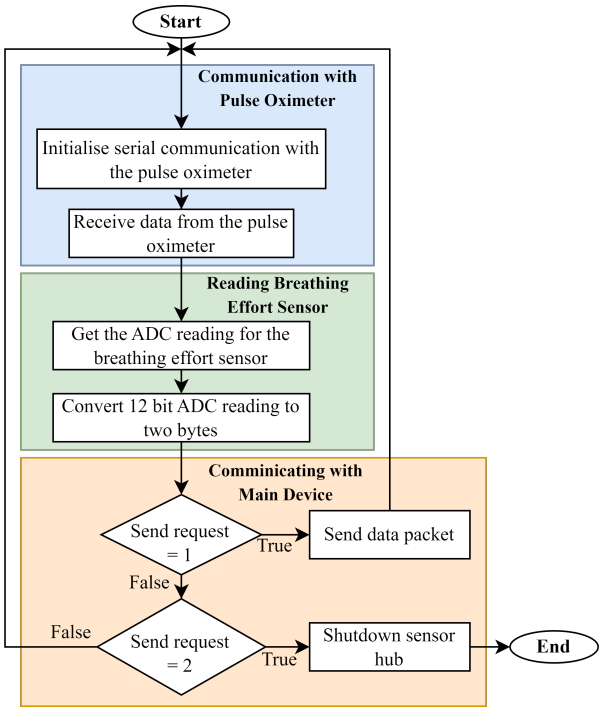

Figure 34: Outline of Sensor Hub Software

The pulse oximeter requires a handshake to be sent to it in order to keep sending data. The handshake was identified using a USB traffic monitoring tool and is sent to the pulse oximeter during initialisation. The initialisation is therefore repeated in each loop to ensure data is continuously sent from the pulse oximeter. The main device sends a request for data before the sensor hub communicates the sensor data. If the send request is "1", the sensor hub will send all of the data required by the main device, but if the request is "2", the sensor hub will shut down, allowing the hub to power off safely.

3.7.2 Detailed Software Development

Some of the components of the software architecture are more complex and require a more detailed explanation and discussion, which is given in the following section.

Output Pressure Control Using PID

A method of controlling the fan is required in order to ensure the pressure delivered to the user is accurately controlled. A PID control loop is selected as the pressure output is assumed to have a linear relationship with the voltage input to the fan. The PID control method can be described by the following equation (Trujano et al., 2012):

$$u(t) \;=\; k_p e(t) \;+\; k_i \int e(t)dt + k_d \frac{de(t)}{dt} \tag{4}$$

The control method can be explained graphically by the control diagram shown in Figure 35. In both Equation 4 and Figure 35, $e(t)$ is the error, or the difference between $f(t)$ (the desired pressure) and $p(t)$ (the pressure reading), k_p is the proportional gain, k_i is the integral gain, and k_d is the derivative gain.

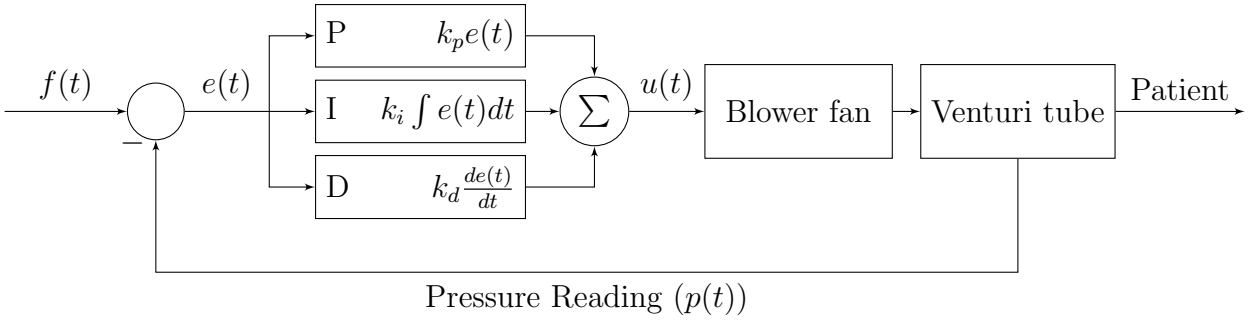

Figure 35: PID Control Loop Diagram

PID control is, however, prone to the following effects, which reduce its robustness:

1. **Derivative Kick**
   When the user or clinician changes the desired pressure ($f(t)$), it changes instantly, causing the error ($e(t)$) to change rapidly. This results in a significantly large derivative term ($\frac{de(t)}{dt}$) for one or more cycles which may saturate the fan input ($u(t)$) (Hedengren, 2020). This can be avoided by using the derivative on measurement method, where the derivative of the desired pressure ($f(t)$) is assumed to be zero (Hedengren, 2020). The following equation shows the result of this assumption.

$$\frac{de(t)}{dt} = \frac{d(f(t) - p(t))}{dt} = \frac{df(t)}{dt} - \frac{dp(t)}{dt} = -\frac{dp(t)}{dt} \tag{5}$$

2. **Integral Windup**
   The PID algorithm does not take into account the physical limitations of the system. For example, the speed input to the fan is set by a 12-bit integer and therefore has a maximum value of 4095. The PID function may, however, set the fan speed to a value greater than this and expect the output to match this input. This results in the integral term reaching a large value and the output will stay at the upper or lower limit until the integral term is reduced (Hedengren, 2020). This effect is mitigated by clamping the integral term to the minimum and maximum values of the fan speed (0 and 4095).

Fan Response Linearisation

PID control requires the system to respond linearly to changes in inputs. During gain tuning of the PID loop it is found that the optimal gains for lower pressures were not the same as the optimal gains for higher pressures and the system became unstable. The response of the fan with a linear input is therefore investigated by measuring the pressure output of the fan when connected to the standard airway resistance as defined in ISO80601-2-70. This response is shown in Figure 36.

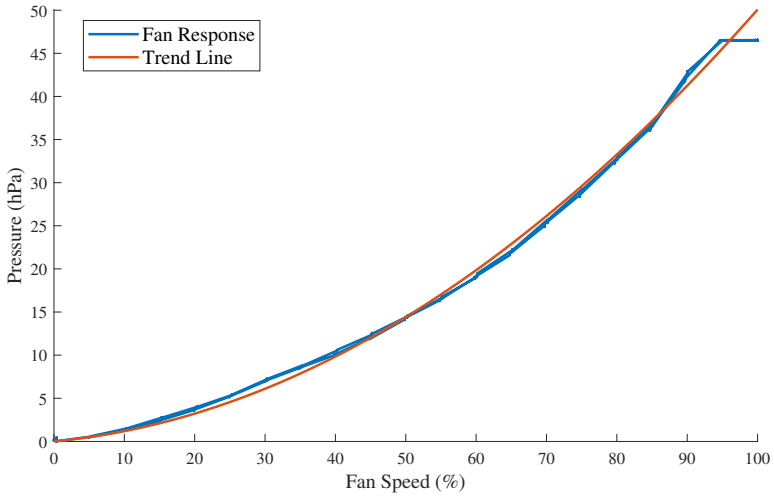

Figure 36: Pressure Output While Varying Fan Speed

From the response, it is noted that a binomial trend line could be used to approximate the response. The general form of a binomial function is:

$$y = ax^2 + bx + c \tag{6}$$

In this case, the pressure output is 0 hPa when the fan speed is set to 0 %. The response, therefore, goes through the origin. Thus, c can be set to 0. The values of a and b that yield the best fit are $a = 2.53305 \times 10^{-6}$ and $b = 1.85557 \times 10^{-3}$. With these values, the coefficient of determination (R^2) is 0.998. Completing the square and taking the inverse of the general binomial form results in the following equation:

$$y = \frac{-b}{2a} \pm \sqrt{\frac{x}{a} + \frac{b^2}{4}} \tag{7}$$

Only the positive root is used as the negative root implies that the fan can generate negative pressure. This function is used to linearise the response of the fan, where x is the desired pressure, and y is the fan speed required to obtain this pressure. A test was repeated using this function and the results are shown in Figure 37. The resulting coefficient of determination of the response when compared to a straight line is 0.998. The response has therefore been successfully linearised.

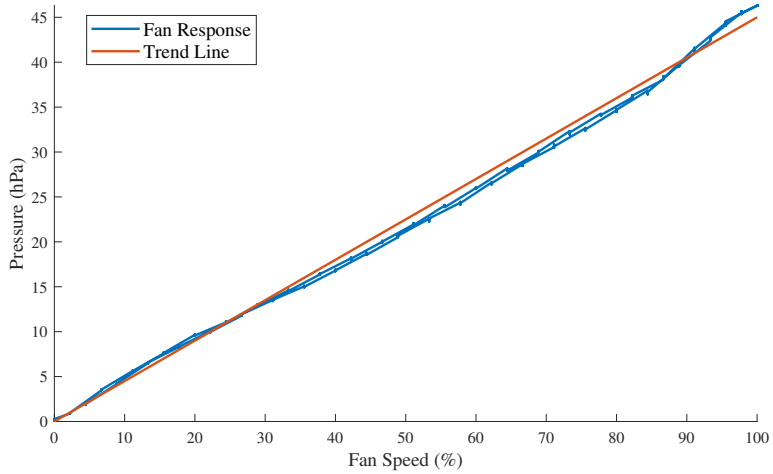

Figure 37: Linearised Fan Response

Mask Removal Detection

The device must be able to track how long the patient receives treatment per night, and what percentage of this time the user is wearing a mask. This gives the treating clinician an indication of how compliant the patient is. The flow rate is used to detect when the mask is removed. To detect when the flow rate is higher than normal (mask has been removed), the expected flow rate must be characterised. A standard airway resistance is used (as defined in ISO80601-2-70) to characterise the flow rate at different pressures. The resulting flow rate measurements are shown in Figure 38.

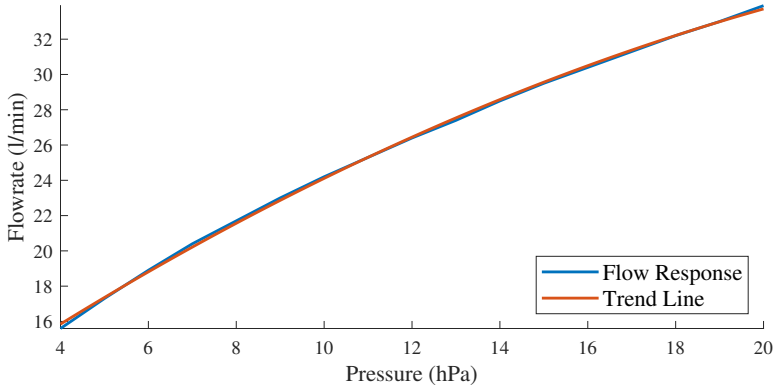

Figure 38: Flow Rate at Different Pressures

A binomial trend line can be fitted to the data with a coefficient of determination of 0.9995. The binomial is therefore used to calculate the expected flow rate at different pressures. If the current flow rate is greater than the expected flow rate multiplied by a certain factor, then the mask is considered to be removed. Increasing the factor makes the device less sensitive to mask removal but allows for some leak in the patient-mask connection. Through testing on a mannequin, the best factor is determined to be 2.3. This, however, may be different for humans, and for different types of masks.

Patient Pressure Approximation

The pressure is measured at the outlet of the device, but there is a pressure drop along the breathing circuit. This pressure drop must be accounted for to ensure the patient receives the correct pressure. This pressure drop can be calculated using the Darcy-Weisbach equation shown below (White, 2015).

$$\Delta p = L \cdot f_d \cdot \frac{\rho}{2} \cdot \frac{v^2}{D_h} \tag{8}$$

Where Δp is the pressure drop, L is the Length of the pipe, f_d is the Darcy friction factor, ρ is the density of the fluid, v is the average fluid velocity, and D_h is the hydraulic diameter of the pipe. The equation can be re-written as follows.

$$\Delta p = K \cdot v^2 \quad where \quad K = \frac{L \cdot f_d \cdot \rho}{2 \cdot D_h} \tag{9}$$

K is comprised of values that do not change as the flow rate changes, except for the Darcy friction factor. Because the pressure drop across the breathing circuit is expected to be relatively small, it is assumed the Darcy friction factor remains constant. This assumption is tested by evaluating the value of K after the device has been calibrated. To calibrate the pressure drop constant, K is varied to ensure the pressure measured at the end of the breathing circuit matches the pressure setting of the device.

After doing the calibration, it is found that $K = 3.00 \times 10^{-7}$ provides the correct pressure drop. This is sufficiently small for the Darcy friction factor to have a negligible effect on the pressure drop. To calculate the pressure drop, the following equation is used, where Q is the flow rate (measured in $\mathrm{L\,min^{-1}}$), and A is the cross-sectional area of the breathing circuit.

$$\Delta p = K \cdot v^2 = C \cdot Q^2 \quad where \quad C = \frac{K \times \frac{0.1^3}{60}}{A^2} \tag{10}$$

$$C = \frac{(3.00 \times 10^{-7}) \times \frac{0.1^3}{60}}{(0.011^2\pi)^2} = 1.5625 \times 10^{-4} \tag{11}$$

This value of C is therefore multiplied by the square of the flow rate before the control loop is executed in interrupt service routine.

Signal Amplitude Detection

The diagnostic algorithm, as defined by the AASM, require the amplitude of the pressure and breathing effort signals to be tracked in order to identify apnoea and hypopnea events. An algorithm, shown in Figure 39, is developed to identify the peaks and troughs in the signal and subsequently measure the amplitude of the signal in order to identify these events.

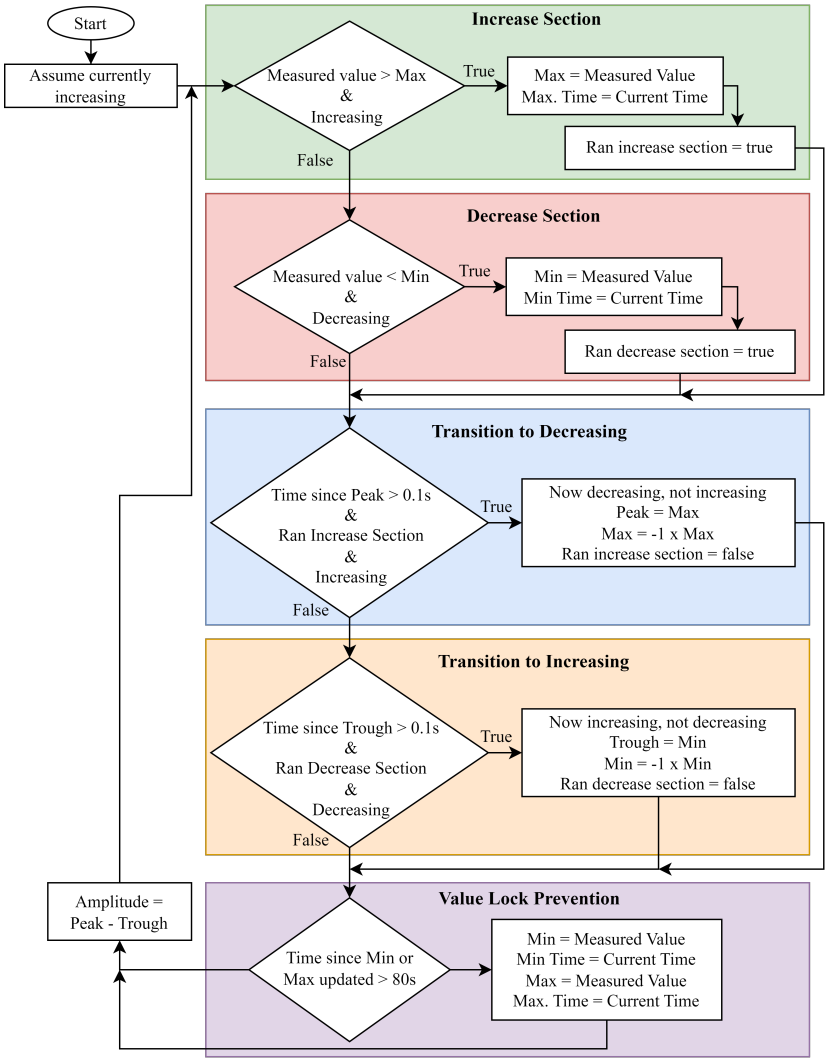

Figure 39: Flow Chart of Amplitude Detection Algorithm

The algorithm works by assuming the signal is currently increasing, and if the current reading is greater than the maximum value, then assigns the current reading as the maximum value and stores the time of the maximum value. If the maximum value has not changed in 0.1 s, then it assigns the maximum value as the peak, and starts decreasing. The algorithm is tested on patient data and it is noted that when a patient moves, a signal can change in amplitude rapidly, and the algorithm fails to pick it up, resulting in the minimum and maximum values being locked on to certain values. A lock prevention mechanism is therefore used to prevent this, where the maximum and minimum values are reset to the current reading if they have not been updated in the last 80 sec.

The result of the algorithm is shown in Figure 40. The peak and trough values are assigned 0.1 s after the peak or trough. The algorithm works well for relatively smooth data, as seen in the pressure graph, where pressure readings from a polysomnography test are used. The same algorithm is used for the readings from the breathing effort sensor, but these readings are less smooth, especially when the patient changes position. Figure 41 shows how the algorithm tracks the peaks when the readings are not cyclical.

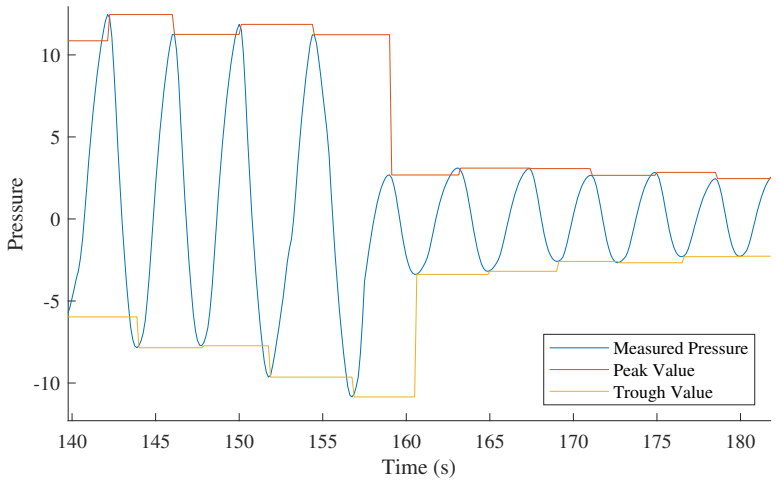

Figure 40: Amplitude Measurement from Flow Reading

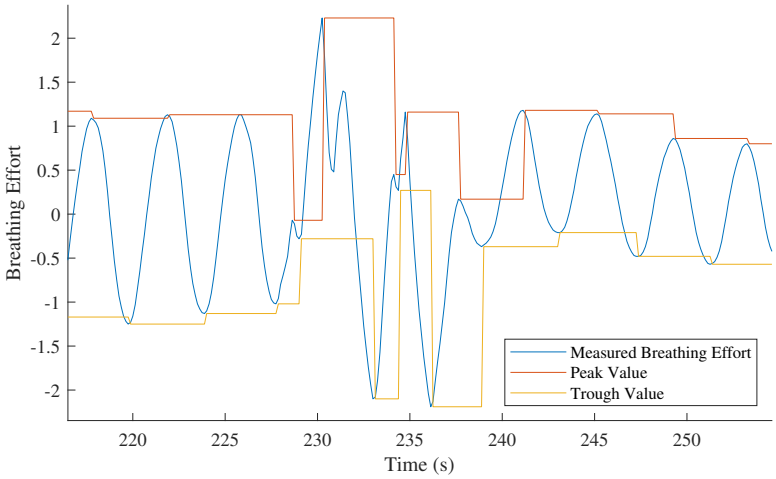

Figure 41: Peak Identification Algorithm Limitations

The algorithm tracks all of the minor and major peaks and troughs except one after the largest peak. This is because at this point the minimum value is at -0.28, and so the tracking value will be set to -1×-0.28. This is less than the minimum value of the smaller dip (0.48) and so the trough value will not be re-assigned to the new trough value. The identification of minor peaks and troughs is also not useful in detecting the overall amplitude of the signal. This can be corrected by increasing the time delay from 0.1 s to half the period of the wave, or by low-pass filtering the readings more aggressively. The identification of apnoea events, however, is also time-dependent (events must last for at least 10 s), which means errors caused by identifying minor peaks and troughs does not have an effect on the identification of the events as they last less than 10 s. This algorithm is therefore used to measure the amplitude of the breathing effort and pressure readings.

Diagnosis algorithm

During diagnosis, the data is logged to an SD card. When the user stops the diagnosis night, the device then processes the logged data and identifies apnoea or hypopnea events. It would be more efficient to process the data as it is being logged. However, this would mean that to test the device, all three diagnostic signals would need to be simulated at the same time, and apnoea events would need to be simulated in these signals. Instead, allowing the data to be processed after the diagnostic night is complete allows the diagnostic signals to be tested individually, and allows existing polysomnography databases to be used to test the diagnostic algorithm.

The diagnostic algorithm is based on the algorithm suggested by the AASM, shown in Figure 6 on page 13. The algorithm is executed in four stages.

Obtain the necessary values: In this stage, the breathing effort and flow signal amplitudes are determined. These values represent the current amplitude. To determine if the amplitude has decreased from a previous value, a more stable value is required. To get this more stable value, two different low-pass filters are used, one more aggressive and one less aggressive. The less aggressive filter is active when an event is not occurring, allowing the stable value to follow long-term trends in the amplitude, for example, if the sensor slowly slides down the user's chest and no longer measures the same amplitude. The more aggressive filter is active during an event and slows the rate of change of the stable value. As a result, the stable value will not change significantly during an event, ensuring the event is not ceased prematurely.

Identify Events Based on Flow: The flow signal is monitored to identify when there is a decrease in the amplitude of the flow signal. When there is a decrease, the filtered SpO_2, breathing effort amplitude, and flow amplitude signals are recorded as the pre-event baseline values.

Event Confirmation: When the flow signal amplitude increases again, the duration event is noted. If there is a confirmed apnoea event, then the hypopnea event is not considered. The AASM algorithm does not require a decrease in SpO_2 values for apnoea events but does require it for hypopnea events. During testing, it is noted that many hypopnea events are excluded because of this condition. The events are therefore noted as suspected hypopnea events.

Event Classification: Once the event is confirmed, it is classified based on the amplitude changes in the breathing effort signal. If there is no significant reduction in breathing effort then the event is obstructive as there is continued breathing effort. If the breathing effort signal amplitude reduced by more than 70% then the event is classified as a central event. All other events are considered mixed events.

The algorithm described above is shown in Figure 42.

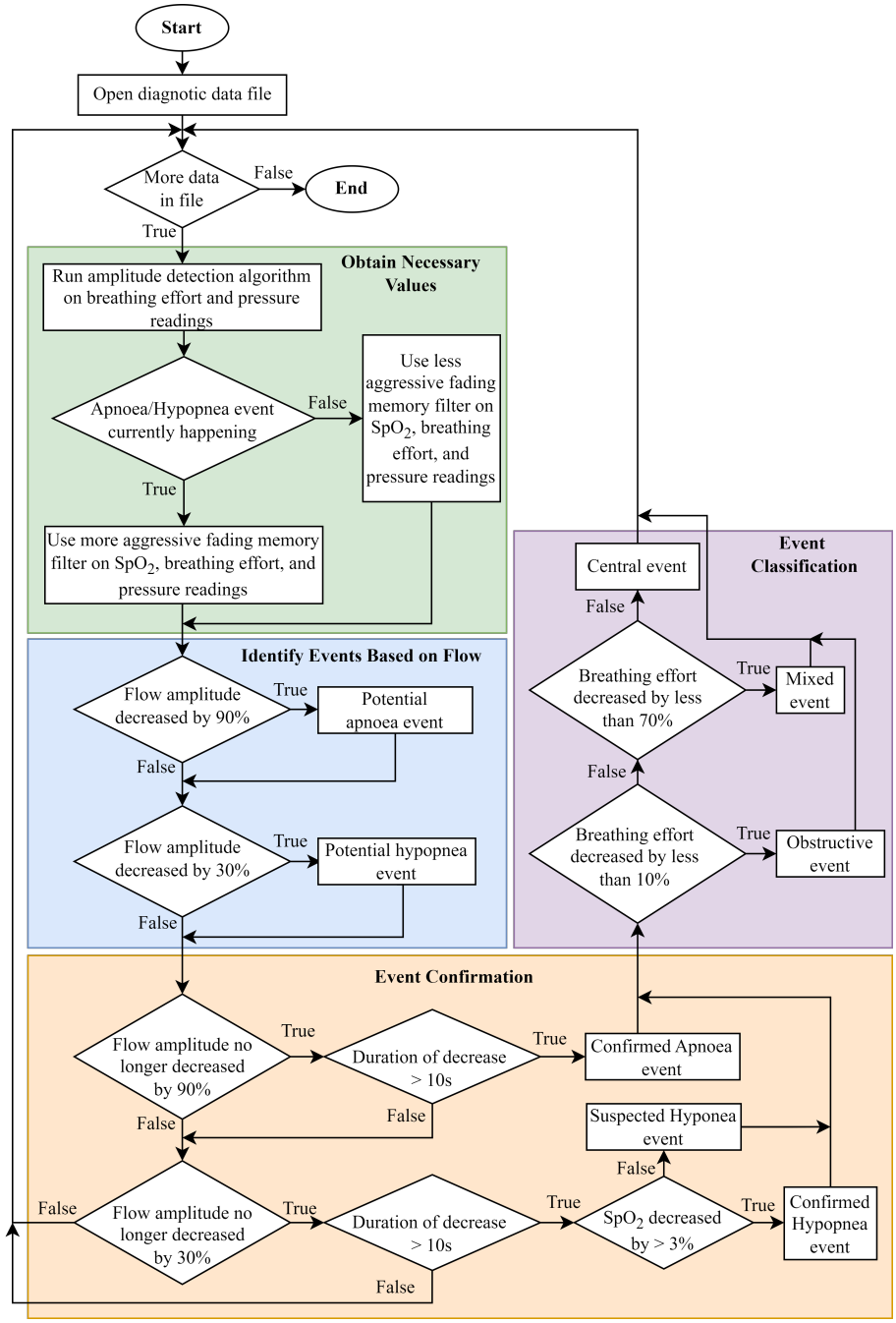

Figure 42: Event Identification and Classification Algorithm

4 Testing and Results

This chapter describes the process followed to test the device, the equipment required, and the results of the tests. The testing protocol was developed such that the performance of the device can be compared to the requirements specifications outlined in Tables 3 and 4. The testing was divided into two sections: the treatment component, and the diagnostic component of the device.

4.1 Treatment component

Where the test protocol was not dictated by the ISO80601-2-70 standard, the protocol was designed to test the device according to the requirement specification.

4.1.1 Mean Static Pressure

Test Protocol

The testing protocol for the mean static was dictated by the ISO 80601-2-70 standard as follows.

1. Set up the sleep apnoea device for normal use in CPAP mode according to Figure 43. Switch off all the comfort features of the device and place the standard resistance (Figure 44) at the patient-connection port.
2. Measure the pressure at a frequency of at least 1 Hz at the patient-connection port for eight hours. Calculate the average pressure for each one minute interval.
3. Determine the most positive and most negative pressure deviation of the calculated average pressures from the set pressure on the sleep apnoea device.

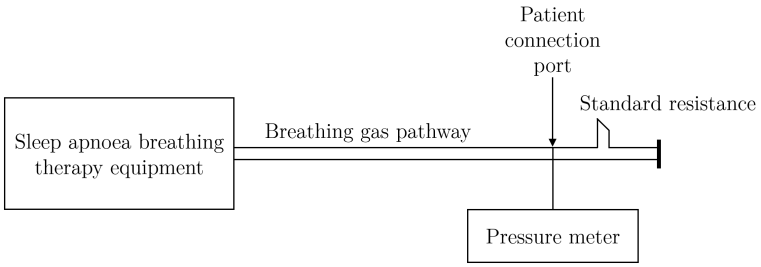

Figure 43: Diagram of Static Pressure Test Layout (International Organization for Standardization, 2020)

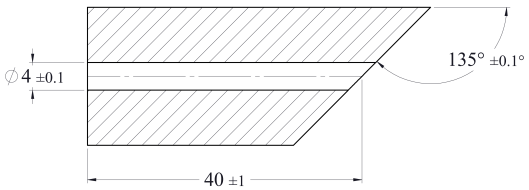

Figure 44: Dimensions of the Fixed Resistance (International Organization for Standardization, 2020)

The ISO standard also dictates that the test must be conducted after the device has been in operation for at least 20 minutes and must be repeated for three pressures: 5 cmH_2O, 10 cmH_2O, and 15 cmH_2O.

Test Setup

The standard airway resistance was 3D printed with an inner diameter of 3.5 mm. The hole was then reamed using a 4.0 mm reamer to ensure the hole is smooth and is the correct diameter. The resulting component is shown in Figure 45.

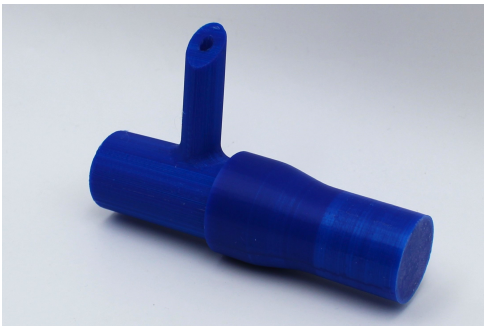

Figure 45: Standard Resistance

A ventilator assessment tool (VAT) developed at the University of Cape Town MedTech Laboratory was used as the pressure-measuring device. This tool has a pressure and flow rate sensor, and logs data to an SD card. For this test, the device was set to log at a frequency of 68 Hz to minimise the effect of noise on the test results. The VAT with the standard resistance connected to the outlet is shown in Figure 46.

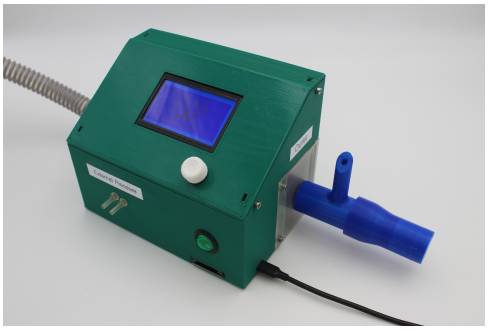

Figure 46: VAT with the Standard Resistance Connected

Test Result

The test was conducted and the results processed using a MatLab script which reads the log files produced by the VAT, averages the pressure readings for each minute, and identifies the minute with the maximum and minimum values. The deviation of these values from the target pressure is shown in Table 6 as well as the difference between the most positive and most negative pressure deviations.

Table 6
Mean Static Pressure Test Results

Pressure Setting (cmH_2O)	**Most Negative Deviation** (cmH_2O)	**Most Positive Deviation** (cmH_2O)	**Pressure Range** (cmH_2O)
5	0.033	0.032	0.065
10	0.042	-0.015	0.027
*10	0.017	0.0019	0.019
15	0.080	0.018	0.098

The results of the 10 cmH_2O test did not fit the trend, as the maximum deviation is less than the pressure setting and the pressure range is significantly smaller than the range of the other two tests. Therefore, the test at 10 cmH_2O was repeated and the results are shown in the table. The results show that the first test is most likely not an anomaly as the range for the second test is even smaller than the first.

Result Synthesis

The results appear to show a trend where at 10 cmH_2O the deviation is at a minimum and the deviation increases as the pressure moves further away from 10 cmH_2O. Further testing would need to be done to confirm if this trend is present. The negative value of the most positive deviation is indicative of a calibration error. Again, further testing is required to determine if this is the case. The mean static pressure performance requirements are shown in Table 7, as well as the results of the test. The results indicate that the device has met the performance requirements.

Table 7
Mean Static Pressure Test Requirements

No.	**Characteristic**	**Requirement**	**Result**
1.1	Mean static pressure	$\pm 0.5\,cmH_2O$ for $P < 10\,cmH_2O$ $\pm 1.0\,cmH_2O$ for $10\,cmH_2O \leq P < 20\,cmH_2O$	$\pm 0.042\,cmH_2O$ $\pm 0.080\,cmH_2O$

4.1.2 Dynamic Airway Pressure Accuracy

Test Protocol

The dynamic airway pressure accuracy will also be tested in accordance with the EN ISO 80601-2-70 standard. The protocol for this test is as follows.

1. Connect the patient-connection port to a pressure-measuring device and a pump as shown in Figure 47. Set the pump to produce a sinusoidal wave with an inspiratory to expiratory ratio of 1:1 and a tidal volume of approximately 500 mL. Ensure the dead space volume of the pump is less than the tidal volume.

2. Set the pump breathing rate to the breathing rate shown in Table 8.
3. Set the device to the minimum pressure setting (4.0 cmH_2O).
4. Measure the flow rate and pressure at the patient connection with a sampling frequency of at least 100 Hz. Filter the readings using a 5 Hz low-pass filter and record the results for at least 5 minutes.
5. Add the test apparatus uncertainties to the results.
6. For each pump cycle, identify the most positive and most negative pressure deviation from the desired pressure and calculate the average of the most positive and most negative readings over the period of 5 minutes.
7. Repeat steps 3 to 6 for each pressure indicated in Table 8.
8. Repeat steps 2 to 7 for each breathing rate indicated in Table 8.

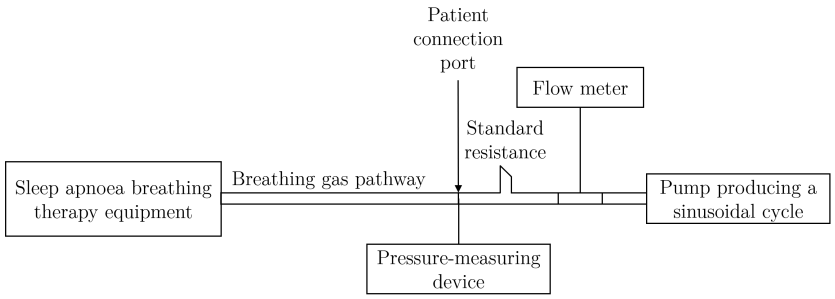

Figure 47: Diagram of Dynamic Pressure Test Layout (International Organization for Standardization, 2020)

Test Setup

The VAT was used in conjunction with a piston-cylinder type pump. The piston was connected to a stepper-motor via a connecting rod and crank. The length of the crank was adjusted to ensure that a tidal volume of approximately 500 mL was achieved. This was calculated by measuring the diameter of the cylinder and the stroke length of the piston to get the volume of each pump cycle. The speed of the stepper motor was controlled to ensure the correct breathing rate. The VAT logs the sensor readings at 210 Hz to the SD card after which the readings are processed. The test setup is shown in Figure 48.

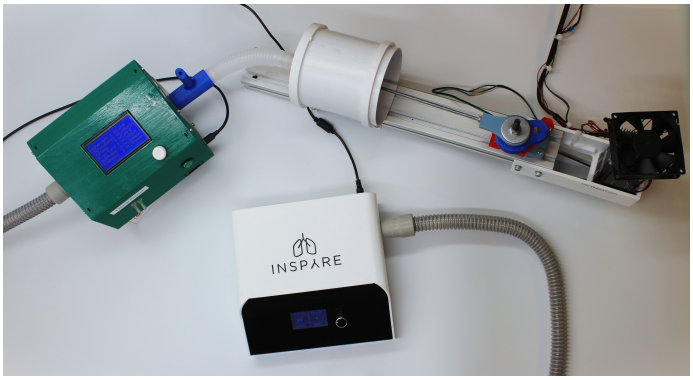

Figure 48: Dynamic Pressure Test Setup

Test Result

A MatLab script was used to analyse the data obtained from the VAT. The script filters the readings as required by the protocol, identifies the peaks and the troughs in the data, and calculates the average peak value and average trough value. The deviation from the pressure setting is shown in Table 8, where $P_{range} = P_{max} - P_{min}$.

Table 8
Dynamic Airway Pressure Test Results

Breaths per minute	Device Pressure Setting (cmH_2O)				
	P_{min}	$P_{min} + \frac{1}{4}P_{range}$	$P_{min} + \frac{1}{2}P_{range}$	$P_{min} + \frac{3}{4}P_{range}$	P_{max}
	4	8	12	16	20
10	-0.67	-0.84	-0.84	-0.95	-0.43
	+0.34	+0.46	+0.54	+0.67	+0.46
15	-1.10	-1.38	-1.62	-1.67	-2.07
	0.63	0.89	1.01	1.08	1.26
20	-2.28	-2.27	-2.43	-2.67	-2.69
	1.83	1.43	1.75	1.73	1.58

Result Synthesis

It is noted that as the breathing rate increases, the deviation from the pressure setting also increases. It is also noted that the negative pressure deviation is larger than the positive pressure deviation in 14 of the 15 tests. The reason for this can be better understood by looking at the test result shown in Figure 49. This shows a section of the results from the test with a pressure setting of 20 cmH_2O, and a breathing rate of 20 breaths per minute.

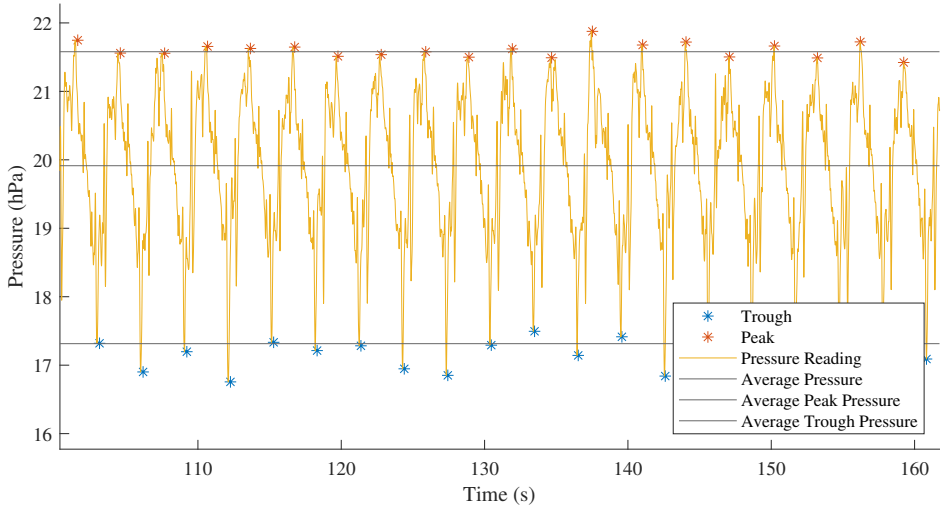

Figure 49: Section of Dynamic Pressure Test at 20 cmH_2O and 20 Breaths per Minute

The average pressure for this test is 19.91 cmH_2O, indicating that the larger negative offset than positive offset is not due to sensor calibration error. The pressure at the patient connection port decreases in the inhalation phase during which the fan increases its angular velocity. A larger negative pressure deviation indicates that the fan is not increasing its speed fast enough to compensate for the pressure drop during the inhalation phase. To reduce this effect, the gains of the PID control loop were changed to make the fan response more sensitive. This reduced the offset slightly but meant the control loop became unstable. The large pressure deviation could be mitigated using one, or a combination, of the following changes:

Altered control loop: A control loop with a better predictive ability may be able to predict periodic disturbances and account for them. This could be implemented through a feed-forward element in the control loop which makes use of flow rate measurement to determine the frequency and amplitude of breathing and adjust the fan speed based on the predicted flow changes (Bohn & Alsogkier, 2017).

Increased control loop frequency: Increasing the frequency of the system may allow it to respond more quickly but may also introduce instability (Åström & Hägglund, 1995). Further testing needs to be done with an increased control loop frequency to determine the optimal frequency. Increased control loop frequency will also require increased sensor sampling frequency.

Use of a different motor driver: The current motor driver is not able to actively slow down the blower and may be limiting the acceleration of the blower. Further testing is required to determine if active breaking may improve the pressure-tracking ability of the device, and if the motor driver is limiting the acceleration of the blower.

Use of a different blower: A blower with a different mechanical design (A blower with reduced output per rotation but reduced angular inertia) may allow for better control of the pressure output, especially if the blower is operating at a higher angular velocity.

The performance of the current system is compared to the performance requirement in Table 9. The system does not meet the requirements of a deviation of less than 1.0 cmH_2O from the pressure setting.

Table 9
Mean Dynamic Pressure Test Requirements

No.	Characteristic	Requirement	Result
1.2	Dynamic Airway Pressure Accuracy	$< 1.0\,cmH_2O$	$\leq 2.69\,cmH_2O$

4.1.3 Pressure Support Range

Test Protocol

The device is required to provide pressure support between 4 cmH_2O and 20 cmH_2O, in 0.5 cmH_2O increments. A test protocol was therefore designed to test if the device is able to provide pressure support at all pressure levels and is shown below.

1. Turn off all comfort features on the device.
2. Set up the device in the same configuration as for the static pressure test, as shown in Figure 43.
3. Set the pressure setting to increase by 0.5 cmH_2O every 30 seconds, starting from 4.0 cmH_2O and ending at 20.0 cmH_2O.
4. Record the pressure at the patient connection port at a frequency of at least 100 Hz and filter the pressure readings with a 5 Hz low-pass filter.
5. For each 30 s increment, remove the first and last 5 s.
6. Record the average pressure reading, and the standard deviation of the pressure reading for each 30 s increment.

Test Result

The resulting pressure readings as well as the pressure settings are shown in Figure 50.

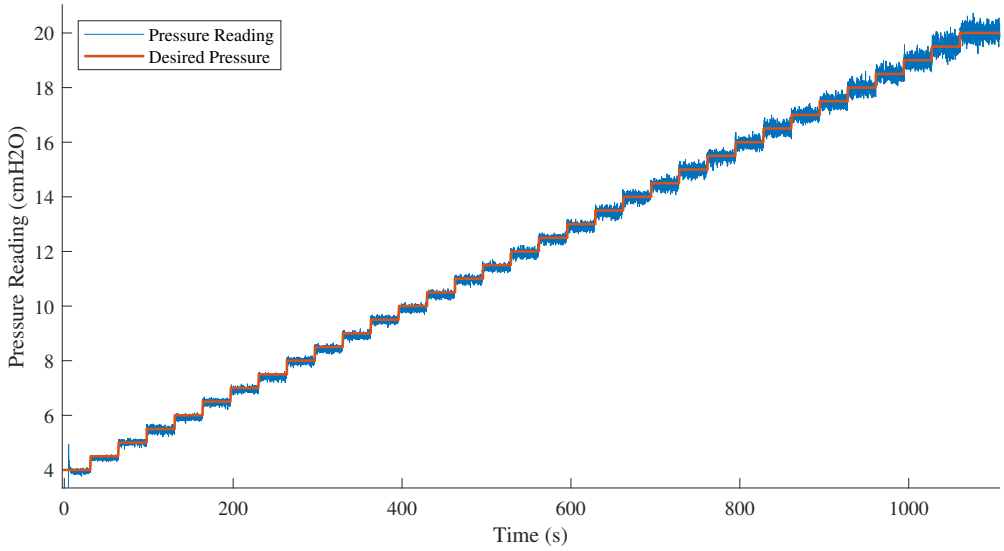

Figure 50: Pressure readings and Pressure Setting for Pressure Support Range Test

This data was processed using a MatLab script as described in the test protocol. For each pressure setting interval, the pressure readings are averaged. The pressure setting at that interval was then subtracted from the average to give the average offset. The average offset and standard deviation of the pressure readings for each interval are plotted in Figure 51.

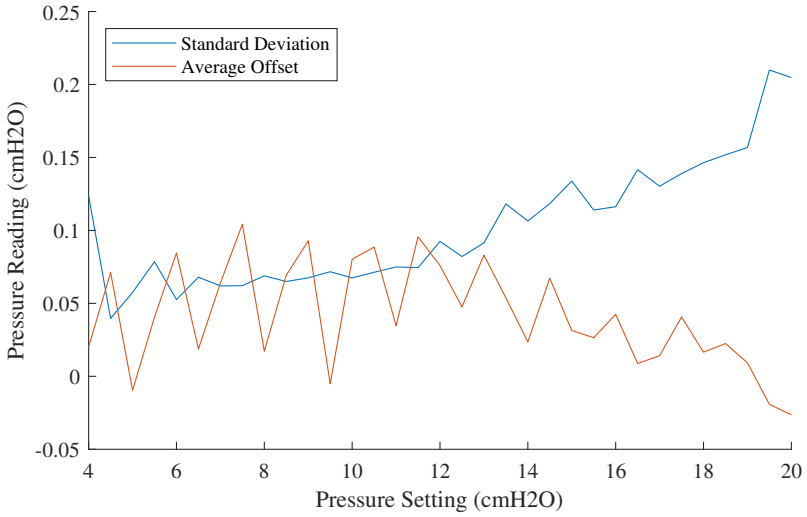

Figure 51: Standard Deviation and Average Offset of Pressure Support Range Test

Result Synthesis

The standard deviation increases as the pressure setting increases which is most likely due to an increase in turbulent flow in the VAT and in the Venturi tube. Despite this, the average offset remains relatively constant and small. The device is therefore considered to be able to provide pressure support at all the desired pressure intervals. The results of the test are compared to the requirements in Table 10.

Table 10
Pressure Support Range Test Requirements

No.	Characteristic	Requirement	Result
2.1	Minimum pressure	4 cmH_2O	4 cmH_2O
2.2	Maximum pressure	20 cmH_2O	20 cmH_2O
2.3	Pressure increments	$\leq$0.5 cmH_2O	0.5 cmH_2O

4.1.4 Maximum Flow Rate

Test Protocol

The maximum flow rate is also tested in accordance with the EN ISO 80601-2-70 standard. The protocol for this test is as follows.

1. Set up the treatment device with all the comfort features disabled and with a breathing circuit that is at least 1.9 ± 0.15 m long.
2. Place a pressure and flow measuring device at the end of the breathing circuit. The pressure and flow measuring device must not have a pressure drop across it of more than 1 cmH_2O when the flow rate through the device is 40 $L\,min^{-1}$.
3. Place an adjustable valve at the outlet of the pressure and flow measuring device as shown in Figure 52.

4. Set the treatment device to its minimum pressure setting and adjust the value until the flow rate is $40 \pm 2\,\mathrm{L\,min^{-1}}$.
5. Record the pressure at the patient connection port.
6. Adjust the valve until the pressure at the patient connection port is reduced by $1.0 \pm 0.1\,\mathrm{cmH_2O}$ and record the corresponding flow rate, and pressure measurement.
7. Repeat steps 4 to 6 ten times and record the average values of those ten measurements.
8. Repeat steps 4 to 7 for each pressure indicated in Table 11.

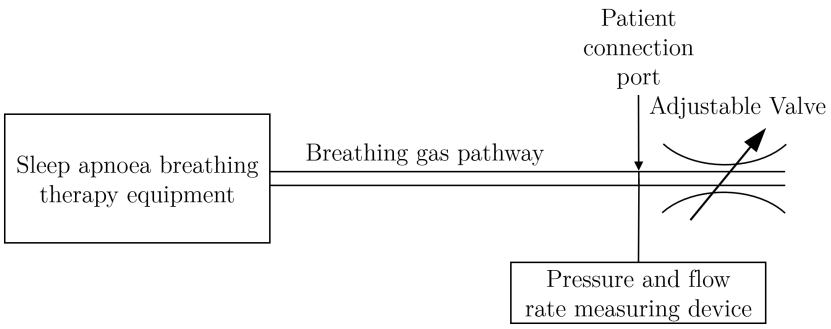

Figure 52: Maximum Flow Rate Test Layout

Test Setup

The device was connected to the VAT set to a logging frequency of 210 Hz, with a large-bore adjustable valve connected to the outlet of the valve. The valve was adjusted as instructed in the protocol. The VAT and adjustable valve are shown in Figure 53.

Figure 53: Maximum Flow Test Setup

Test Result

The results for the ten tests at each flow rate are recorded and the averaged results are shown in Table 11. The standard deviation of the flow rate readings is also added, to indicate how dispersed the data is.

Table 11
Maximum Flow Rate Test Results

Readings at patient connection port	Test Pressures (cmH_2O)				
	P_{min}	$P_{min} + \frac{1}{4}P_{range}$	$P_{min} + \frac{1}{2}P_{range}$	$P_{min} + \frac{3}{4}P_{range}$	P_{max}
	4	8	12	16	20
Pressure (cmH_2O)	3.06	7.07	11.11	15.03	19.01
Average flow ($L\,min^{-1}$)	125.12	121.54	117.64	113.55	109.32
σ_{flow} ($L\,min^{-1}$)	0.09	0.13	0.09	0.14	0.13

The maximum flow rate can be plotted as a function of the pressure setting, as shown in Figure 54.

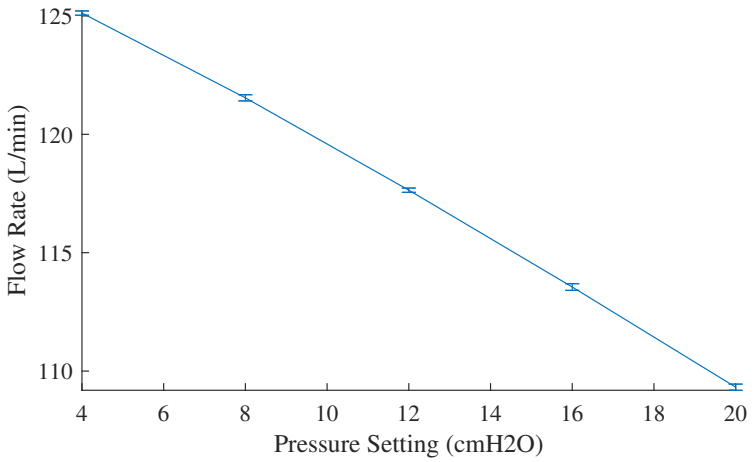

Figure 54: Maximum Flow Rate at Different Pressure Settings

Result Synthesis The maximum flow rate of the device is considered as the minimum flow rate in the table above. This result is compared to the requirement specification in Table 12. The result exceeds the minimum requirement and so the requirement is considered satisfied.

Table 12
Maximum Flow Rate Test Requirements

No.	**Characteristic**	**Requirement**	**Result**
3.1	Maximum flow rate	$80\,L\,min^{-1}$	$109.32\,L\,min^{-1}$

4.1.5 Automatic Leak compensation

Test Protocol

The treatment device is required to automatically adjust the flow rate in case there is a small leak in the mask, so that the correct treatment pressure is maintained. This test is therefore designed to ensure that the correct pressure is maintained, even at higher flow rates. The test protocol is shown below.

1. Set up the treatment device with all the comfort features disabled and with a breathing circuit that is at least 1.9 ± 0.15 m long.
2. Set up the test equipment the same as for the maximum flow rate test, as shown in Figure 52.
3. Set the pressure setting of the treatment device to 4 cmH_2O.
4. Adjust the valve position such that the flow rate measured at the patient connection port is 0% ($\pm 2.0\,L\,min^{-1}$) of the maximum flow rate at a current pressure setting.
5. Record the pressure and flow rate at the patient connection port for 5 minutes.
6. Filter the recorded pressure and flow rate readings using a 5 Hz low-pass filter.
7. Record the average flow rate and pressure readings, as well as the standard deviation of the pressure readings.
8. Repeat steps 4 to 7 for 50% and 90% of the maximum flow rate.
9. Repeat steps 3 to 8 with the pressure settings indicated in Table 13.

Test Result

The results of the test are summarised in Table 13. The desired flow was calculated from the maximum pressure test results, and the measured flow was within $2.0\,L\,min^{-1}$ of the desired flow rate. The positive flow rate when the valve is completely closed (at 0% of the maximum flow rate) is most likely due to small leaks in the connection between the VAT and the valve. The difference between the average pressure and the pressure setting is shown in Figure 55. The offset generally increases with an increasing flow rate, with the offset reaching a maximum of 0.56 cmH_2O at a pressure setting of 20 cmH_2O and 90% of the maximum flow rate.

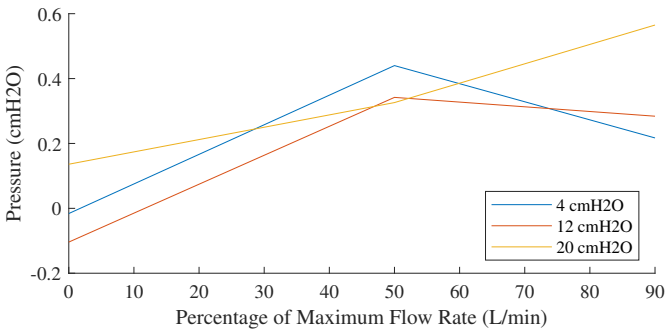

Figure 55: Standard Deviation of the Pressure Readings at Different Flow Rates

Table 13
Automatic Leak Compensation Test Results

Percentage of Max. Flow Rate	Sensor Readings	Device Pressure Setting (cmH_2O)		
		4	12	20
0%	$P_{average}$ (cmH_2O)	3.98	11.90	20.14
	$\sigma_{pressure}$ (cmH_2O)	0.060	0.165	0.220
	Desired Flow ($L\,min^{-1}$)	0.00	0.00	0.00
	Measured Flow ($L\,min^{-1}$)	0.14	0.38	0.53
50%	$P_{average}$ (cmH_2O)	4.44	12.34	20.33
	$\sigma_{pressure}$ (cmH_2O)	0.399	0.727	0.940
	Desired Flow ($L\,min^{-1}$)	62.56	58.82	54.66
	Measured Flow ($L\,min^{-1}$)	64.45	58.60	54.72
90%	$P_{average}$ (cmH_2O)	4.22	12.28	20.56
	$\sigma_{pressure}$ (cmH_2O)	0.356	0.762	1.038
	Desired Flow ($L\,min^{-1}$)	112.61	105.88	98.39
	Measured Flow ($L\,min^{-1}$)	112.22	106.13	97.68

Result Synthesis
As seen in Table 13, the flow rate automatically compensates to ensure the correct pressure is delivered to the patient. While the flow rate compensation is automatic, increasing the flow rate generally reduces the pressure accuracy, as seen in Figure 55. It is interesting to note that as the flow rate increases, the pressure delivered to the patient tends to decrease, however, further testing is required to confirm this trend. The test result and the performance requirement are shown in Table 14. tends to decrease.

Table 14
Automatic Leak Compensation Test Requirements

No.	**Characteristic**	**Requirement**	**Result**
3.2	Leak compensation	Automatic	Automatic

4.1.6 User Modes

The settings for the device are stored on the SD card, in a text file. When the device powers on, it reads the settings from the SD card, and only some of the settings are adjustable by the user. The SD card is located at the back of the device and is not accessible unless the user has a tool to remove it (a pair of tweezers to press the SD card and disconnect it from the SD card reader). The location of the SD card is shown in Figure 56.

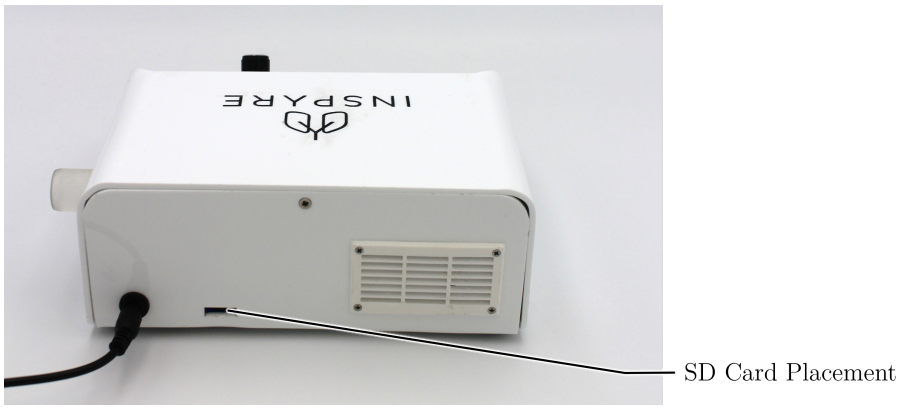

Figure 56: Location of SD card

Once the SD card is removed, a clinician has access to the settings of the device through the settings text file. The contents of this file are shown in Figure 57.

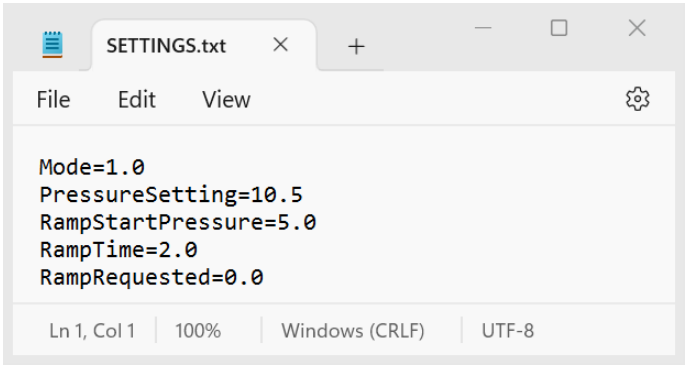

Figure 57: Contents of the Settings File

The first row of the file determines if the device is set to diagnostic or treatment mode. In Figure 57, it is set to treatment mode. If the text read “Mode=0.0” then the device would be in diagnostic mode. The clinician is also able to adjust the “PressureSetting” which determines the level of pressure support provided to the patient. The rest of the settings are adjustable by both the clinician and the user.

The user is able to adjust the settings through the “Settings” menu on the device. The workflow of this menu is shown in Figure 58.

Figure 58: Settings Adjustable by User

Result Synthesis

From the workflow, it is evident that the patient is not able to adjust the mode of the device or the pressure setting. The workflow also shows that the user is able to adjust some of the settings, thus satisfying the requirement specifications shown in Table 15.

Table 15
User Modes Requirements

No.	Characteristic	Requirement	Result
4.1	Operational modes	Clinician and user modes	Achieved
4.2	Features of clinician mode	All settings are adjustable	Achieved
4.3	Features of user mode	Limited settings are adjustable	Achieved

4.1.7 Pressure Ramp

Test Protocol

The device is required to provide a pressure ramp feature, where the user can adjust the starting pressure and the duration. This test was designed to ensure the user can adjust the duration and starting pressure, and that the device delivers the correct pressure during the ramp period.

1. Set up the device the same as for the static pressure test, as shown in Figure 43.
2. Enable the ramp feature and set the device to a pressure setting of 20 cmH_2O.
3. Set the ramp duration to 1 minute.
4. Set the ramp starting pressure to 4.0 cmH_2O.
5. Record the pressure at the patient connection port, sampling the pressure sensor at at least 100 Hz. Filter the sampled pressure readings using a 5 Hz low-pass filter.
6. Calculate the expected pressure reading for each time value by assuming a linear increase in pressure from the starting pressure to the pressure setting over the ramp duration.
7. Subtract the pressure setting from the readings to get the pressure offset of each reading.
8. Record the average and the standard deviation of the pressure offset readings.
9. Repeat steps 4 to 8, using the starting pressures indicated in Table 16.
10. Repeat steps 3 to 9 for each ramp duration indicated in Table 16.

Test Result

For each test, the pressure was recorded for the duration of the test. The desired pressure was calculated by assuming a linear increase between the starting pressure and pressure setting for the duration of the ramp period. The difference between the desired pressure and the pressure readings can also be calculated. These three graphs are shown in Figure 59 for a starting pressure of 12.5 cmH_2O and a duration of one minute.

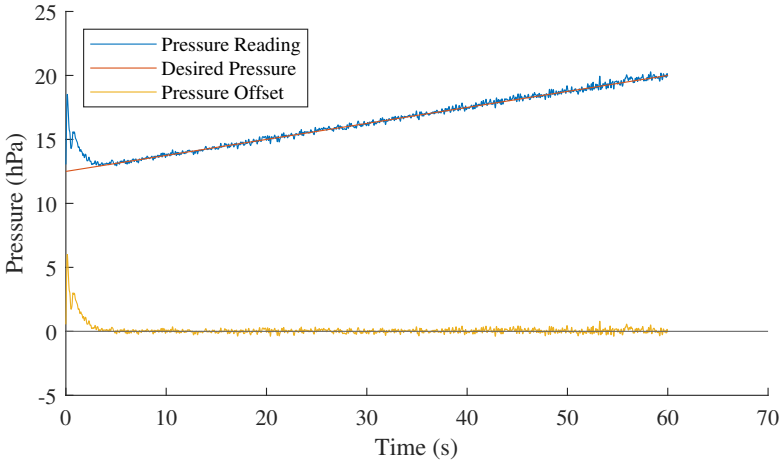

Figure 59: Typical Results of a Pressure Ramp Test

This is repeated for all the ramp durations and starting pressures shown in Table 16. The average pressure offset from the expected linearly increasing pressure is also shown in Table 16, as well as the standard deviation of the pressure around the expected pressure.

Table 16
Pressure Ramp Test Results

Ramp Duration (min)	Sensor Readings (cmH_2O)	Ramp Starting Pressure (cmH_2O)			
		4	4.5	12	12.5
1	Average Offset	0.20	0.18	0.21	0.12
	$\sigma_{pressure}$	0.334	0.303	0.486	0.502
20	Average Offset	0.06	0.07	0.10	0.08
	$\sigma_{pressure}$	0.110	0.131	0.175	0.171
45	Average Offset	-0.03	-0.12	-0.11	-0.08
	$\sigma_{pressure}$	0.1095	0.1137	0.1502	0.1606

Result Synthesis

It is noted that there is a slight overshoot as the device reaches the starting pressure. This overshoot has a larger effect on the standard deviation and average pressure offset in tests with a shorter duration. This is a result of PID gains that are close to the limit of instability to improve the response of the system for the dynamic pressure test. Despite this, the device shows a clear ability to track a steady increase in pressure that is user adjustable, as is summarised in Table 17.

Table 17
Pressure Ramp Requirements

No.	Characteristic	Requirement	Result
5.1	Pressure ramp	User able to initiate ramp at their discretion	Achieved
5.2	Ramp period	User adjustable from 1 min to 45 min	Achieved
5.3	Ramp starting pressure	User adjustable from 4 cmH_2O in ≤ 0.5 cmH_2O increments	Achieved

4.1.8 Mask Removal Detection

Test Protocol

The device must be able to determine whether or not the user has the mask on or not so that the clinician has an indication of compliance. A test protocol was designed to check whether the device can reliably determine when the mask has been removed.

1. Set up the test equipment as shown on Figure 60. A mannequin with reasonable facial contours should be used at the end of the breathing gas pathway.
2. Turn off all comfort features on the device.
3. Set the pressure setting of the therapy equipment to 4 cmH_2O and turn off all comfort features.
4. Start treatment with the mask on.
5. Slowly remove the mask and note the pressure reading on the pressure and flow meter as soon as the therapy equipment indicates that the mask has been removed.
6. Repeat step 4 ten times.
7. Record the average and the standard deviation of the flow rate readings.
8. Repeat steps 2 to 6 for each pressure setting indicated in Table 18.

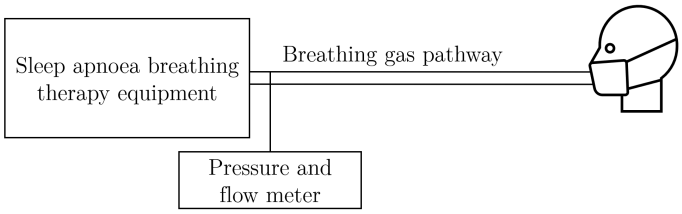

Figure 60: Layout of Equipment for Mask Removal Detection Test

Test Setup

An airway management training with mannequin was used with an oronasal mask, as shown in Figure 61.

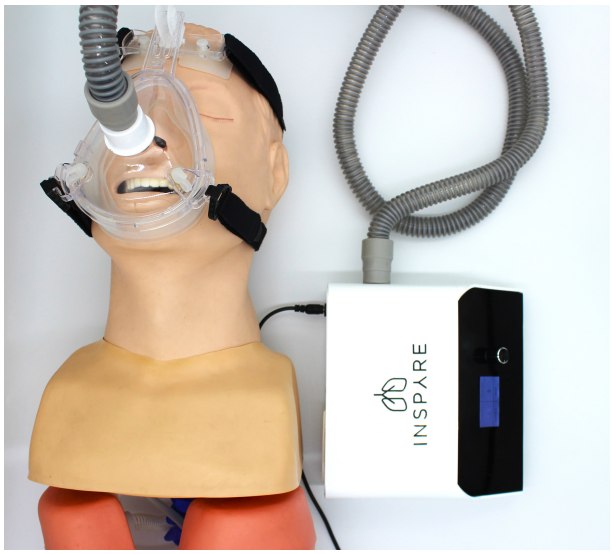

Figure 61: Photograph of Mannequin with Oro-nasal Mask

Test Result

The test results are shown in Table 18 and plotted in Figure 62.

Table 18
Connection Detection Results

Pressure Setting (cmH_2O)	Average Flow Rate ($L\,min^{-1}$)	Standard Deviation ($L\,min^{-1}$)
4	36.68	0.457
8	50.07	0.586
12	62.19	0.763
16	71.17	0.840
20	79.28	0.895

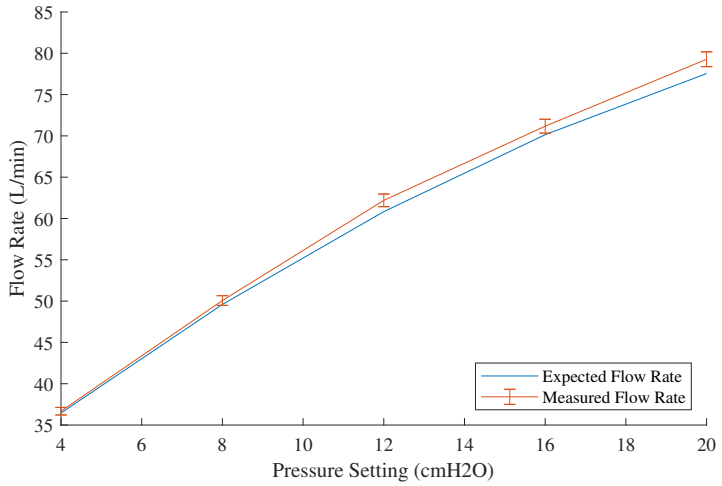

Figure 62: Expected and Measured Flow Rate at which Mask is Considered Removed

The calculated flow rate at which the device should indicate that the mask has been removed is also shown in the graph as "Expected Flow Rate".

Result Synthesis

The results show that the device is able to use the measured flow rate to identify when the mask is removed from the patient. As such, the performance requirement is considered achieved, as highlighted in Table 19.

Table 19
Mask Removal Detection Requirements

No.	**Characteristic**	**Requirement**	**Result**
6.1	Connection Detection	Device must identify when it is connected to the patient	Achieved

4.1.9 Compliance and Usage History

Test Protocol

The device must be able to use the mask detection function to report the user's compliance (percentage of time the user has the mask on while being treated) and report the average time the device is used per night. This data is stored on the SD card in the form of the number of nights used, the total time the device is used in seconds, and the total time the device is used with the mask on in seconds. A clinician is able to access the records on the SD card, and reset the values to zero, while the user is not able to adjust the values. The following test protocol was used to check if the device stores and presents the correct data. The test simulates a history of four nights of use for 8 hours 30 minutes of use each night and a compliance of 95%. A new night of treatment was then run and the changes in the data are compared to the expected changes.

1. Remove the SD card from the device and open the "USAGE" text file.
2. Change the values to reflect the following:
   Nights=2
   TotalTime=612000
   TotalTimeWithMask=55080
3. Turn off all comfort features and set up the device the same as for the mask removal detection test, as shown in Figure 60.
4. Start the treatment with the mask on.
5. After 30 minutes, remove the mask from the mannequin.
6. After 60 minutes stop the treatment.
7. Record the average use time and compliance as displayed on the device.
8. Record the updated numbers in the "USAGE" text file.
9. Compare the expected compliance, average use time, and records to the actual readings.

Test Result

The test was conducted and the results were recorded in Table 20. The results as displayed on the device screen are shown in Figure 63.

Table 20

Compliance and Usage History Test Results

	Initial Values	Expected Value	Results
Nights of use	4	5	5
Total Use Time (s)	122400	129600	129593
Use Time with Mask (s)	110160	113760	113756
Average Use Time (hh:mm)	8:30	7:12	7:12
Compliance (%)	90	88	88

Figure 63: Displayed Average Time and Compliance on the Device

Result Synthesis

The difference between the expected and results column in Table 20 can be accounted for by a few seconds delay in stopping the treatment (7 seconds more than 1 hour) and by not removing the mask at precisely 30 minutes. The device, however, operates as expected and correctly displays the required usage data, as summarised in Table 21.

Table 21

Compliance and Usage History Requirements

No.	Characteristic	Requirement	Result
6.2	Information reporting	Device must store historical data regarding its use for review by a clinician.	Achieved

4.1.10 Power Supply

The power supply was purchased as an off-the-shelf component. The data sheet was therefore consulted to obtain the electrical operating conditions of the component. The following text is an extract from the data sheet (RS Pro, 2023).

Input: **90-264V, 47/63Hz**

Nominal full load input current: 2A max.

Inrush current (cold start): 50A max.

Nominal efficiency @ 230V: 89.19%

Off load stand-by power: 0.1W max.

Output voltage (±5%): 24VDC

Maximum output current: 2500mA

Result Synthesis

The input voltage range and frequency are smaller than the limits stated on the data sheet. The power supply can therefore continuously supply power to the device at the required voltage and current, even when the input power to the power supply is at the extremes of the frequency and voltage input. This requirement is therefore satisfied.

Table 22

Power Supply Requirements

No.	Characteristic	Requirement	Result
7.1	Input power supply frequency	50 Hz to 60 Hz	47 Hz to 63 Hz
7.2	Input power supply voltage	220 V to 240 V	90 V to 2264 V

4.2 Diagnostic Component

4.2.1 Pulse Oximeter

Test Protocol

The pulse oximeter is purchased as an off-the-shelf component. As mentioned in the component selection section, the Contec CMS60C pulse oximeter is used. It has a USB port, through which it is able to stream data. The following test protocol is developed to test the sampling frequency and the reading averaging time.

1. Setup the device in the same configuration as would be used during diagnosis.
2. Connect the pulse oximeter to a pulse oximeter simulator.
3. Set the pulse oximeter to a pulse rate of 60 beats per minute.
4. Set the blood oxygen saturation (or SpO_2) to 40%.
5. Start recording on the device.
6. After 2 minutes and 30 seconds, step the simulator SpO_2 to 80%.
7. Stop the recording after 5 minutes.
8. Record the average and average offset from the correct value for the readings for the first and last two minutes of the test.
9. Record the time it took for the reading to reach the correct value.
10. Repeat steps 4 to 9 for the SpO_2 values shown in Table 23.

Test Setup

A Fluke ProSim 8 vital signs simulator from the Groote Schuur Hospital, department of clinical engineering, as shown in Figure 64, is used for the testing. The device and the sensor hub were set up in the clinical engineering laboratory, and the test was completed. The simulator was set to the default settings for pulse oximeter testing and calibration, as shown in Figure 64.

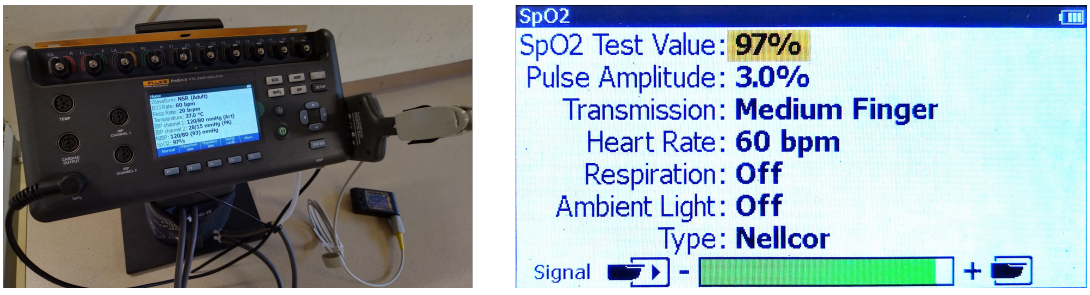

Figure 64: Photograph of Fluke ProSim 8 Vital Signs Simulator

Test Result

Initially, the test is conducted with the data logging function run in an interrupt service routine on the Arduino set at 25 Hz. The data received from the sensor hub was therefore logged at 25 Hz and the SpO_2 results of this logging are shown in Figure 65a. There are many errors in the received data. It was also noted that during testing, the device would

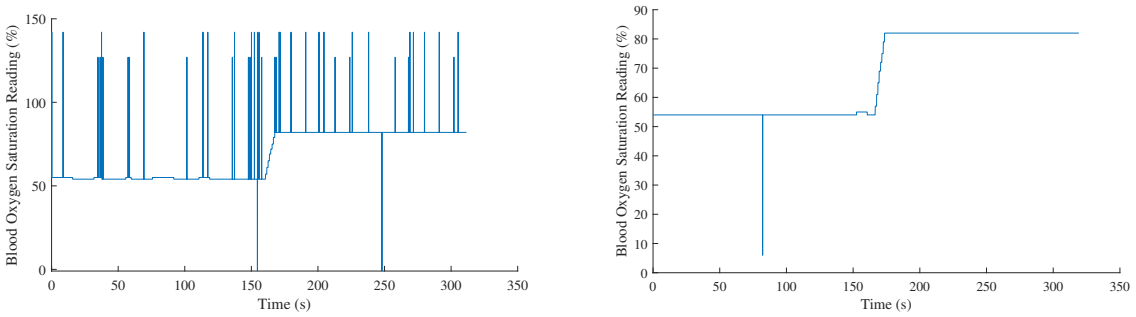

(a) 25 Hz (b) 10 Hz

Figure 65: Pulse Oximeter Test Result

freeze frequently and the test would need to be repeated. The method of data logging was therefore changed such that a flag is raised in the 25 Hz interrupt service routine, and then the data is saved in the main loop which would check if the flag were raised and then log the data if the flag was raised. This reduced the logging frequency to 9.80 Hz, but significantly reduced the error rate, as shown in Figure 65b. The Sensor hub, however, still received data from the pulse oximeter at approximately 40 Hz. This method of data logging is selected, and the frequency of logging is a limitation of the microcontroller. The results of the test are shown in Table 23.

Table 23
Pulse Oximeter Test Results

Starting SpO_2 (%)	40	50	60	70
Average Sensor Reading (%)	53.95	61.00	68.00	74.99
Offset (%)	13.95	11.00	8.00	4.99
Reading Delay (s)	7.11	7.03	8.32	8.64
Gradient (%/s)	3.95	4.13	3.25	2.78
Ending SpO_2 (%)	80	90	95	99
Average Sensor Reading (%)	82.00	90.00	95.00	99.00
Offset (%)	2.00	0.00	0.00	0.00
Average Sampling Frequency (Hz)	42.1	41.4	41.7	41.9

During the test, it was noted that at lower SpO_2 values, the pulse oximeter reading was offset from the simulator setting, despite the pulse oximeter being rated to function at SpO_2 values between 35% and 99%. The offset plotted against the increasing simulated SpO_2 percentage is shown in Figure 66. It was also noted during the test that the power management PCB had a sharp rise in temperature when the sensor hub was powered on. This indicates that the power management PCB is not able to provide sufficient current to the sensor hub, so an external power supply is used for the sensor hub.

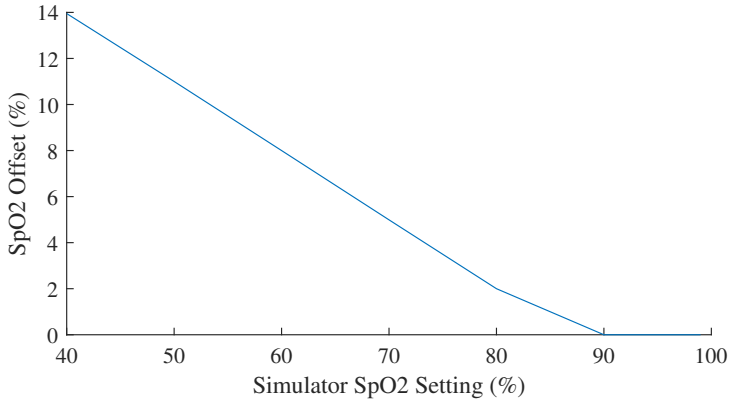

Figure 66: Pulse Oximeter Reading Offset

Result Synthesis

The offset at normal oxygen saturation (between 95% and 99%) is 0% but increases linearly as the simulator saturation decreases. Further testing is required to determine the lowest blood oxygen saturation at which the offset is zero, however, due to the nature of the test, the test equipment is not available for additional testing. The accuracy of the pulse oximeter is also out of the scope of this research, but the constant linear increase in offset could be accounted for by the device.

The average rate at which the SpO_2 reading changes when given a step input is $3.52\,\%\,s^{-1}$. There does seem to be a decreasing trend in the rate of change as the SpO_2 increases, however, further testing is required to confirm if this is true. From Table 23, the average time taken for the reading to reach the simulated value is 7.8 s, indicating the reading averaging time is also approximately 7.8 s. This is significantly longer than the requirement of less than 3 s. The performance of the pulse oximeter in comparison to the performance requirements is shown in Table 24.

Table 24
Pulse Oximeter Requirements

No.	Characteristic	Requirement	Result
8.1	Interface type	USB	USB
8.2	Reading averaging time	$\leq 3\,s$	7.8 s
8.3	Minimum sampling frequency	10 Hz	41.8 Hz

The maximum rate of SpO_2 decrease during an apnoea event is $1.5\,\%\,s^{-1}$ which is less than the pulse oximeter maximum rate of change, suggesting the pulse oximeter reading is able to change quickly enough to identify apnoea events even though it does not meet the requirement. Further testing is required with a simulator that is able to adjust the SpO_2 value over time, and not just a step input. The sampling frequency is limited by the logging frequency of the device and not the pulse oximeter, and so the sampling frequency would increase if an alternative microcontroller with a higher clock frequency is used.

4.2.2 Breathing Effort Sensor

Test Protocol

The breathing effort sensor is also an off-the-shelf component, and interfaces with the sensor hub. The following protocol is developed to test the device's ability to read data from the breathing effort sensor and log the data to the SD card.

1. Set up the device in the same configuration as would be used during diagnosis.
2. Connect the breathing effort sensor to a device that mimics the movement of a chest while breathing.
3. Set the breathing rate to 10 breaths per minute and at a constant amplitude.
4. Start a diagnosis night and wait for 5 minutes.
5. Stop the diagnosis.
6. Record the sampling frequency and process the logged signal, recording the average breathing amplitude, and the standard deviation of the signal amplitude.
7. Repeat steps 3 to 6 for the breathing rates shown in Table 25.

Test Setup

The breathing effort sensor is testing using SimMan 3G medical scenario simulator at the clinical skills centre at Groote Schuur Hospital, Cape Town, shown in Figure 67 . The patient simulator can breathe at a breathing rate set externally, but the breathing effort amplitude is not adjustable. The breathing effort sensor connected to the SimMan 3G is shown in Figure 67.

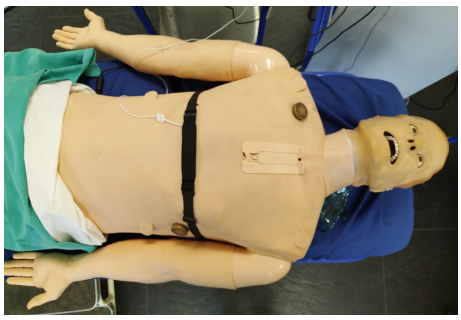

Figure 67: Photograph of SimMan 3G Medical Scenario Simulator

Test Result

The data is recorded by the sensor hub at just over 40 Hz, filtered on the sensor hub using a bandpass filter set at 0.1 Hz and 15 Hz, and the logged to the SD card at 10 Hz. An example of the data logged to the SD card (from the 10 breaths per minute test) is shown in Figure 68.

The data is processed using a Matlab script that identifies peaks and troughs. Each trough is subtracted from the subsequent peak and then halved to get the amplitude of each wave. The average wave amplitude is then recorded, as well as the standard deviation. These results are shown in Table 25. The breathing effort sensor is uncalibrated, so the sensor readings are unitless.

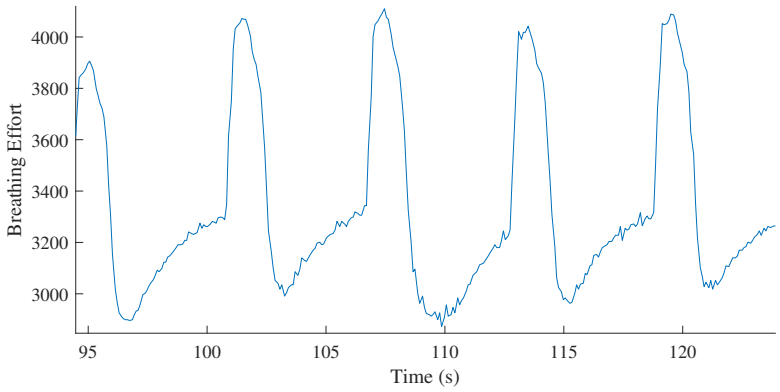

Figure 68: Breathing Effort Test Result

Table 25
Breathing Effort Sensor Test Results

Breaths per minute	**10**	**15**	**20**
Average amplitude	546.7	521.7	522.8
Standard Deviation	79.4	52.8	52.3
Sampling frequency (Hz)	41.5	42.0	41.3
Logging frequency (Hz)	10.99	10.96	10.97

Result Synthesis

The SimMan 3G is not able to provide a smooth breathing motion but rather gasps at a set rate. This is indicated by the waveform shown in Figure 68. Despite this, the data from the breathing effort sensor is clearly able to track the chest movement accurately. The test results are compared to the performance requirements in Table 26. The table shows that the sensor meets all of the minimum performance requirements.

Table 26
Breathing Effort Sensor Requirements

No.	**Characteristic**	**Requirement**	**Result**
9.1	Interface type	USB type B	USB type B
9.2	Minimum sampling frequency	25 Hz	41.6 Hz
9.3	Low frequency filter cut-off frequency	0.1 Hz	0.1 Hz
9.4	High frequency filter cut-off frequency	15 Hz	15 Hz
9.5	Sensor Type	Single/dual thoracoabdominal RIP/PVDF/Piezo belt (calibrated or uncalibrated)	Single uncalibrated thoracoabdominal piezo belt

4.2.3 Airflow Sensor

Test Protocol

The test protocol was developed to assess the accuracy of flow rate measurement, as required by the AAST. The AAST mandates the use of an oro-nasal thermal airflow sensor or nasal pressure transducer for flow rate measurement. In this case, the outlet pressure sensor serves as an equivalent to the nasal pressure transducer, approximating the pressure at the mask. While the Venturi tube would provide more accurate flow rate measurements for diagnosing sleep apnoea, the pressure readings will be used to comply with the AAST requirements. The test protocol below aims to evaluate the device's ability to approximate the pressure at the end of the breathing circuit.

1. Setup the device in the same configuration as would be used during diagnosis.
2. Connect the breathing circuit to the breathing simulator, standard resistance, and pressure measuring device (VAT), as shown in the dynamic pressure test protocol.
3. Set the breathing simulator to a breathing frequency of 10 breaths per minute.
4. Start recording on the VAT and on the diagnostic device at the same time and record for at least 5 minutes.
5. Stop recording on the VAT and diagnostic device at the same time.
6. Filter the pressure readings from the VAT using a 5 Hz low-pass filter.
7. Find the peaks in both the VAT recording and in the diagnostic device recording.
8. Calculate the difference between the pressure readings for each peak.
9. Divide the difference by the VAT peak pressure reading and multiply by 100, to get the error percentage and record the average peak error percentage for all peaks.
10. Repeats steps 7 to 10 for the troughs.
11. Record the average error percentage of the peak and trough error percentages, ensuring the absolute value of the error percentage is used.
12. Repeat steps 3 to 12 for the breathing rates shown in Table 27.

Test Result

The resulting data was processed using a Matlab script which filters the VAT readings with a 5 Hz low-pass filter, identifies the peaks and troughs in both the VAT data and diagnostic device data, and calculates the percentage error. Figure 69 shows an extract of the pressure measurements from the VAT and diagnostic device from the 15 breaths per minute test. The results of the tests are summarised in Table 27.

Table 27
Pressure Measuring Test Results

Breaths per minute	**10**	**15**	**20**
Peak Pressure Error (%)	8.97	8.66	1.52
Trough Pressure Error (%)	-12.12	1.44	-6.85
Average Error (%)	10.54	5.05	4.19

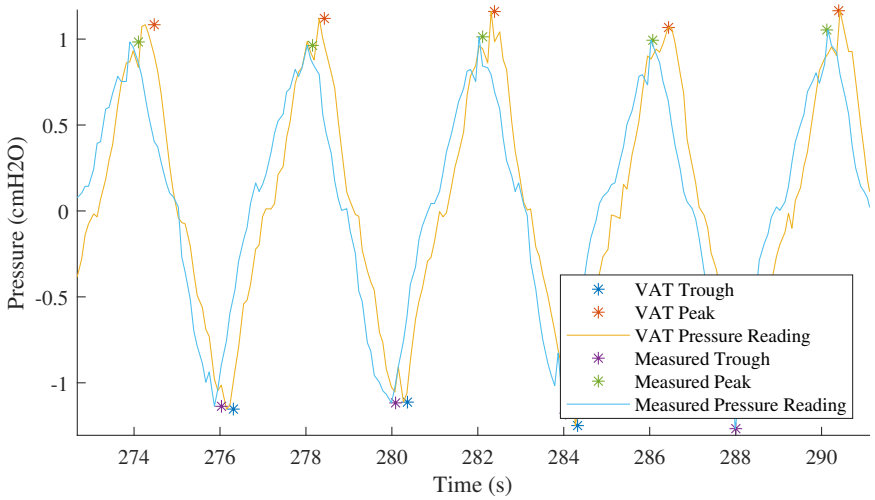

Figure 69: Pressure Measuring Test Result

Result Synthesis

The VAT measurements seen in Figure 69 are slightly delayed in comparison to the diagnostic device measurements. This can be accounted for by a slight delay when starting the recording. The delay does not affect the error calculation as the peak value is used in the calculation and there is no comparison of the time values.

The error tends to be positive for the peaks and negative for the troughs. This indicates that the VAT readings have a slightly larger amplitude than the diagnostic device readings. This could be explained by the compressibility of the air in the breathing circuit and the flex in the walls of the breathing circuit.

The performance requirements of the airflow sensor are compared to the test results in Table 28. In this case, the maximum flow rate of the Venturi tube is considered. The maximum flow rate reading is recorded as the maximum flow rate from the treatment component testing. The minimum flow rate is based on the observed readings when the device is powered off.

Table 28
Airflow Sensor Requirements

No.	Characteristic	Requirement	Result
10.1	Sensor Type	Oronasal thermal airflow sensor or nasal pressure transducer	Nasal pressure transducer
10.2	Sensor Accuracy	±5%	±10.54%
10.3	Maximum reading	$80\,\mathrm{L\,min^{-1}}$	$125.12\,\mathrm{L\,min^{-1}}$
10.4	Minimum reading	$10\,\mathrm{L\,min^{-1}}$	$0\,\mathrm{L\,min^{-1}}$

4.2.4 Diagnostic Data Analysis

Test Protocol

After the data is logged to the SD card, it must be processed by the diagnostic algorithm. This algorithm requires a decrease in flow rate and the duration of the decrease to be identified, as well as a decrease in blood oxygen saturation and breathing effort. The following test protocol was developed to check if these characteristics can be identified by the device.

1. From existing patient data, identify 3 apnoea events.
2. Extract the data for each apnoea event as well as for a minute before and after the apnoea event.
3. Pass this data through the diagnostic event detection algorithm.
4. Graphically display the data and take readings from the graph that correspond to the characteristics being measured by the device.
5. Compare the graphically measured values to the reported values from the device.

Test Setup

Typically, polysomnography (PSG) recordings are stored in the European Data Format (EDF) and, as such, need to be converted into a different format before they can be processed by the device. This pre-processing is conducted using a Matlab script which converts the EDF file into comma-separated values (CSV file) and reduces the sampling frequency from 100 Hz to 10 Hz. PSG recordings from the Wisconsin sleep cohort are used (Young et al., 2009; Zhang et al., 2018). For this test, the first visit of patient 10241 is used because they have a relatively high AHI (18.3). The events used from this recording are highlighted in Table 29. These events have been identified and annotated by a qualified sleep technologist.

Table 29
Summary of Events Used for Diagnostic Data Analysis Test

Event No.	Event Type	Time
1	Hypopnea	1:33:13
2	Obstructive apnoea	5:26:06
3	Obstructive apnoea	5:38:06

Test Result

The events are processed by the device and the characteristics reported. These reported values are compared to the measured values, which are obtained by taking readings from the graphs. The comparison is shown in Table 30.

Table 30
Results of Diagnostic Data Analysis Test

Data Characteristic	Event 1		2		3	
	Measured	Reported	Measured	Reported	Measured	Reported
Decrease in flow (%)	95.1	82.0	98.0	96.9	88.8	97.7
Duration of decrease in flow (s)	10.8	10.1	13.2	11.3	10.1	10.2
Drop in SpO_2 (%)	-3.50	-3.46	0.98	0.74	0.74	0.00
Decrease in breathing effort (%)	77.9	99.4	89.9	27.6	83.1	52.8

Result Synthesis

Table 30 indicates that the device is able to identify the event and the characteristics of the event. The accuracy of the reported values varies significantly; however, the device has demonstrated its ability to identify when the characteristics of the signal change and place these changes into categories based on the magnitude of the change. Therefore, diagnostic data analysis requirements are considered achieved, as shown in Table 31.

Table 31
Diagnostic Data Analysis Requirements

No.	Characteristic	Requirement	Result
11.1	Identify a drop in flow rate	$\geq 30\,\%$ decrease in flow rate in comparison to pre-event baseline	Achieved
11.2	Identify duration of a drop in flow rate	$\geq 10\,$s duration of decrease in flow rate	Achieved
11.3	Identify a drop in blood oxygen saturation	$\geq 3\,\%$ drop in blood oxygen saturation	Achieved
11.4	Identify a cessation of breathing effort	Decrease of $20\,\%$ in amplitude of breathing effort	Achieved

4.2.5 Algorithm Execution

Test Protocol

The information obtained from the identification of the characteristics of the data needs to be combined to correctly identify apnoea events. The following test protocol was designed to test if the device can identify apnoea events from patient data.

1. From an existing PSG test, extract the SpO_2, breathing effort, and airflow data.
2. Process this data using the diagnostic algorithm on the device.

3. Record the AHI score recorded from the device and compare it to the sleep technologist-scored result.
4. Record the time taken for the device to process that data.
5. Repeat steps 1 and 3 for another 4 PSG recordings.

Test Setup

Five PSG recordings from the Wisconsin Sleep Cohort (WSC) are used for this test (Young et al., 2009; Zhang et al., 2018). The recordings contain 16 data channels, of which the nasal pressure (channel 11), thorax breathing effort (channel 12), and SpO_2 (channel 16) channels are used. A Matlab script is used to convert the data from EDF for CSV files, and to reduce the sampling frequency from 100 Hz to 10 Hz.

Test Result

The CSV files are converted to text files and processed by the device. The results are summarised in Table 32. The table shows the identification number of the patient used by the Wisconsin sleep cohort (WSC) to anonymise the patient.

Table 32
Algorithm Execution Test Results

PSG Recording	WSC ID	Scored AHI	Suspected AHI	Confirmed AHI	Processing time (min)
Recording 1	10119	0.5	5.51	3.81	17.6
Recording 2	10191	0.0	3.38	1.45	19.2
Recording 3	10198	7.3	14.8	6.5	17.6
Recording 4	10226	18.1	23.9	5.2	18.6
Recording 5	10241	18.3	21.3	2.85	17.7

Result Synthesis

During the test, it was noted that the PSG data was not as clean as expected. When the patient moves, the amplitude of their breathing effort reading changes, but an apnoea or hypopnea event has not necessarily occurred. The AASM algorithm relies heavily on the breathing effort signal, so it is prone to both false positives and false negatives, especially if the signal amplitude changes when the patient movies. The algorithm also requires a drop in blood oxygen saturation of at least 4% in order for an event to be classified as a hypopnea event. It is noted that very few events have such a significant drop in SpO_2 and so many hypopnea events are considered "suspected hypopnea events". The algorithm takes, on average, 18.1 min to process a full recording. This highlights the limitation of the Arduino's clock speed, as well as the need to process the data as it is being logged to the SD card. Despite this, the test has demonstrated the device's ability to process the data and identify events. The performance requirement, as shown in Table 33, is considered achieved.

Table 33
Algorithm Execution Performance Requirement

No.	Characteristic	Requirement	Result
11.5	Apnoea event identification	Combine breathing effort, flow rate, and blood oxygen saturation event identifications to identify obstructive or central sleep apnoea.	Achieved

4.2.6 Information Presentation

Test Protocol

The device must be able to present the AHI score as well as the list of identified events to a clinician. The following test protocol was used to test if the device is capable of doing this.

1. From an existing PSG test, extract the SpO_2, breathing effort, and airflow data.
2. Process this data using the diagnostic algorithm on the device.
3. Open the files containing the AHI and list of identified events, as well as the file containing the recorded data.
4. Ensure all required information is present in these files.

Test Result

The recording of patient 10119 from the WSC is used for this test. The resulting diagnostic summary file is shown in Figure 70 and illustrates how the information is presented to a clinician. All of the events identified by the device are listed in the file, however, most of them have been removed from the figure and shown as "// List of events" to ensure the contents of the whole file are visible.

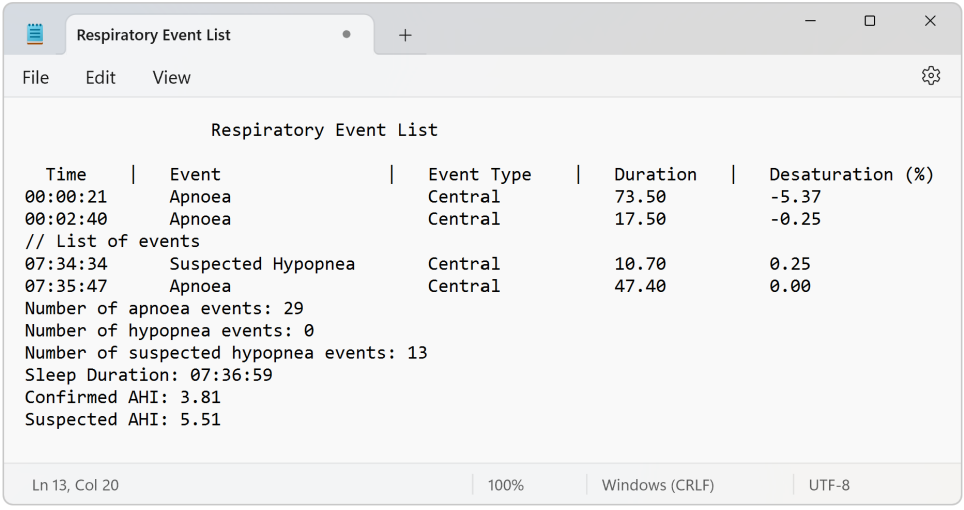

Figure 70: Diagnostic Information Reporting Test Result

Figure 71 shows the how the raw data is presented to a clinician which would allow them to check the scoring of the diagnostic night. Each row contains the time since starting the test, the SpO_2 value, breathing effort value, flow rate value, and heart rate. The heart rate is not used in the AASM diagnostic algorithm, so it is not extracted from the PSG recordings and is set to zero.

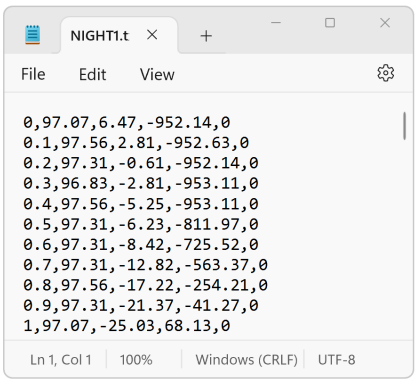

Figure 71: Data used for Diagnosis

Result Synthesis

The diagnostic results clearly present the time and type of event, as well as its duration and the blood oxygen desaturation during the event (a negative desaturation percentage indicates the SpO_2 value increased during the event). The results also clearly display the AHI, sleep duration, and the number of the different events.

The file containing the data displays the data, albeit without headings. The data is in an accessible format but is not in the industry standard EDF format. The requirement of presenting the raw sensor reading, as shown in Table 34, is, however, satisfied. Additional software would, however, need to be developed that would graphically present the data, thus allowing clinicians to identify apnoea events.

Table 34
Diagnostic Data Presentation Performance Requirements

No.	Characteristic	Requirement	Result
12.1	Present event identification	Present all events to a clinician as well as AHI score	Achieved
12.2	Present sensor readings	Present raw sensor readings	Achieved

5 Discussion

The testing chapter highlighted the performance characteristics of the device in comparison to the performance requirements. Further synthesis and analysis of the results are done in this chapter, focusing specifically on the treatment and diagnostic components of the device.

5.1 Treatment Component

Dynamic Pressure Accuracy

Although the device showed strong performance characteristics in the static pressure test, it performed poorly in the dynamic airway pressure accuracy test, where it did not meet the requirements. There are multiple factors that could improve the dynamic pressure response of the device, as mentioned in the results synthesis section of the dynamic airway pressure accuracy test and further analysis needs to be done to understand which of the improvements would be most effective. This analysis could involve characterising the response of the system by feeding a step function to the linearisation function and thus to the fan. This would give a better indication of the response time of the system. This could be repeated with the fan stepped from 0% to 100%, as well as from 100% to 0%, thus giving an indication of the time required for the fan to slow down, and the pressure to drop.

Most of the tests (pressure support range, maximum flow rate, leak compensation, and mask removal tests) are conducted using the standard resistance, meaning the effect of the patient's breathing is not considered in the results. Further testing needs to be done using the breathing simulator to gain insight into how the device responds when connected to a patient. The breathing simulator, as required by ISO 80601-2-70, is relatively simple and does not account for changes in inspiratory time to expiratory time (I:E) ratio, or changes in breathing amplitude. A more advanced breathing simulator should be used to test the device with known patient breathing waveforms (pressure and volume).

Accounting for the Bernoulli Effect

In the maximum flow rate tests, it is noted that, at higher flow rates, the pressure delivered to the patient is higher than the pressure setting. This is most likely due to the Bernoulli effect, where the pressure decreases as the fluid velocity increases. As a result, the pressure measured at the outlet of the device would decrease as the flow rate decreases. As a result, the device would increase the blower speed to ensure the pressure measured at the outlet matches the pressure setting, resulting in a higher pressure being

delivered to the patient. This response needs to be characterised and accounted for by the device to ensure the pressure delivered to the patient is the correct pressure, regardless of the flow rate.

Limitations of the Patient and Clinician Modes

One of the requirements of the treatment component of the device is that the patient is not able to access all of the settings, while the clinician has full access. This is achieved by limiting the settings adjustable through the user interface but allowing all settings to be adjustable when a clinician accesses the SD card. Theoretically, this means, the patient can also remove the SD card and change the settings. This design decision was made, however, to ensure that when the device is used in resource-limited settings (without internet access to download software, or without the ability to purchase specific tools or equipment to change settings) the clinician would be able to change the settings using just an SD card reader. Most modern cellphones also make use of the same SD card for data storage so the SD card could also be inserted into a cellphone and the settings changed using a text editor on the cell phone. A further layer of security could be added by encrypting the information on the SD card that can be decoded using software, either on a clinician's computer or cellphone. The software could require the clinician to register using their professional registration number (for example a health professionals council of South Africa (HPCSA) registration number). This would, however, limit the use of the device to settings with internet connectivity.

Pitfalls of the User Interface

The user interface consists of a black and white screen with a push-button and rotary encoder. This means that users do not need to search for different buttons when the device is used in the dark and can interact with the device using just one connection point. The rotary encoder, however, protrudes from the device quite far, making it easy for the user to bump the encoder and damage it. The encoder is also placed on the right-hand side of the screen, meaning it is easy for right-handed users to operate the device, but less ergonomic for left-handed users. The screen is also not currently configured to be dimmable, so the backlight is constantly powered on. This would not be convenient when the user is trying to sleep and would need to be corrected on future versions of the device.

Runaway Blower when Mask Removed

When the user removes the mask, the screen displays "Please refit mask.", and the blower goes to its maximum speed until the mask is fitted correctly. This is inconvenient and noisy, especially if the user removes the mask so they can go to the bathroom. The fan should, instead, reduce its speed while still producing sufficient flow to detect when the mask is correctly fitted again.

5.2 Diagnostic Component

Sensor Hub Design and Power Consumption

During the initial design phase of the project, the electronic and software requirements in order to connect with the pulse oximeter were not well understood. The Arduino Mega was selected as the primary microcontroller, however, it does not have the capability to act as a USB host. As a result, an additional microcontroller is required in order to communicate with the pulse oximeter. Initially, a Raspberry Pi Pico was considered as it can act as a USB host and is relatively inexpensive. Using the Pico, however, would have extended the development time as it is significantly more complex to program and to get it to interface with the pulse oximeter. Instead, the Raspberry Pi 4B is used as it is significantly simpler to program and debug. This does, however, mean that the sensor hub had to be external to the device. The Pi 4B also requires significantly more power than the Pico and requires more power than the power management PCB can safely provide. An external power supply is therefore used for the Pi 4B.

The overheating of the power management PCB while powering the Pi 4B highlighted that there is no cooling mechanism for the internal components. The device was able to conduct the eight-hour static pressure tests with no overheating issues, but simulations and testing needs to be done to understand which components heat up, and how they behave with limited cooling. This would determine if additional active or passive internal cooling is required.

Pulse Oximeter Selection

To diagnose sleep apnoea, an off-the-shelf pulse oximeter is used. The performance specifications for these oximeters are not advertised or available (specifically the sampling rate and reading averaging time). Furthermore, there are a limited number of pulse oximeters that can continuously stream pulse oximetry data over a USB connection. Borsini and Nigro (2022), however, makes use of a Nonin OEM III module with fingertip pulse oximeter to read pulse oximetry data for sleep apnoea diagnosis. This pulse oximeter was used with a sampling frequency of 1 Hz and an averaging time of four to eight heart beats. This equates to roughly 1.5 sec to 3 sec. A similar sensor is used in the Resmed Apnealink, a diagnostic device commonly used for conducting home sleep tests (Stansbury et al., 2022). These two devices utilise pulse oximeters designed specifically for sleep apnoea diagnosis. Further research needs to be done to identify any similar pulse oximeters that can be purchased as a single component, and not part of a home sleep test kit.

Error Handling During Diagnosis

When the device reads the data from the SD card to identify apnoea events, there are no error handling techniques used. The values are read sequentially until the end of the

file is reached. If there is one value missing (for example, the SpO_2 reading) then the rest of the values will all be offset by one position and the nextSpO_2 reading will be the time value. To prevent this, each line should be read as a packet, with a start and end identifier. If the identifiers are not correct, then the packet can be discarded. Despite this, the diagnostic algorithm was able to operate correctly as there were no missing values in the data used.

Implications of Mask Use for Flow Rate Monitoring

In the PSG readings used, there are three different values that give an indication of flow rate. These are oral flow, nasal flow, and oral pressure. For the algorithm testing, the nasal pressure is used, but a combination of these values would give the most accurate indication of the flow rate. The device developed makes use of an oro-nasal mask which would encapsulate both the flow to the mouth and nose and would have significantly less leak than the sensors used in the PSG test. The readings from the device would therefore be more accurate than the flow rate from the PSG readings. One of the major drawbacks, however, is that the pressure drop over the breathing circuit may make it more difficult for the patient to inhale, thereby increasing the patient's AHI score. The use of the mask and breathing circuit may also mean that the patient is re-breathing air that they have exhaled. To overcome this issue, the blower could be controlled to ensure the pressure at the patient's mask is maintained at the environmental pressure. This would ensure the mask and breathing circuit have no effect on the patient's AHI score. To prevent re-breathing, a slight positive pressure could be provided during exhalation to ensure the exhaled air leaks out the mask and not back into the device. Further development and testing are, however, required to investigate how the fan could be used to ensure the device does not affect the patient's AHI, and prevent re-breathing of exhaled air.

Limitations of the Diagnostic Algorithm

It is noted that the AHI reported by the device is often different to the AHI identified by a sleep technologist. The intention of the diagnostic algorithm is to screen the results and identify possible events, and not definitively identify all the events. This definitive event identification is conducted by a qualified sleep technologist. The role of the diagnostic algorithm is purely to assist this process by screening the data. That being said, the better the algorithm at identifying the events, the easier it is for the sleep technologist and the easier it is to diagnose sleep apnoea. The algorithm developed by the AASM is relatively simple but apnoea events can, however, be more complex and difficult to identify. For example, as a result of an apnoea or hypopnea event, a patient's blood oxygen saturation may decrease. This decrease might not be identifiable during the event but rather be noted a few seconds after the event. The AASM algorithm does not dictate a time frame in which the decrease in blood oxygen saturation must occur. A more advanced algorithm is therefore required to improve the event identification process. One method that could

work is the use of a trained neural network to identify events. Research into its use in identifying events in PSG readings is currently being conducted and it has been able to reach an accuracy of 84% in sleep apnoea detection (Piorecky et al., 2021). This method could also be used for home sleep test data.

Implications of a Device that Diagnoses and Treats a Condition

Devices that both diagnose and treat a condition may be subject to high levels of scrutiny, especially if the device over-diagnoses the condition. If this type of device over-diagnoses a condition, then more of the same device are likely to be sold. It is therefore beneficial for the company selling the device if the device over-diagnoses the condition. It is critical that the device is able to demonstrate that it makes use of standardised diagnostic processes and performs comparatively to other diagnostic devices. For this reason, the AASM algorithm was used to identify events. In any further development of the device, this must also be considered, and the diagnostic performance of the device should be compared to similar devices.

6 Conclusion

The purpose of the study was to design and develop a device capable of diagnosing sleep apnoea as well as providing CPAP therapy such that the prevalence of untreated and undiagnosed sleep apnoea could be reduced. This was achieved by developing a device with two modes, diagnosis and treatment mode.

When in treatment mode, the device provides a basic level of CPAP treatment. This was achieved through the use of a blower and Venturi tube, where a microcontroller controls the speed of the blower to ensure the correct output pressure is maintained. The output pressure setting can be adjusted by a clinician, while the patient has no access to this setting via the user interface. The device also incorporated comfort features such as pressure ramping and provides pressure support between 4.0 cmH_2O and 20.0 cmH_2O. Various tests were conducted on the device to determine if it meets the performance characteristics specified by the ARTP. It met requirements for mean static pressure and maximum flow rate tests but exceeded the allowable range for dynamic airway pressure accuracy. Further device development is necessary to improve test results and ensure the device delivers accurate pressure to the patient throughout the breathing cycle.

In diagnostic mode, the device records physiological signals (blood oxygen saturation, breathing effort, and flow rate) such that apnoea events can be identified. The breathing effort signal is measured using an off-the-shelf breathing effort sensor, and an existing pulse oximeter is used to measure the blood oxygen saturation. The performance of this pulse oximeter does not meet the minimum performance requirements as the reading averaging period is longer than the maximum specified by the ARTP. An oro-nasal mask is used instead of a nasal pressure sensor to measure the flow rate. Therefore, the measurement is more accurate as the mask captures the airflow going through the mouth and the nose, instead of only measuring the flow at the nose. This may, however, result in the re-breathing of air and further research is required to determine the extent of the re-breathing and how this could be avoided.

Once the signals have been recorded, the device processes the data and identifies apnoea events. Using the algorithm proposed by the AASM, the device can process the recorded signals, identify events, and present this information to a clinician. The algorithm's reliance on flow rate measurements, especially when obtained from the nose using a pressure sensor for testing purposes, makes it more susceptible to errors.

The device has demonstrated that it is possible for a single device to provide a basic level of CPAP therapy and the information required to make a diagnosis. The diagnosis method used is a Level 3 type home sleep test, meaning sleep apnoea diagnosis would be more accessible than the overnight polysomnography test.

7 Recommendations

Although the developed system answers the research question, it requires improvements and additional features to improve its functionality. These improvements and additional features are highlighted below.

Data Processing Algorithm
A more advanced algorithm is required for sleep apnoea diagnosis that does not significantly emphasise one signal over another. This may take the form of a neural network, or a more complex threshold-based algorithm.

Diagnostic Data Streaming
One of the features of a Level 1 type of sleep apnoea diagnosis is that the sleep technologist is with the patient for the duration of the night and has access to the signals for the entire time. Thus, if the signal no longer reads correctly, then the sleep technologist can prompt the patient to correct the sensor placement. It would therefore be helpful if the device could stream the data during the test, allowing the sleep technologist access to it during the test which could allow them to phone the patient if the sensor readings are not giving the correct values. If streaming is not possible, then the device should be able to upload the data after the test. This could allow the sleep technologist to diagnose remotely, removing the need for the patient to visit the sleep technologist again.

Software Development for APAP Mode
Following diagnosis, a patient would typically return to the technologist and receive an APAP device that can do a titration study to determine what level of pressure support the patient requires. If the system that has been developed could also do the titration study, then the patient would not need to visit the sleep technologist again and could go straight from diagnosis to titration and to treatment.

Pressure Control
As highlighted in the dynamic pressure test, the device needs to be able to control the pressure more accurately when connected to the patient. Further development and testing are required to ensure this is the case. It would be important to develop and test the device while connected to a more realistic breathing simulator, where the patient-mask connection and the patient's breathing characteristics are better simulated.

Sound Abatement
The system is designed to be placed on the patient's bedside table while they are sleeping. It is, therefore, essential that it is relatively quiet while in use to ensure it does not wake up the patient or anyone else sleeping close to them. Currently, the air inlet's shape

means that the fan's sound is amplified. The solid mechanical connection between the fan and the device's chassis also means that any fan vibrations are transferred and not damped. Therefore, further consideration of the noise generated by the device is required to ensure that it does not disrupt the patient's sleep.

Mobile Application Development

The user interface is relatively simple, meaning it is difficult for the user to interact meaningfully with the data generated by the device. A mobile application should be developed that connects to the device and displays additional data to the user. This data could also be sent to the sleep technologist, allowing them to monitor the patient's treatment.

Re-breathing during diagnosis

The system developed proposes a new method of measuring the flow rate of air entering and leaving a patient. This new method makes use of an oro-nasal mask instead of sensors placed on or close to the patient's nose and mouth. Further research needs to be done to understand how this new method compares to the old one, and if the new method promotes re-breathing of exhaled air.

These improvements, as well as adherence to regulatory requirements, may result in a device that significantly enhances the patient treatment pathway and improves accessibility to sleep apnoea diagnostic and treatment devices.

References

AASM. (2014). *International classification of sleep disorders* (3rd).

American Academy of Sleep Technologists. (2020). *AAST Technical Guideline* (tech. rep.).

Antonescu-Turcu, A. & Parthasarathy, S. (2010). CPAP and Bi-level PAP Therapy: New and Established Roles. *Respiratory Care*, *55*(9).

Arduino. (2022). Arduino Mega 2560 Rev3. https://store.arduino.cc/products/arduino-mega-2560-rev3

Arlotto, P., Grimaldi, M., Naeck, R. & Ginoux, J.-M. (2014). An Ultrasonic Contactless Sensor for Breathing Monitoring. *Sensors*, *14*(8), 15371–15386. https://doi.org/10.3390/s140815371

ARTP. (2018). *Association for Respiratory Technology and Physiology Standards of Care-CPAP Devices (Technical and Performance), Version 4* (tech. rep.). ARTP Sleep Apnoea Consortium. Stafforshire.

Åström, K. J. & Hägglund, T. (1995). *PID controllers: Theory, design, and tuning.* (2nd ed.). Instrument Society if America.

Bailey Maimilian. (2010). The Respiratory System. Pearson Education, Inc. Nasal cavity Nostril Oral cavity Pharynx Larynx Trachea Left main (primary) bronchus. - ppt download. https://slideplayer.com/slide/8294547/

Ball, E. M., Simon, R. D., Tall, A. A., Banks, M. B., Nino-Murcia, G. & Dement, W. C. (1997). Diagnosis and treatment of sleep apnea within the community. The Walla Walla Project. *Archives of internal medicine*, *157*(4), 419–24.

Benjafield, A. V., Ayas, N. T., Eastwood, P. R., Heinzer, R., Ip, M. S., Morrell, M. J., Nunez, C. M., Patel, S. R., Penzel, T., Pépin, J. L. D., Peppard, P. E., Sinha, S., Tufik, S., Valentine, K. & Malhotra, A. (2019). Estimation of the global prevalence and burden of obstructive sleep apnoea: a literature-based analysis. *The Lancet Respiratory Medicine*, *7*(8), 687–698. https://doi.org/10.1016/S2213-2600(19)30198-5

Berry, R., Quan, S., Abreu, A., Bibbs, M., DelRosso, L., Harding, S., Mao, M.-M., Plante, D., Pressman, M., Troester, M. & Vaughn, B. (2020). *The AASM Manual for the Scoring of Sleep and Associated Events* (Version 2.6). American Academy of Sleep Medicine.

Bikov, A. & Dragonieri, S. (2020). *Obstructive Sleep Apnea Epidemiology, Pathomechanism and Treatment* (tech. rep.). www.mdpi.com/journal/medicina

Bohn, C. & Alsogkier, I. (2017). Rejection and Compensation of Periodic Disturbance in Control Systems. *THE INTERNATIONAL JOURNAL OF ENGINEERING AND INFORMATION TECHNOLOGY (IJEIT)*, *4*(1), 44. www.ijeit.misuratau.edu.ly

Borsini, E. & Nigro, C. A. (2022). Proposal of a diagnostic algorithm based on the use of pulse oximetry in obstructive sleep apnea. *Sleep and Breathing*. https://doi.org/10.1007/s11325-022-02757-1

Bradley, T. D., Logan, A. G., Kimoff, J. R., Sériès, F., Morrison, D., Ferguson, K., Belenkie, I., Pfeifer, M., Fleetham, J., Hanly, P., Smilovitch, M., Tomlinson, G. & Floras, J. S. (2005). Continuous Positive Airway Pressure for Central Sleep Apnea and Heart Failure. *New England Journal of Medicine*, *353*(19), 2025–2033. https://doi.org/10.1056/NEJMoa051001

Chang, S. (2022). 12/24V Brushless DC Motor Fan Blower. https://www.alibaba.com/product-detail/12-24V-brushless-dc-motor-fan_60657146534.html?spm=a2700.shop_index.86.9.15cb7dffFyMVUt%20[2023,%20January%205]

Colten, H. R. & Altevogt, B. M. (2006). Sleep Disorders and Sleep Deprivation: An Unmet Public Health Problem. *Sleep Disorders and Sleep Deprivation: An Unmet Public Health Problem*, 1–404. https://doi.org/10.17226/11617

Day, M. (2002). Understanding low drop out (LDO) regulators. *Texas Instruments, Dallas*, *16*.

Doherty, L. S., Kiely, J. L., Swan, V. & McNicholas, W. T. (2005). Long-term Effects of Nasal Continuous Positive Airway Pressure Therapy on Cardiovascular Outcomes in Sleep Apnea Syndrome. *Chest*, *127*(6), 2076–2084. https://doi.org/10.1378/chest.127.6.2076

Domínguez-Mayoral, A., Sánchez-Gómez, J., Guerrero, P., Ferrer, M., Gutiérrez, C., Aguilar, M., Fouz-Rosón, N., Benítez, J. M., Pérez-Sánchez, S., Gamero-García, M. Á., De Torres-Chacón, R., Barragán-Prieto, A., Algaba, P., Ruiz-Bayo, L. & Montaner, J. (2021). High prevalence of obstructive sleep apnea syndrome in Spain's Stroke Belt. *The Journal of International Medical Research*, *49*(10). https://doi.org/10.1177/03000605211053090

Ebben, M. R., Oyegbile, T. & Pollak, C. P. (2012). The efficacy of three different mask styles on a PAP titration night. *Sleep Medicine*, *13*(6), 645–649. https://doi.org/10.1016/j.sleep.2012.02.004

Ejury, J. (2013). Buck converter design. *Infineon Technologies North America (TFNA)*, *1*, 1.

Epstein, L. J., Kristo, D., Strollo, P. J., Friedman, N., Malhotra, A., Patil, S. P., Ramar, K., Rogers, R., Schwab, R. J., Weaver, E. M. & Weinstein, M. D. (2009). Clinical Guideline for the Evaluation, Management and Long-term Care of Obstructive Sleep Apnea in Adults. *Journal of Clinical Sleep Medicine : JCSM : Official Publication of the American Academy of Sleep Medicine*, *5*(3), 263. https://doi.org/10.5664/jcsm.27497

Ferrie, J. E., Kumari, M., Salo, P., Singh-Manoux, A. & Kivimäki, M. (2011). Sleep epidemiology—a rapidly growing field. *International Journal of Epidemiology*, *40*(6), 1431–1437. https://doi.org/10.1093/IJE/DYR203

Flemons, W. W., Douglas, N. J., Kuna, S. T., Rodenstein, D. O. & Wheatley, J. (2004). Access to Diagnosis and Treatment of Patients with Suspected Sleep Apnea. *American Journal of Respiratory and Critical Care Medicine*, *169*(6), 668–672. https://doi.org/10.1164/rccm.200308-1124PP

Gallitto, A. A., Zingales, R., Battaglia, O. R. & Fazio, C. (2021). An approach to the Venturi effect by historical instruments. *Physics Education*, *56*(2), 025007. https://doi.org/10.1088/1361-6552/ABC8FA

Ge, X., Han, F., Huang, Y., Zhang, Y., Yang, T., Bai, C. & Guo, X. (2013). Is Obstructive Sleep Apnea Associated with Cardiovascular and All-Cause Mortality? *PLoS ONE*, *8*(7), e69432. https://doi.org/10.1371/journal.pone.0069432

Gottlieb, D. J. & Punjabi, N. M. (2020). Diagnosis and Management of Obstructive Sleep Apnea: A Review. *JAMA - Journal of the American Medical Association*, *323*(14), 1380–1400. https://doi.org/10.1001/jama.2020.3514

Harsch, I. A., Schahin, S. P., Radespiel-Troger, M., Weintz, O., Jahreib, H., Fuchs, F. S., Wiest, G. H., Hahn, E. C., Lohmann, T., Konturek, P. C. & Ficker, J. H. (2004). Continuous positive airway pressure treatment rapidly improves insulin sensitivity in patients with obstructive sleep apnea syndrome. *American journal of respiratory and critical care medicine*, *169*(2), 156–162. https://doi.org/10.1164/RCCM.200302-206OC

Hedengren, J. (2020). Dynamics and Control: Proportional Integral Derivative (PID). https://apmonitor.com/pdc/index.php/Main/ProportionalIntegralDerivative

Higurashi, N., Kikuchi, M., Miyazaki, S. & Itasaka, Y. (2002). Effectiveness of a tongue-retaining device. *Psychiatry and Clinical Neurosciences*, *56*(3), 331–332. https://doi.org/10.1046/j.1440-1819.2002.01003.x

International Organization for Standardization. (2020). Medical electrical equipment - Part 2-70: Particular requirements for the basic safety and essential performance of sleep apnoea breathing therapy equipment (ISO 80601-2-70:2020).

Jaradat, M. & Rahhal, A. (2015). Obstructive Sleep Apnea, Prevalence, Etiology \&; Role of Dentist \&; Oral Appliances in Treatment: Review Article. *Open Journal of Stomatology*, *05*(07), 187–201. https://doi.org/10.4236/OJST.2015.57024

Javaheri, S. & Dempsey, J. A. (2013). Central Sleep Apnea. *Comprehensive Physiology*, *3*(1), 141–163. https://doi.org/10.1002/CPHY.C110057

Llamas, M. & Clifton, S. (2022). Philips CPAP — How a CPAP Treats Sleep Apnea, Side Effects and Recall. https://www.drugwatch.com/philips-cpap/

Man Lo, H., Yee Leung, J. H., Yin Chau, G. K., HS Lam, M., Lee, K. Y. & Ho, A. (2017). Factors Affecting Sleep Quality among Adolescent Athletes. *Sports Nutrition and Therapy*, *02*(02). https://doi.org/10.4172/2473-6449.1000123

Maurer, J. T. (2009). *Update on surgical treatment for sleep apnoea 1* (tech. rep.). www.smw.ch

McCormick, B. W. (2003). V/STOL Airplanes. *Encyclopedia of Physical Science and Technology*, 621–630. https://doi.org/10.1016/B0-12-227410-5/00911-X

McDaid, C., Griffin, S., Weatherly, H., Durée, K., van der Burgt, M., van Hout, S., Akers, J., Davies, R., Sculpher, M. & Westwood, M. (2009). Continuous positive airway pressure devices for the treatment of obstructive sleep apnoea–hypopnoea syndrome: a systematic review and economic analysis. *Health Technology Assessment*, *13*(4). https://doi.org/10.3310/hta13040

Merchant, A. (2022). Oral Devices for Obstructive Sleep Apnea: A Literature Review. *ECS Transactions*, *107*(1), 14499–14510. https://doi.org/10.1149/10701.14499ecst

Mosquera-Lopez, C., Leitschuh, J., Condon, J., Hagen, C. C., Rajhbeharrysingh, U., Hanks, C. & Jacobs, P. G. (2019). Design and Evaluation of a Non-ContactBed-Mounted Sensing Device for AutomatedIn-Home Detection of Obstructive Sleep Apnea:A Pilot Study. *Biosensors*, *9*(3). https://doi.org/10.3390/BIOS9030090

Narkiewicz, K. & Somers, V. K. (2003). Sympathetic nerve activity in obstructive sleep apnoea. *Acta physiologica Scandinavica*, *177*(3), 385–390. https://doi.org/10.1046/J.1365-201X.2003.01091.X

Natsky, A., Vakulin, A., Chai Coetzer, C. & Kaambwa, B. (2021). Economic evaluation of diagnostic sleep studies for obstructive sleep apnoea in the adult population: a systematic review. *SLEEP Advances*, *2*(Supplement_1), A53–A54. https://doi.org/10.1093/sleepadvances/zpab014.145

Natsky, A. N., Vakulin, A., Coetzer, C. L. C., McEvoy, R. D., Adams, R. J. & Kaambwa, B. (2021). Economic evaluation of diagnostic sleep studies for obstructive sleep apnoea: a systematic review protocol. *Systematic Reviews*, *10*(1), 104. https://doi.org/10.1186/s13643-021-01651-3

Nieto, F. J., Peppard, P. E., Young, T., Finn, L., Hla, K. M. & Farré, R. (2012). Sleep-disordered breathing and cancer mortality: Results from the Wisconsin Sleep Cohort Study. *American Journal of Respiratory and Critical Care Medicine*, *186*(2), 190–194. https://doi.org/10.1164/rccm.201201-0130OC

Nogueira, J. F., Poyares, D., Simonelli, G., Leiva, S., Carrillo-Alduenda, J. L., Bazurto, M. A., Terán, G., Valencia-Flores, M., Serra, L., de Castro, J. R., Santiago-Ayala, V., Pérez-Chada, D., Franchi, M. E., Lucchesi, L., Tufik, S. & Bittencourt, L. (2020). Accessibility and adherence to positive airway pressure treatment in patients with obstructive sleep apnea: a multicenter study in Latin

America. *Sleep and Breathing*, *24*(2), 455–464. https://doi.org/10.1007/s11325-019-01881-9

Nogueira, J. F., Simonelli, G., Giovini, V., Angellotti, M. F., Borsini, E., Ernst, G. & Nigro, C. (2018). Access to CPAP treatment in patients with moderate to severe sleep apnea in a Latin American City. *Sleep Science*, *11*(3), 174. https://doi.org/10.5935/1984-0063.20180032

Pantin, C. C., Hillman, D. R. & Tennant, M. (1999). Dental Side Effects of an Oral Device to Treat Snoring and Obstructive Sleep Apnea. *Sleep*, *22*(2), 237–240. https://doi.org/10.1093/sleep/22.2.237

Parra, O., Arboix, A., Bechcich, S., Garcia-Eroles, L., Montserrat, J. M., Lopex, J. A., Ballester, E., Guerra, J. M. & Sopena, J. J. (2000). Time Course of Sleep-related Breathing Disorders in First-Ever Stroke or Transient Ischemic Attack. *American Journal of Respiratory and Critical Care Medicine*, *161*(2), 375–380. https://doi.org/10.1164/ajrccm.161.2.9903139

Patel, S. R., Ayas, N. T., Malhotra, M. R., White, D. P., Schernhammer, E. S., Speizer, F. E., Stampfer, M. J. & Hu, F. B. (2004). A Prospective Study of Sleep Duration and Mortality Risk in Women. *Sleep*, *27*(3), 440–444. https://doi.org/10.1093/sleep/27.3.440

Patil, S. P., Schneider, H., Schwartz, A. R. & Smith, P. L. (2007). Adult Obstructive Sleep Apnea: Pathophysiology and Diagnosis. *Chest*, *132*(1), 325–337. https://doi.org/10.1378/CHEST.07-0040

Peppard, P. E., Young, T., Palta, M. & Skatrud, J. (2000). Prospective Study of the Association between Sleep-Disordered Breathing and Hypertension. *New England Journal of Medicine*, *342*(19), 1378–1384. https://doi.org/10.1056/NEJM200005113421901

Piorecky, M., Bartoň, M., Koudelka, V., Buskova, J., Koprivova, J., Brunovsky, M. & Piorecka, V. (2021). Apnea Detection in Polysomnographic Recordings Using Machine Learning Techniques. *Diagnostics*, *11*(12), 2302. https://doi.org/10.3390/diagnostics11122302

Punjabi, N. M. (2008). The Epidemiology of Adult Obstructive Sleep Apnea. *Proceedings of the American Thoracic Society*, *5*(2), 136. https://doi.org/10.1513/PATS.200709-155MG

Punjabi, N. M. & Beamer, B. (2005). *Sleep Apnea and Metabolic Dysfunction* (4th ed.). Elsevier/Saunders.

Punjabi, N. M., Shahar, E., Redline, S., Gottlieb, D. J., Givelber, R. & Resnick, H. E. (2004). Sleep-disordered breathing, glucose intolerance, and insulin resistance: the Sleep Heart Health Study. *American journal of epidemiology*, *160*(6), 521–530. https://doi.org/10.1093/AJE/KWH261

Pushpak R. Shinde, Rahul H. Chaudhari, Prayag S. Patil & Satish S. Marathe. (2020). Modelling and Simulation of Venturi Parameters in Relation to Geometries and Discharge Coefficient with Computational Fluid Dynamics Technique. *International Journal of Engineering Research and*, *V9*(05). https://doi.org/10.17577/IJERTV9IS050556

ResMed. (2022). What is the air filter for the S9/Air Sense 10? https://ap.resmed.com/knowledge/air_filter

Roche, J., Rae, D. E., Redman, K. N., Knutson, K. L., von Schantz, M., Gómez-Olivé, F. X. & Scheuermaier, K. (2021). Impact of obstructive sleep apnea on cardiometabolic health in a random sample of older adults in rural South Africa: building the case for the treatment of sleep disorders in underresourced settings. *Journal of Clinical Sleep Medicine*, *17*(7), 1423–1434. https://doi.org/10.5664/jcsm.9214

RS Pro. (2023). *Datasheet RS PRO 60W Switching Power Supply* (tech. rep.). https://docs.rs-online.com/ad24/0900766b8169ce99.pdf

Rundo, J. V. & Downey, R. (2019). Polysomnography. *Handbook of clinical neurology*, *160*, 381–392. https://doi.org/10.1016/B978-0-444-64032-1.00025-4

Sánchez, A. I., Martínez, P., Miró, E., Bardwell, W. A. & Buela-Casal, G. (2009). CPAP and behavioral therapies in patients with obstructive sleep apnea: Effects on daytime sleepiness, mood, and cognitive function. *Sleep Medicine Reviews*, *13*(3), 223–233. https://doi.org/10.1016/j.smrv.2008.07.002

Shahar, E., Whitney, C. W., Redline, S., Lee, E. T., Newman, A. B., Javier Nieto, F., O'Connor, G. T., Boland, L. L., Schwartz, J. E. & Samet, J. M. (2001). Sleep-disordered breathing and cardiovascular disease: cross-sectional results of the Sleep Heart Health Study. *American journal of respiratory and critical care medicine*, *163*(1), 19–25. https://doi.org/10.1164/AJRCCM.163.1.2001008

Shayeb, M. E., Topfer, L. A., Stafinski, T., Pawluk, L. & Menon, D. (2014). Diagnostic accuracy of level 3 portable sleep tests versus level 1 polysomnography for sleep-disordered breathing: A systematic review and meta-analysis. *CMAJ*, *186*(1), E25. https://doi.org/10.1503/CMAJ.130952/-/DC1

Skalna, M., Novak, V., Buzga, M., Skalny, P., Hybaskova, J., Stransky, J. & Stembirek, J. (2019). Oral Appliance Effectiveness and Patient Satisfaction with Obstructive Sleep Apnea Treatment in Adults. *Medical Science Monitor*, *25*, 516–524. https://doi.org/10.12659/MSM.911242

Stansbury, R., Badami, V., Rojas, E., Naqvi, S. F., Easterling, J., Abdelfattah, M., Quan, S. F. & Sharma, S. (2022). Addressing rural health disparity with a novel hospital sleep apnea screening: Precision of a high-resolution pulse oximeter in screening for sleep-disordered breathing. *Sleep and Breathing*, *26*(4), 1821–1828. https://doi.org/10.1007/s11325-021-02559-x

Stats SA. (2017). Public healthcare: How much per person? — Statistics South Africa. http://www.statssa.gov.za/?p=10548

Stradling, J. R. & Crosby, J. H. (1991). Predictors and prevalence of obstructive sleep apnoea and snoring in 1001 middle aged men. *Thorax*, *46*(2), 85–90. https://doi.org/10.1136/THX.46.2.85

Trujano, M., Garrido, R. & Soria, A. (2012). *Stable Visual PID Control of Redundant Planar Parallel Robots*. InTech. https://doi.org/10.5772/652

Vasta, C. (2022). Types of CPAP Masks. *the CPAP shop*. https://www.thecpapshop.com/blog/types-of-cpap-masks/#:~:text=CPAP20masks20are20broken20down,own20mask20preference20for20comfort.

Wang, Y.-H., Chen, C.-P., Chang, C.-M., Lin, C.-P., Lin, C.-H., Fu, L.-M. & Lee, C.-Y. (2009). MEMS-based gas flow sensors. *Microfluidics and Nanofluidics*, *6*(3), 333–346. https://doi.org/10.1007/s10404-008-0383-4

White, F. M. (2015). *Fluid Mechanics* (8th). McGraw Hill.

Won, C. H., Li, K. K. & Guilleminault, C. (2008). Surgical treatment of obstructive sleep apnea: Upper airway and maxillomandibular surgery. *Proceedings of the American Thoracic Society*, *5*(2), 193–199. https://doi.org/10.1513/pats.200708-121MG

Yaggi, K. H., Concato, J., Kernan, W. N., Lichtman, J. H., Brass, L. M. & Mohsenin, V. (2005). Obstructive Sleep Apnea as a Risk Factor for Stroke and Death. *New England Journal of Medicine*, *353*(19), 2034–2041. https://doi.org/10.1056/NEJMoa043104

Yalamanchali, S., Farajian, V., Hamilton, C., Pott, T. R., Samuelson, C. G. & Friedman, M. (2013). Diagnosis of Obstructive Sleep Apnea by Peripheral Arterial Tonometry: Meta-analysis. *JAMA Otolaryngology-Head and Neck Surgery*, *139*(12), 1343–1350. https://doi.org/10.1001/JAMAOTO.2013.5338

Young, T., Evans, L., Finn, L. & Palta, M. (1997). Estimation of the clinically diagnosed proportion of sleep apnea syndrome in middle-aged men and women. *Sleep*, *20*(9), 705–706. https://doi.org/10.1093/SLEEP/20.9.705

Young, T., Palta, M., Dempsey, J., Peppard, P. E., Nieto, F. J. & Hla, K. M. (2009). Burden of Sleep Apnea: Rationale, Design, and Major Findings of the Wisconsin Sleep Cohort Study. *WMJ : official publication of the State Medical Society of Wisconsin*, *108*(5), 246. /pmc / articles / PMC2858234 / %20 / pmc / articles / PMC2858234 / ?report = abstract%20https://www.ncbi.nlm.nih.gov/pmc/articles/PMC2858234/

Young, T., Palta, M., Dempsey, J., Skatrud, J., Weber, S. & Badr, S. (1993). *The Occurrence of Sleep-Disordered Breathing among Middle-Aged Adults* (tech. rep.).

Zancanella, E., do Prado, L. F., de Carvalho, L. B., Machado Júnior, A. J., Crespo, A. N. & do Prado, G. F. (2021). Home sleep apnea testing: an accuracy study. *Sleep and Breathing*, 1–7. https://doi.org/10.1007/S11325-021-02372-6/FIGURES/3

Zhang, G.-Q., Cui, L., Mueller, R., Tao, S., Kim, M., Rueschman, M., Mariani, S., Mobley, D. & Redline, S. (2018). The National Sleep Research Resource: towards a sleep data commons. *Journal of the American Medical Informatics Association : JAMIA*, *25*(10), 1351–1358. https://doi.org/10.1093/jamia/ocy064

Appendices

A Ethics Letter for Patient Data Use

UNIVERSITY OF CAPE TOWN
Faculty of Health Sciences
Human Research Ethics Committee

Room 45, E-52 Old Main Building
Groote Schuur Hospital
Observatory 7925
Email: hrec-enquiries@uct.ac.za
Website: www.health.uct.ac.za/fhs/research/humanethics/forms

27 September 2022

HREC REF NO: 603/2022

Prof Sudesh Sivarasu
Division of Biomedical Engineering
Human Biology
Email: sudesh.sivarasu@uct.ac.za
Email: joelphilpott@gmail.com

Dear Prof Sivarasu

PROJECT TITLE: DESIGN AND DEVELOPMENT OF A DEVICE TO DIAGNOSE AND TREAT OBSTRUCTIVE SLEEP APNEA

Thank you for submitting your request to the Faculty of Health Sciences Human Research Ethics Committee.

The HREC note that the proposed study is using data from numerous existing open source databases that provides polysomnography results of patients.

As this uses published literature available through publicly accessible electronic databases, research ethics review and approval is not required.

This is in accordance with Section 1.1.8 of the Department of Health's Ethics in Health Research: Principles, Processes and Structures (South African Department of Health, 2015), which states: *"Research that relies exclusively on publicly available information or accessible through legislation or regulation usually need not undergo formal ethics review. This does not mean that ethical considerations are irrelevant to the research."*

The HREC recommend that researchers refer to the PRISMA website, for the PRISMA statement and checklist, to facilitate the reporting of systematic reviews and meta-analyses. For more information, please refer to http://www.prisma-statement.org/.

Further, fundamental ethical principles for health-related research should be considered in the objectives and methods of the systematic review. See, for example, the Declaration of Helsinki (Fortaleza, Brazil, 2013) and the Department of Health's Ethics in Health Research: Principles, Processes and Structures (South African Department of Health, 2015).

The HREC acknowledges that MMED candidate- Joel Philpott, is also involved in this project.

Yours sincerely

Signed by candidate

PROFESSOR MARC BLOCKMAN
CHAIRPERSON, FACULTY OF HEALTH SCIENCES HUMAN RESEARCH ETHICS COMMITTEE

B Component Selection

Some of the components or subsystems shown in Figure 13 can be purchased as off-the-shelf products, while others require detailed design and manufacturing. This section indicates the requirements of each ready-made component that will be purchased and the product that is selected to satisfy the requirements.

Blower

The selected blower must satisfy the following requirements:

- Provide positive static pressure in the range of 4 cmH_2O to 20 cmH_2O.
- Maintain a positive pressure of 20 cmH_2O with a flow rate of 80 $L\,min^{-1}$.

The WM7040 (24V) centrifugal blower is selected for use as it is available from multiple suppliers and is relatively inexpensive. It is also compact and is designed to be used in CPAP devices and respirators (Chang, 2022). Figure 72 shows the selected fan and Figure 73 shows its pressure-flow rate characteristic curve. The standard motor driver that comes with the motor is purchased as well which requires a Pulse Width Modulation (PWM) signal to control the speed of the fan.

Figure 72: WM7040 Brushless DC Blower Fan (Chang, 2022)

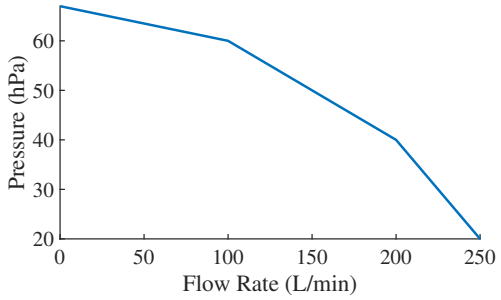

Figure 73: Fan Pressure and Flow Characteristic Curve (Chang, 2022)

Microcontroller

The selected microcontroller must satisfy the following requirements:

- Interface with the storage subsystem, sensor hub, pressure sensors, flow meter, motor driver, screen, and rotary encoder.
- Have a sufficiently high Analog to Digital Converter (ADC) resolution to measure small pressure changes even in a broad range of pressures.
- Have a sufficiently fast clock speed to execute the fan control algorithm, read sensor data, and allow the user interface to operate smoothly.

The Arduino Mega, with an ATmega2560 chip, is selected to be used. The following characteristics make it well-suited to the current application:

- It is readily available from multiple local suppliers.
- It has a 16 MHz crystal oscillator, meaning it will be able to complete the processing requirements without delays.
- It has UART, SPI, and I^2C communication ports and 15 PWM pins.
- It has 54 digital input/output pins.
- It has a maximum ADC resolution of 12 bits and 16 analogue input pins.
- It can be programmed with C++ code, making it relatively simple and quick to develop software for it.

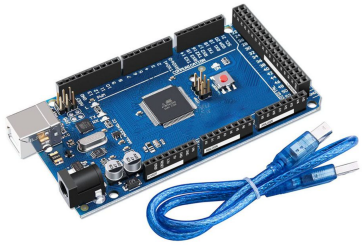

Figure 74: Arduino Mega with and ATmega2560 chip (Arduino, 2022)

Filter

An industry standard filter will be used at the inlet of the device. A standard Resmed Airsense disposable replacement filter is purchased and will be cut to size based on the mechanical design. The selected filter is shown in Figure 75. It is made of non-woven polyester fibre and has an efficiency of greater than 75 % for dust particles approximately 7 µm in diameter (ResMed, 2022).

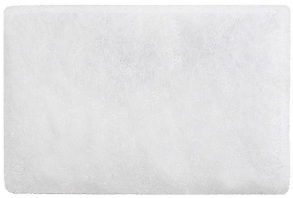

Figure 75: Selected Inlet Filter (ResMed, 2022)

Pressure Sensors

The selected pressure sensors must satisfy the following requirements:

- Measure pressures in at least the range of 4 cmH_2O to 20 cmH_2O.
- Display a linear relationship between the sensor pressure value and the actual pressure.

The XGZP6847 pressure sensor module is selected because it has the following specifications:

- It has a pressure sensing range of between $-50\,cmH_2O$ and $50\,cmH_2O$.

- The pressure sensor is connected to an integrated circuit that corrects for the effects of temperature changes and non-linearities in the reading.
- It outputs an analogue voltage that can be read by the Arduino mega.
- It has a maximum overpressure value of 100 cmH_2O, so the blower cannot damage it.

Figure 76: XGZP6847 Pressure Sensor Module

User Interface

The selected user interface must satisfy the following requirements:

- Allow the user to use the device with a light on or off.
- Allow the user to enable or disable the ramp mode, set the ramp start pressure and set the ramp duration.
- Display usage history.

To satisfy these requirements, a liquid-crystal display (LCD) will be used in conjunction with a continuous rotation rotary encoder with a built-in push button. This means that the user does not need to select from different buttons, but can use the encoder to control the device. The selected LCD screen and rotary encoder are shown in Figure 77.

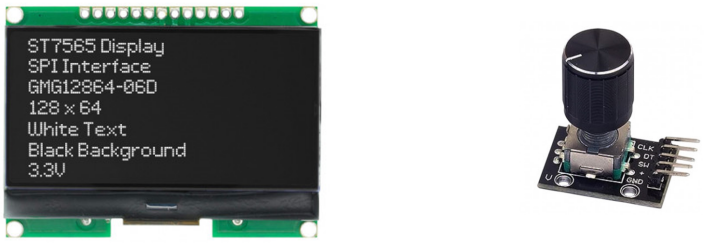

Figure 77: Selected LCD Screen and Rotary Encoder

Data Storage

The selected data storage method must satisfy the following requirements:

- Allow the clinician to access the storage.
- Store at least 3 nights of diagnostic data (at least 36 hours).
- Store at least 1 year of treatment data.
- Store the settings prescribed by the clinician (the pressure support level).

- Store the data in an accessible format.

A microSD card is selected as an appropriate storage method because the storage size can be adjusted by using different microSD cards. It is also compact, and a relatively common storage method so components are readily available. A Catalex microSD card module, as seen in Figure 78, is used as a method of interfacing the SD card with the microcontroller.

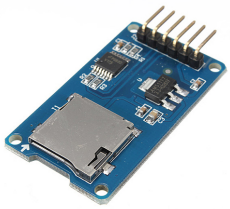

Figure 78: Selected MicroSD Card Reader

Pulse Oximeter

The selected pulse oximeter must satisfy the following requirements:

- Have a minimum sampling frequency of 10Hz.
- Have a reading averaging time of less than 3 s.
- Be able to communicate over USB to the sensor hub and stream data continuously.

The Contec CMS60C pulse oximeter (shown in Figure 79) is selected due to the following specifications:

- It has a 60Hz sampling frequency.
- The device streams the raw data over the USB interface.

Figure 79: Selected Pulse Oximeter

Breathing Effort Sensor

The selected breathing effort sensor must satisfy the following requirements:

- Have a minimum sampling frequency of 25 Hz.

- Have a low frequency filter cut-off frequency of 0.1 Hz
- Have a high frequency filter cut-off frequency of 15 Hz
- Be a sensor of the type Single/dual thoracoabdominal RIP/PVDF/Piezo belt (calibrated or uncalibrated).

Not many breathing effort sensors with a USB interface are available. Therefore, a Plux Biosignals piezo-electric respiration sensor is selected in conjunction with an adapter that converts the connection type to USB. The sensor transmits an analogue voltage, so the sampling frequency and filter cut-off frequencies depend on the microcontroller, not the sensor itself. The sensor, shown in Figure 80, therefore, satisfies all of the requirements.

Figure 80: Selected Piezo-electric Respiration Sensor

Sensor Hub

An interfacing hub is required between the diagnostic sensors and the microcontroller because the pulse oximeter needs to be connected to a device capable of acting as a USB host. The selected Arduino Mega cannot perform this function, so a Raspberry Pi single-board is used. The Raspberry Pi is not used as the main microcontroller as it would increase the cost of the device. (The user does not need the sensor hub containing the Raspberry Pi to receive treatment, but only to be diagnosed. The sensors and the sensor hub can, therefore, be returned after diagnosis). The Raspberry Pi cannot access hardware in real time so if the central processing unit is busy, hardware access will be interrupted. This makes the Raspberry Pi suitable as a method of reading data from the pulse oximeter, but not as the main controller of the device.

Figure 81: Raspberry Pi 4B

Power Supply

It is not possible to calculate the exact power requirements of the device at the outset of the research as the power consumption of each component is difficult to estimate until the device is constructed. For this reason, a bench power supply is used during the construction of the device. The current supplied to the device is measured and a suitable power supply is then purchased based on the current consumption. It is found that a 24 V, 2.5 A power supply, as shown in Figure 82, is suitable.

Figure 82: Selected Power Supply

C Circuit and PCB Design

In this appendix, the circuit design of the different subsystems is discussed, followed by the main PCB. The schematic, PCB design and resulting PCB is shown for each of the circuits.

C.1 Screen PCB

The screen operates on the I^2C communication protocol but requires a 3.3 V logic level. An eight-channel logic level converter with a breakout board is therefore required to change the 5 V logic level from the Arduino to the 3.3 V logic level. The Arduino has a library for I^2C communication and so no additional circuitry is required, just a connection to the Arduino. The resulting schematic is shown in Figure 83.

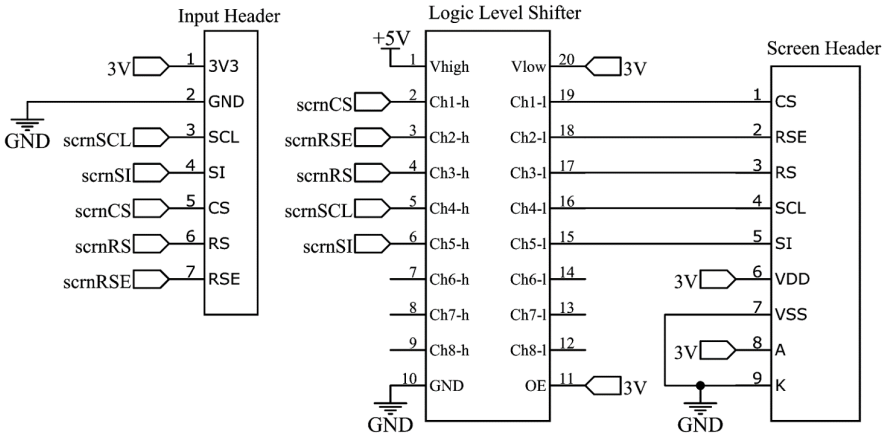

Figure 83: Screen PCB Schematic

The input header is to connect directly to the main PCB. The signals then go through the logic level shifter, and the screen is connected directly to the screen header.

The schematic is converted to a PCB design, as seen in Figure 84. The left side of Figure 84 shows the PCB design, with the top layer nets shown in red and the bottom layer nets shown in blue. The right side of Figure 84 shows the silkscreen of the PCB.

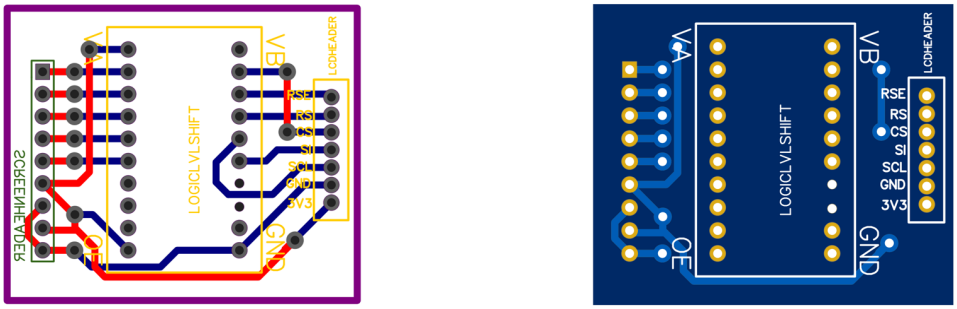

Figure 84: Screen PCB Design

The PCB is manufactured using a desktop computer numerical control (CNC) mill. This allows for PCBs to be prototyped and tested rapidly. The resulting PCB is shown in Figure 85.

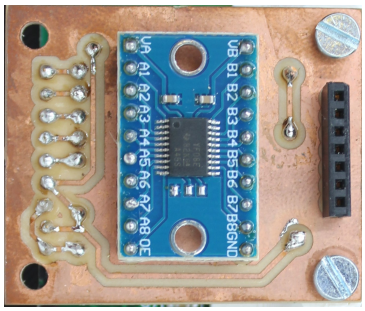

Figure 85: Photograph of Screen PCB

C.2 Encoder PCB

The encoder consists of the push button circuit and the encoder circuit. The push button is connected to ground (GND) and to a digital interrupt pin on the Arduino (encBTN). An internal pull-up resistor is applied to the pin, so the voltage at the pin is ground when pushed and 5 V when not pushed. The circuit is shown on the left side of Figure 86.

The encoder makes use of two pins to indicate when it has been turned and in which direction. A similar method to the button circuit is used to read the information from the pins. This information will be processed in software to determine the direction in which the encoder is being rotated. The circuit is shown in the middle of Figure 86.

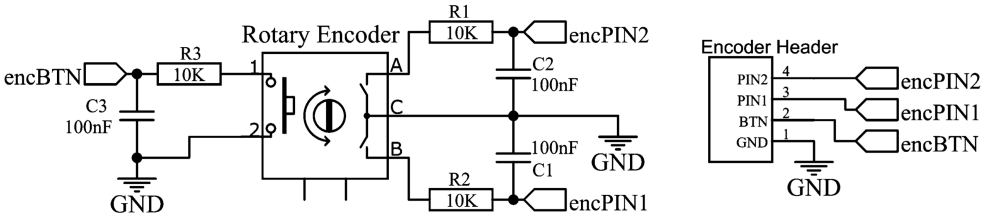

Figure 86: Encoder PCB Schematic

During initial testing, the circuit was unreliable and would sometimes register a double press on the button or double rotation. To mitigate this a passive low-pass filter is used. This is achieved by a resistor and capacitor placed at all the pins as seen in Figure 86. The schematic is converted to the PCB design shown in Figure 87. The rotary encoder is mounted to the back of the PCB while the rest of the components are mounted to the front. This allows the PCB to be mounted close to the front face of the device with the encoder still soldered directly to the PCB.

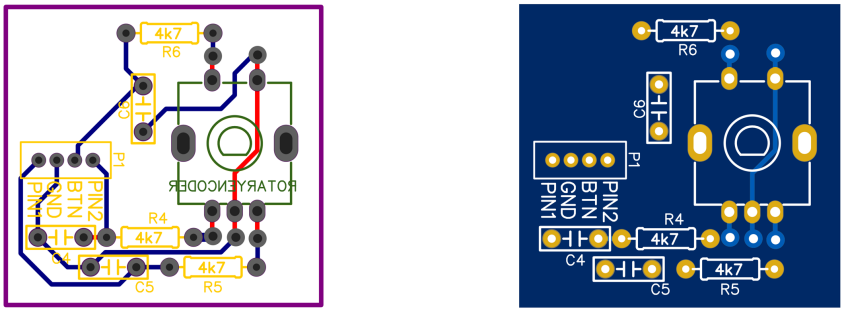

Figure 87: Encoder PCB Design

The PCB is again manufactured using the desktop CNC mill. The resulting PCB is shown in Figure 88.

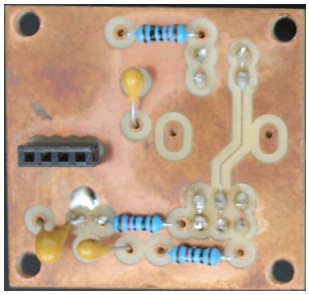

Figure 88: Photograph of Encoder PCB

C.3 Sensor Hub PCB

The sensor hub is required to interface with the pulse oximeter and breathing effort sensor and feed this information back to the Arduino. The pulse oximeter will connect directly to one of the USB ports on the Raspberry Pi and thus does not require any additional circuitry. The breathing effort sensor requires a 5 V power supply and provides an analogue voltage in return that indicates the strain voltage. The Raspberry Pi has no built-in ADC so an external one is required. Finally, the Arduino has a logic level of 5 V while the Raspberry Pi has a logic level of 3.3 V. A logic level converter is therefore required in order for the two devices to communicate with each other. Figure 89 shows the schematic for the sensor hub.

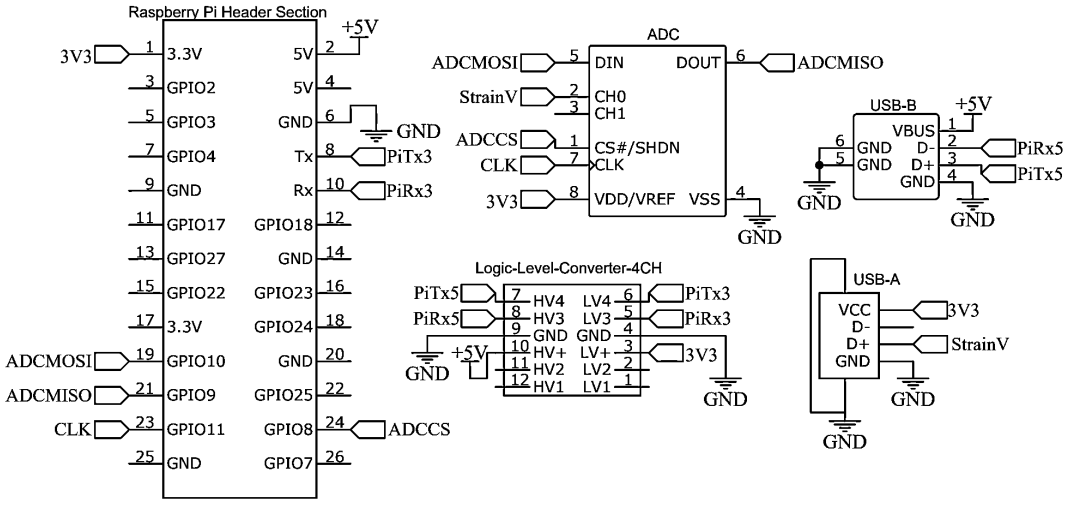

Figure 89: Sensor Hub PCB Schematic

A PCB is designed that accommodates the components shown in the schematic. The PCB will fit onto the first 26 pins of the Raspberry Pi general purpose input/output (GPIO) pins as shown in Figure 90. USB type-A ports are used for the inputs to the sensor hub, and a USB type-B port is used for the output of the sensor hub.

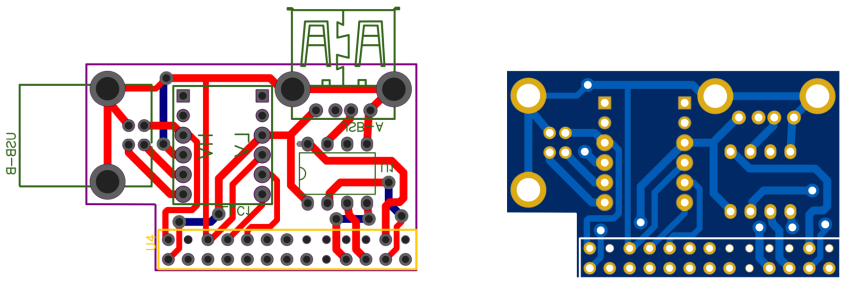

Figure 90: Sensor Hub PCB Design

The PCB design is manufactured and assembled as shown in Figure 91.

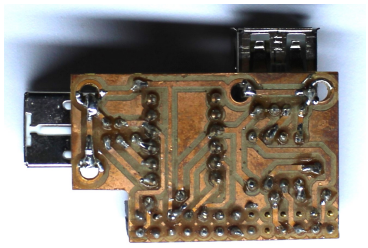

Figure 91: Photograph of Sensor Hub PCB

A basic housing is also designed and constructed using 3D printed components to protect the electronic components. The housing is shown in Figure 92.

Figure 92: Photograph of Sensor Hub Casing

C.4 Power Management PCB

Although the blower requires a voltage of 24 V, most of the other electrical components only require a voltage input of 5 V. In order to accommodate this, the device input voltage is 24V, but a means of reducing the voltage is required. This is typically done using one of the following methods:

Linear Voltage Regulator: A voltage regulator reduces the voltage releasing the excess energy as heat (Day, 2002). It produces a smooth voltage level, but the greater the voltage drop across it, the more heat is produced (Day, 2002). It is also inefficient as the power is dissipated as heat (Day, 2002).

Buck Converter: Buck converters make use of a switch, often in the form of a transistor, to switch the output on and off very quickly (Ejury, 2013). The proportion of time the switch is on affects the output voltage. The output from the switch is smoothed using a capacitor and inductor (Ejury, 2013). This is therefore far more efficient than a voltage regulator, but the output is usually not smooth and contains ripples from the switching of the transistor.

Neither of these methods are well suited to the current application as a large voltage drop is required (from 24 V to 5 V), and the voltage level needs to be smooth in order to reduce noise in the pressure sensor readings. A combination of these two methods will therefore be used. A buck converter is used to step down the majority of the voltage (from 24 V to 8 V). A linear regulator is then used to step down the voltage from 8 V to 5 V. The resulting circuit is shown in Figure 93.

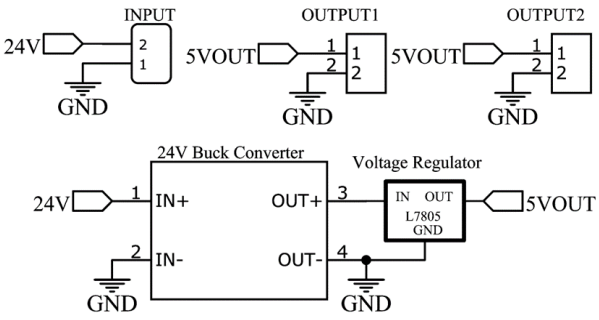

Figure 93: Power Management PCB Schematic

The input header is connected to the 24 V input to the device. The two output headers are connected to the main PCB. This is to reduce the risk of one of them disconnecting and the device losing power.

The schematic is converted to a PCB design as seen in Figure 94. The linear voltage regulator is connected to a heatsink to avoid overheating.

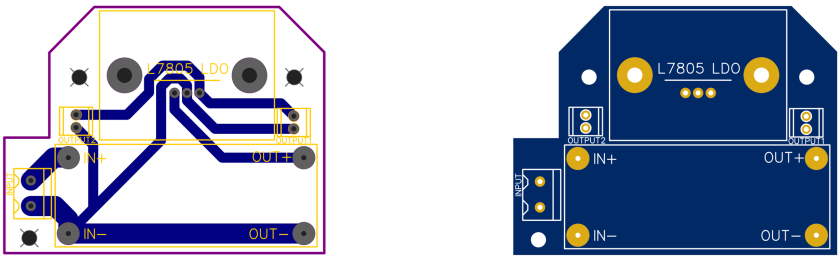

Figure 94: Power Management PCB Design

This PCB is also manufactured by a desktop CNC mill and assembled. The heatsink is soldered to the PCB and then connected to the linear regulator with thermal paste. The resulting circuit is shown in Figure 95.

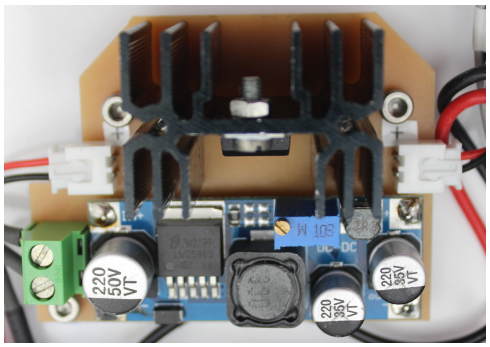

Figure 95: Photograph of Power Management PCB

C.4.1 Main PCB

The main PCB is required to host multiple subsystems and interface with different subsystems. The circuit design is, therefore, broken into smaller components and each component is discussed below.

Pressure and Flow Sensing

The pressure sensors (for pressure sensing and flow sensing) produce analogue output voltages and thus need to be processed by an analogue to digital converter (ADC). The Arduino has a built-in ADC which will be used to process the signal. During the initial testing of the sensors, it is noted that the signal has a significant amount of high-frequency noise. To reduce this, a hardware low-pass RC filter is used. The cut-off frequency for RC filters can be calculated using the following equation:

$$f_c = \frac{1}{2\pi RC} \tag{12}$$

A cut-off frequency of 300 Hz is selected as it is sufficiently higher than the maximum signal frequency but is also lower than the noise frequency. A resistor and capacitor combination is selected that allows for the closest cutoff frequency to 300 Hz. A 4.7 kΩ resistor and 100 nF capacitor are selected and produce a cut-off frequency of 338 Hz. The RC filter is applied to the inputs from all the sensors. The resulting circuit is shown in Figure 96

Blower Control

The design of the blower control component is discussed in the Mechanical Design and Assembly section of Chapter 3. The resulting schematic required to interface with the DAC is shown in Figure 97.

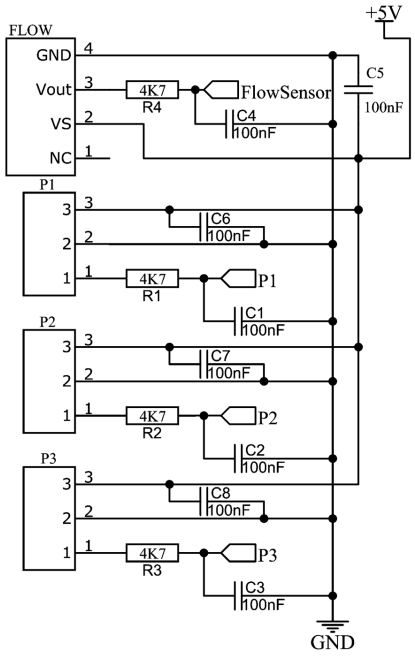

Figure 96: Pressure Sensors Connection Schematic

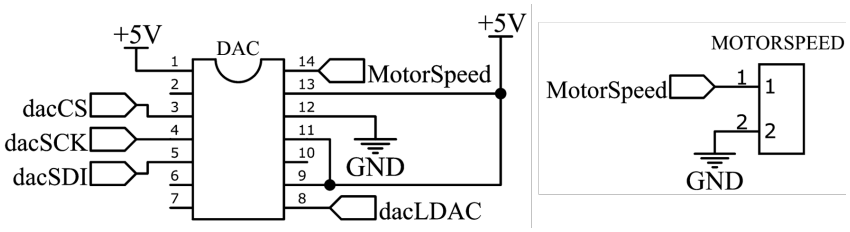

Figure 97: DAC Connection Schematic

External Subsystem Interface

There are five different external subsystems with which the main PCB must interface. These include the screen, encoder, sensor hub, SD card module, and power management subsystem. Connection to the screen, SD card module, and sensor hub is made using standard headers. A JST (Japan Solderless Terminal) connector is used for the power connections to ensure the connection is not disrupted. Eventually, all the connections should be converted to JST connectors to make the device safer, but for debugging and prototyping purposes, simple header connections are used.

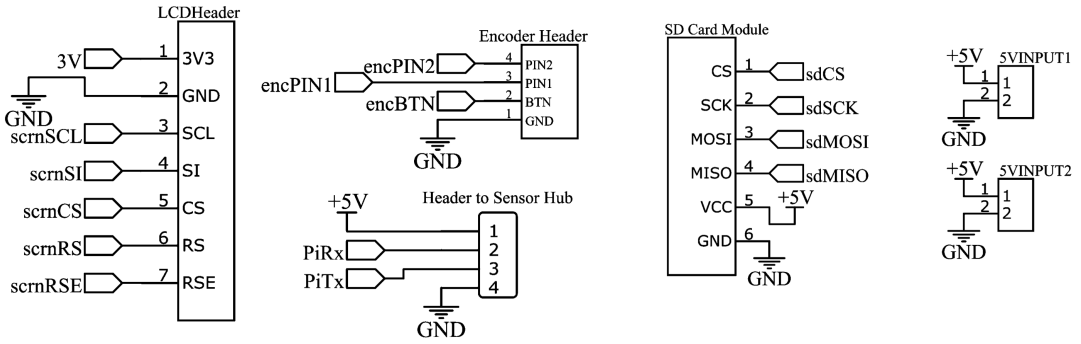

Figure 98: External Subsystem Connection Schematic

Microcontroller Pin Connection

The subsystem connections to the Arduino are carefully considered and selected based on the functionality of the pin, and the location of the pin on the microcontroller PCB. The pin choices are detailed below.

Power Connections: All of the 5 V and ground connectors are connected to a common net.

Sensors: The pressure and flow sensors are connected to the analogue pins, allowing the analogue signal to be processed using a built in ADC.

SD Card Module and DAC: The SD card module and DAC both make use of the SPI protocol and thus are connected to the SPI pins on the Arduino. The chip select connections for the DAC and SD card module are connected to different pins on the Arduino. These pins which will be used to indicate to the DAC and SD card module when the Arduino is communicating with them.

Screen: The screen makes use of the I^2C protocol and is thus connected to the pins on the Arduino capable of communicating using this protocol.

Encoder Pins: An interrupt must be generated when the encoder is rotated or pressed. The pins from the encoder are therefore connected to pins capable of generating an interrupt.

Sensor Hub: The sensor hub will communicate with the Arduino using UART communication, and is, therefore, connected to pins capable of processing this protocol.

The selected pins are shown in Figure 99.

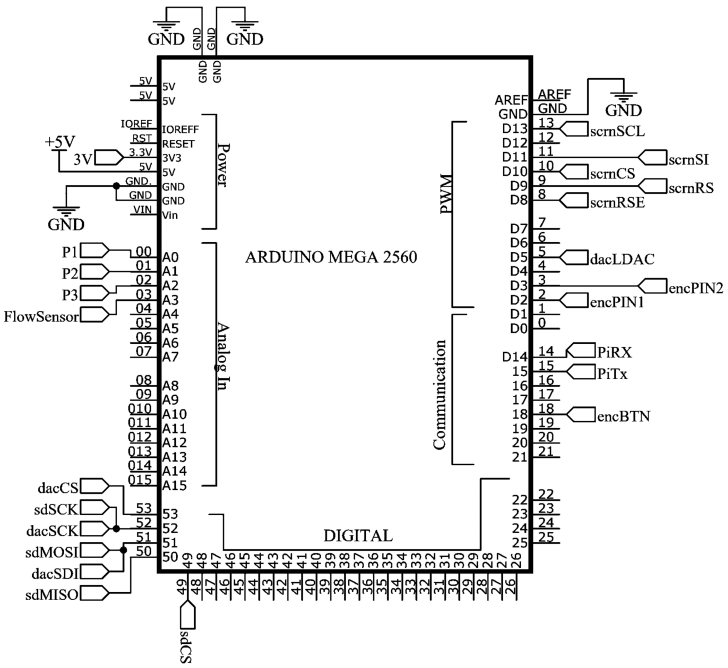

Figure 99: Microcontroller Connection Schematic

The schematic discussed above is converted to a two-layer PCB design, as shown in Figure 100. Tabs with alignment holes are added to the corners of the PCB so that when the board is manufactured, it can be flipped over and the components and holes will still align correctly. No components are placed in the centre column of the PCB as the Venturi tube is placed above the PCB in this region, limiting the space for and access to electronic components.

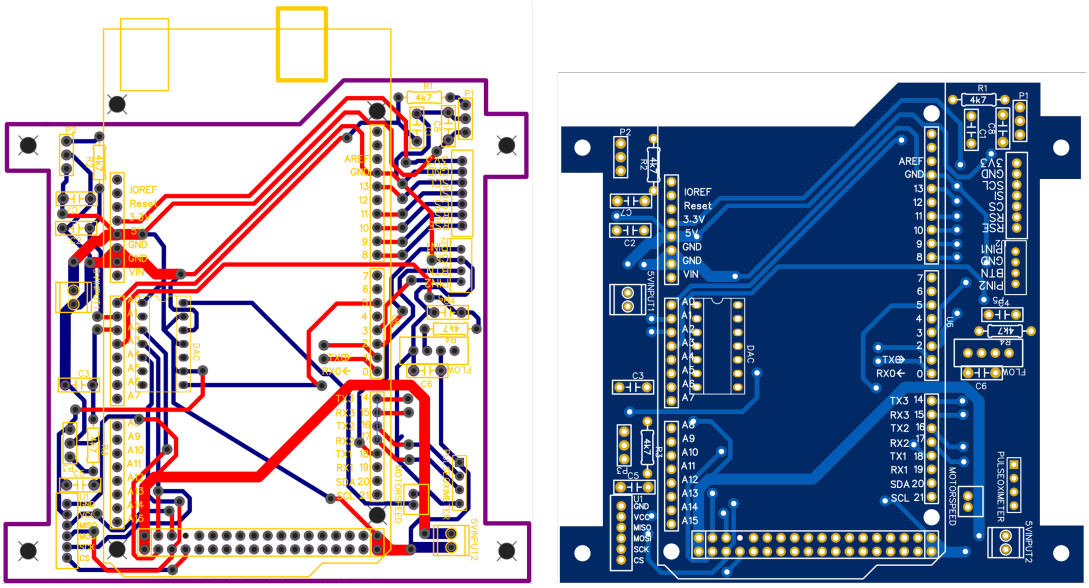

Figure 100: Main PCB Design

The PCB design is again prototyped using a desktop CNC milling machine. The nets are designed to be as thick as possible, to reduce the chance of breakage. The power nets (5 V and ground) leading from the source terminals have an increased width as they carry more current than the other nets and are therefore more prone to heating. The manufactured PCB is shown in Figure 101.

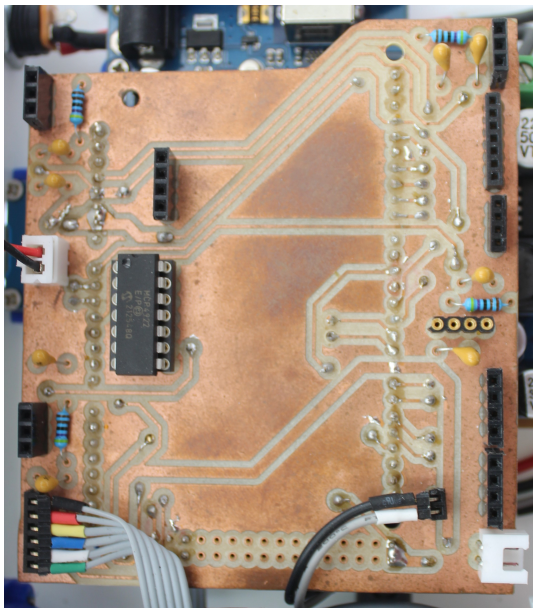

Figure 101: Photograph of Main PCB

D Mechanical Subsystem Assemblies

The different subsystems within the device are assembled after which the device can be assembled. A description of the assembly process for the different subsystems is described below.

D.1 Power Management PCB Assembly

The power management PCB must be securely mounted to ensure that the integrity of all the electrical connections relating to the power management PCB is maintained. A mounting bracket with threaded inserts is therefore designed to secure the PCB. The mounting bracket will be glued to the base of the device. This allows the power management PCB to be positioned optimally after the main PCB is fitted and ensure that the cables connecting to it do not bend at a very tight angle. The PCB mount and assembled PCB is shown in Figure 102.

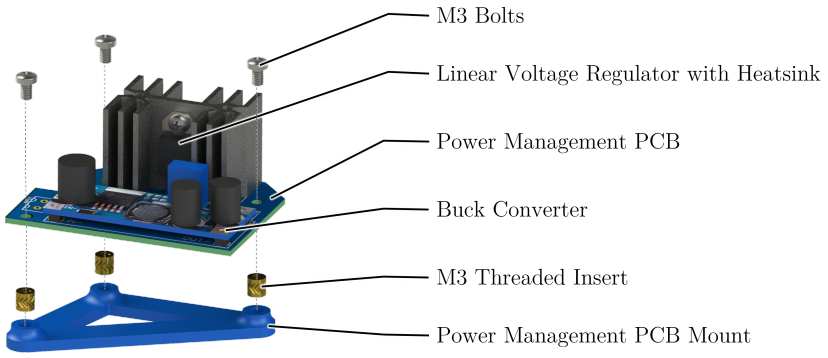

Figure 102: Power Management PCB Assembly

D.2 Motor Driver Assembly

The motor driver is a purchased component so it is modelled and a mount for it designed based on the model. The mount is 3D printed and threaded inserts are melted into the 3D printed part with the holes used as a guide. The PCB is secured to the mount using four M2 bolts, as shown in Figure 103.

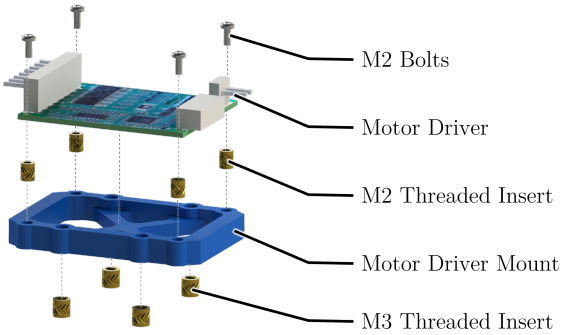

Figure 103: Motor Driver Assembly

D.3 USB Port Assembly

The USB ports are mounted at the front face of the device to make them easily accessible. They will experience a significant amount of force as the user inserts the USB connection into the device. To ensure the port does not break, a supporting place is mounted behind the port and connected to the front face with four bolts that screw into threaded inserts in the front face. The assembly of the ports is shown in Figure 104.

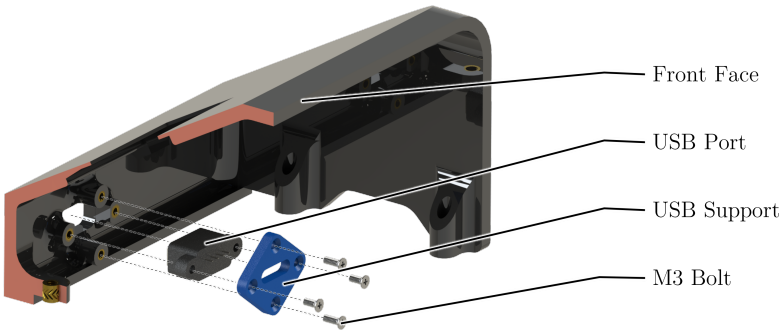

Figure 104: USB Port Assembly

D.4 Rotary Encoder Assembly

The rotary encoder has a threaded shaft. This is used in combination with a washer and thin nut to secure the encoder to the front face. The PCB is soldered to the encoder so if the encoder is secure then so is the PCB. The encoder knob is press fitted onto the end of the encoder shaft, which will allow the user to rotate and press the shaft. The assembly process is shown in Figure 105.

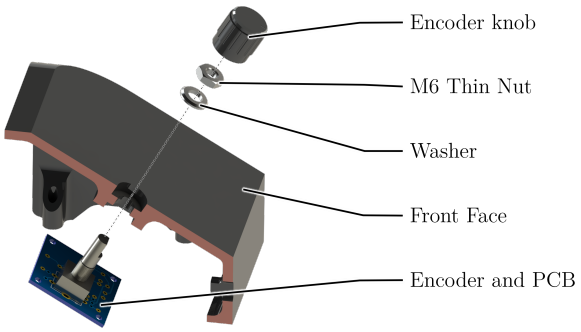

Figure 105: Rotary Encoder Assembly

D.5 Screen Assembly

The screen is bolted to the front face using four M3 bolts and threaded inserts in the front face. The bottom two bolts are also used to secure the screen PCB support and the screen PCB is bolted to the support and connected to the screen header as shown in Figure 106.

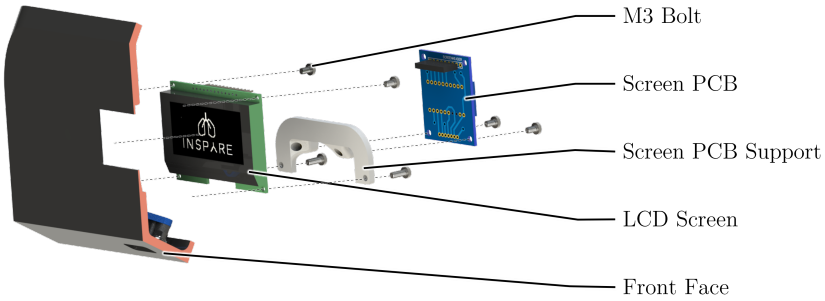

Figure 106: Screen assembly

D.6 Electronics Hub assembly

The main PCB is designed to fit directly onto the Arduino. If the Arduino is mounted securely, then the main PCB will also be secure. The SD card reader is also mounted in the same assembly as it needs be mounted close to the edge of the device to make it accessible. A mount is designed which bolts to the device base. The SD card reader and Arduino are then bolted to the mount, as shown in Figure 107. The assembly is designed to be compact, so that it fits underneath the Venturi tube.

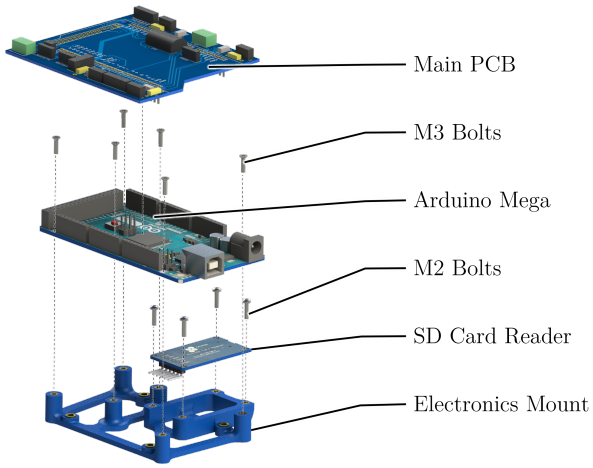

Figure 107: Electronics Hub assembly

D.7 Inlet Assembly

The inlet assembly, as discussed in the flow path design section, is assembled as shown in Figure 108. The fan is bolted and glued to the blower mount, while the inlet funnel is also glued to the blower mount.

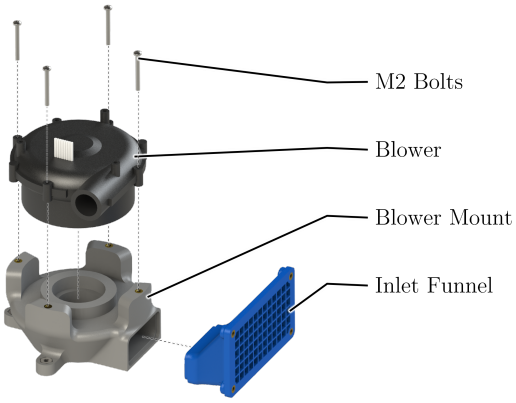

Figure 108: Inlet Assembly

D.8 Flow Path and Electronics Hub Assembly

Once the inlet and electronics hub is assembled, the assembly of the flow path can be completed. The device is designed to be compact, so the flow path cannot be assembled before the electronics hub is inserted between the inlet assembly and outlet support. First the electronics assembly is placed next to the inlet assembly. The outlet support is then placed in front of the electronics assembly, with a cutout in the outlet support that allows for access to the USB port of the Arduino so that the software can be updated. The Venturi tube is then glued to the blower outlet and bolted to the outlet support as shown in Figure 109. The pressure sensors can then be connected directly to the main PCB.

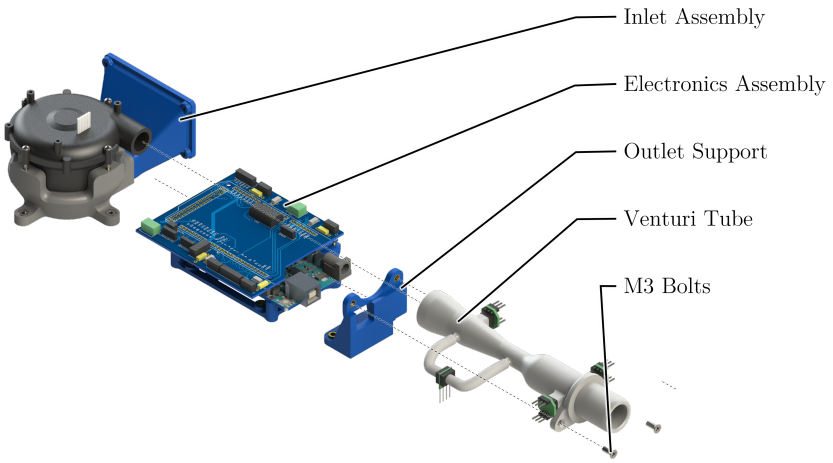

Figure 109: Flow Path and Electronics Hub Assembly

D.9 Top Casing and Device Base Manufacturing and Assembly

The top casing and device base are made by laser cutting a piece of white Perspex, and then bending it into shape using a heat gun and a mould. as discussed in the casing manufacturing section in Chapter 3. Once the top casing has been bent, five casing mounts are glued to it. The casing mount surfaces to be glued are lightly sanded and glued to the Perspex in the positions shown in Figure 110.

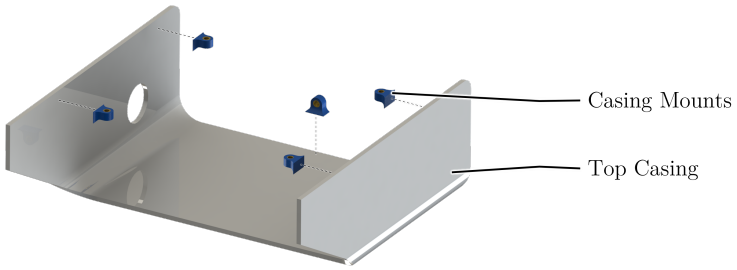

Figure 110: Top Casing Assembly

D.10 Device Assembly

Once the subcomponents of the device are assembled, the device in its entirety can be assembled. This is discussed below.

Step 1: Feet Insertion
The rubber feet are press-fitted into the device base as shown in Figure 111. The feet have a small lip on them that makes the difficult to remove once inserted.

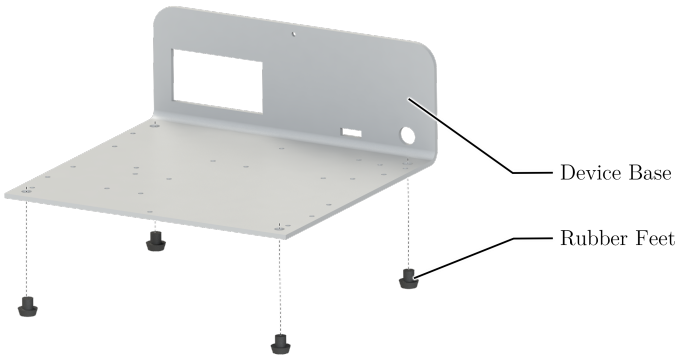

Figure 111: Feet Insertion

Step 2: Flow Path and Electronics Hub Mounting
The flow path and electronics hub is then bolted to the device base using ten M3 bolts. The filter is then inserted, followed by the vent plate. All of the bolts used on the bottom surface of the device are countersunk so that the surface is smooth.

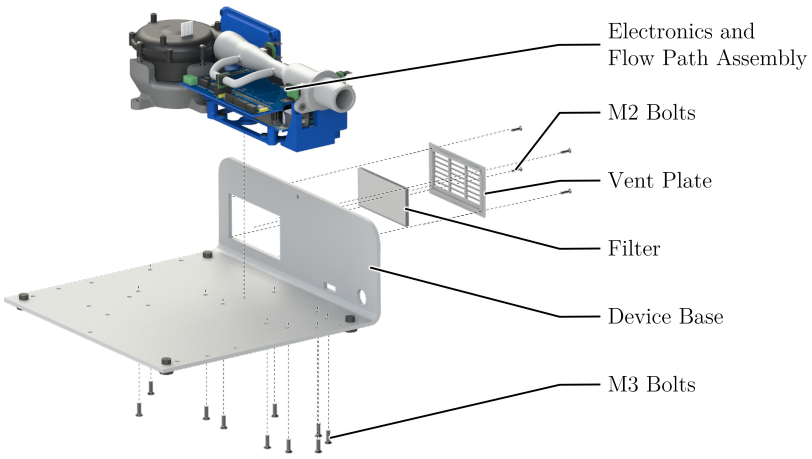

Figure 112: Flow Path and Electronics Hub Mounting

Step 3: Motor Driver and Power Management PCB Mounting

Once the flow path and electronics hub assembly are mounted, the motor driver and power management assemblies can be mounted. The motor driver assembly is bolted onto the device base as shown in Figure 113. The power management assembly is slid onto the device base so that some of it can fit underneath the overhang of the main PCB. The assembly is placed close to the electronics hub assembly, with the terminals on power management PCB still accessible and the heatsink not making contact with the main PCB. This allows for more space for the cables from the screen and encoder at the front of the device, behind the front face. Figure 117 shows the device at the end of step 4, with the motor driver and power management PCB mounted to the device base.

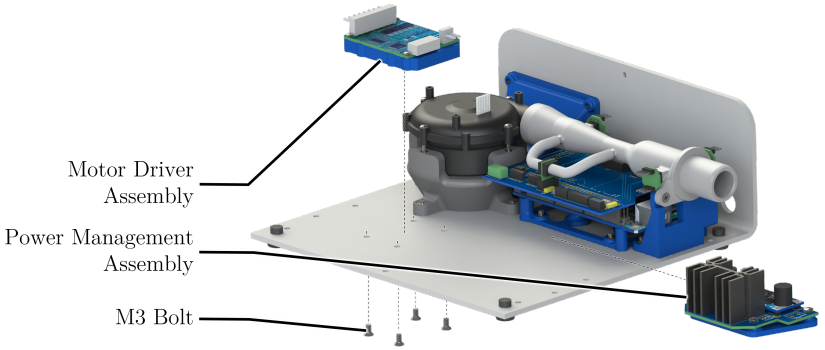

Figure 113: Motor Driver and Power Management PCB Mounting

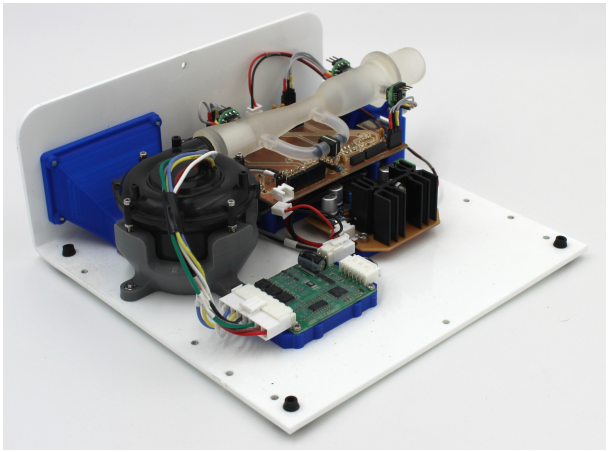

Figure 114: Photograph of the Device at the End of Step 4

Step 4: Front Face and Power Jack Mounting

The power jack is bolted to the back of the device after the power management PCB is mounted so that the cable lengths can be accurately measured. The front face assembly is then bolted to the device base using five M3 bolts as shown in Figure 115. The front face overlaps the device base at the front edge so that the device base is not visible from the front of the device. As a result, the front face relies on the overlap to support it when the encoder button is pushed instead of the bolts.

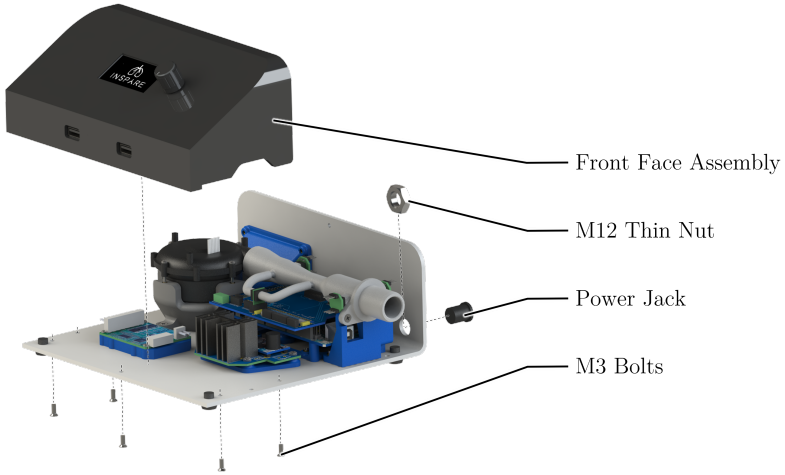

Figure 115: Front Face and Power Jack Mounting

Step 5: Top Casing Mounting

Finally, the top casing is mounted to the device base. The hole in the top casing is slid over the outlet of the Venturi tube. The casing is then rotated. The casing needs to be flexed slightly so that the left side can fit over the front face. Once the top casing is in the correct position, five M3 bolts are used to secure in in place, as shown in Figure 116. Figure 117 shows photographs of the device after steps 3, 4, and 5.

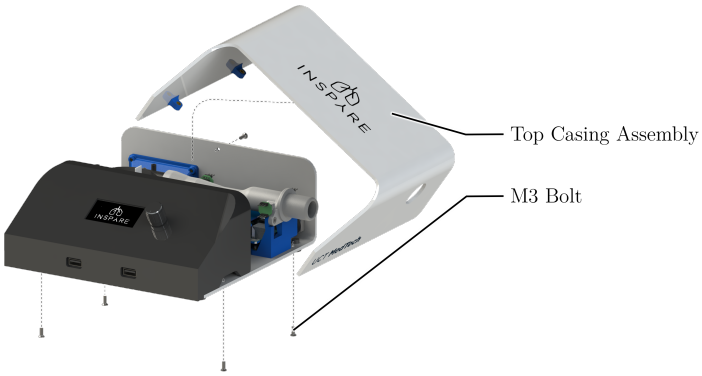

Figure 116: Top Casing Mounting

Figure 117: Photograph of Assembled Device